

15th DOE NUCLEAR AIR CLEANING CONFERENCE

CHARACTERIZATION OF AIRBORNE PLUTONIUM-BEARING PARTICLES FROM A NUCLEAR REPROCESSING PLANT*

S. M. Sanders
Savannah River Laboratory
E. I. du Pont de Nemours & Co.
Aiken, SC 29801

Abstract

The elemental compositions, sizes, structures, and ^{239}Pu contents were determined for 558 plutonium-bearing particles isolated from airborne particles collected at various locations in the exhaust from a nuclear fuel reprocessing facility. These data were compared with data from natural aerosol particles. Most of the collected particles were composed of aggregates of crustal materials. 3.6 percent of the particles were organic and 1.7 percent were metallic, viz., iron, chromium, and nickel. High enrichment factors for titanium, manganese, chromium, nickel, zinc, and copper were evidence of the anthropogenic nature of some of the particles. Plutonium contents of most particles were very low (less than one femtocurie of ^{239}Pu). Plutonium concentrations were determined by the fission track counting method. Only one particle contained sufficient plutonium for detection by electron microprobe analysis. This was a 1- μm diameter particle containing 73% PuO_2 by weight (estimated to be 170 fCi of ^{239}Pu) in combination with Fe_2O_3 and mica. The plutonium-bearing particles were generally larger than natural aerosols. The geometric mean diameter of those collected from the mechanical line exhaust point where plutonium is converted to the metal, was larger than that of particles collected from the wet cabinet exhaust (12.3 μm vs. 4.6 μm). Particles from the mechanical line also contained more plutonium per particle than those from the wet cabinets. The amount of plutonium per particle decreased with the distance of each sampling point from the mechanical line which is considered the major source of plutonium contamination in the reprocessing facility.

Introduction

Nuclear fuel reprocessing facilities at the Savannah River Plant release to the atmosphere minute quantities (<1 mCi/yr) of ^{239}Pu in particulate form. To provide information about the chemical and physical form of these particles, samples were collected from nine locations in the two systems which exhaust air from the plutonium finishing operation (JB-Line) in Building 221-F. Particles bearing plutonium were identified, isolated from other collected particles, and characterized as to size, elemental composition, and radioactive properties.

Sampling Locations

Particles were collected from air in both exhaust systems in a nuclear fuel reprocessing facility at the Savannah River Plant. A schematic diagram of these systems is given in Figure 1. System I takes room air from inside wet cabinets (where plutonium is in solution) and from work areas and exhausts it via the JB-line stack.¹ System II takes air from the mechanical line (where plutonium is handled in metallic form) and exhausts it via the 291-F stack.² In System I, samples were taken of unfiltered cabinet air from the fifth and sixth levels

* Work done under Contract No. AT(07-2)-1.

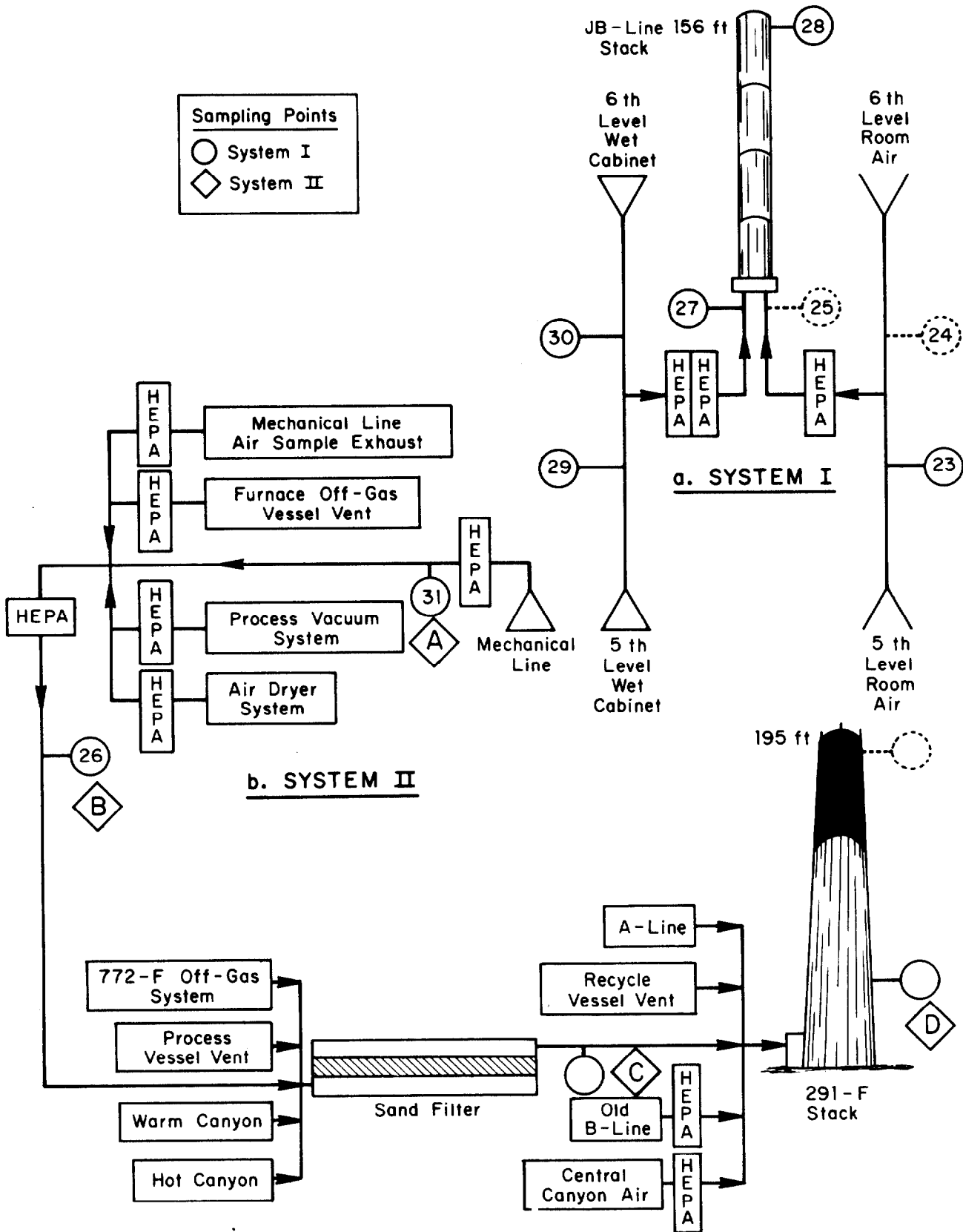


FIGURE 1
EXHAUST SYSTEMS FROM JB-LINE

(Sampling Points 29 and 30, respectively), of filtered air from both locations (Sampling Point 27), and of unfiltered room air from the fifth level (Sampling Point 23), and of air at the 156-foot level of JB-Line stack (Sampling Point 28). In System II, samples were taken of mechanical line air from just beyond the first high-efficiency, particulate air (HEPA) filters located in back of the cabinets (Sampling Point A or 31); of the combined air from the mechanical line, air sample exhaust, furnace off-gas vessel vent, process vacuum system, and air dryer system after the second HEPA filter (Sampling Point B or 26); of the air leaving the sand filter which also contained air from the support laboratory off-gas system of Building 772-F, the fuel dissolving and extraction process vessel vent system and Building 221-F canyons containing the process vessels (Sampling Point C); and of air from the 50-foot level in the 291-F stack where air from the sand filter mingles with that from the uranium recovery A-Line and other sources (Sampling Point D). Air was sampled almost continuously at all locations (except at Sampling Point A) during June 1975 for System I and October 1975 for System II. The level of radioactivity at Sampling Point A was so high that samples were collected only during the first two days.

Only 22 particles could be found on filters used at Sampling Point C and D during October 1975. These points were sampled again from the middle of May to the end of September 1977 with the collection of 163 additional particles. Thus, a total of 121 particles were analyzed from System I (16 from sampling point 23; 68 from point 29; and 38 from point 30) and 417 from System II (125 from Sampling Point A; 107 from Point B; 114 from Point C; and 71 from Point D). These figures do not include 20 particles which contained no elements with atomic numbers greater than 9 and were assumed to be organic.

Methods and Materials

Particle Collection

Particles were collected by drawing a fraction of exhaust air through membrane filters. These filters were polycarbonate films 47 mm in diameter with 0.1- μ m diameter pores supported in a polycarbonate aerosol holder.* Air was drawn through the holder by a small diaphragm pump at a rate of four liters per minute to give a face velocity at the filter of 3.8 cm/sec. Since samples were collected from exhaust ducts having varying linear velocities, the sampling technique was anisokinetic. At the above sampling flow rate, the total efficiency for particle collection by the processes of impaction, diffusion, and interception, calculated according to Spurney,³ is 100% for all particles with diameters of 0.001 μ m (the diameter of gas molecules) or larger.

Arrangement of the air sampling system is shown in Figure 2. To determine the fraction of the exhaust sampled, integrated air flow was measured with a dry type test meter** in series with the diaphragm pump. When nitrogen dioxide was present, exhaust gas was passed through two gas drying towers between the filter and the pump. The first tower contained indicating *Drierite*[†] to remove moisture from the air and save the *Ascarite*^{††} in the second tower. The self-indicating

* The aerosol holders and membrane filters were produced by Nuclepore Corporation, Pleasanton, California, and obtained from them or Bio-Rad Laboratories, Richmond, California.

** Manufactured by the American Meter Division of Singer.

† Trademark of W. S. Hammond Drierite Company.

†† Trademark of Arthur H. Thomas Company.

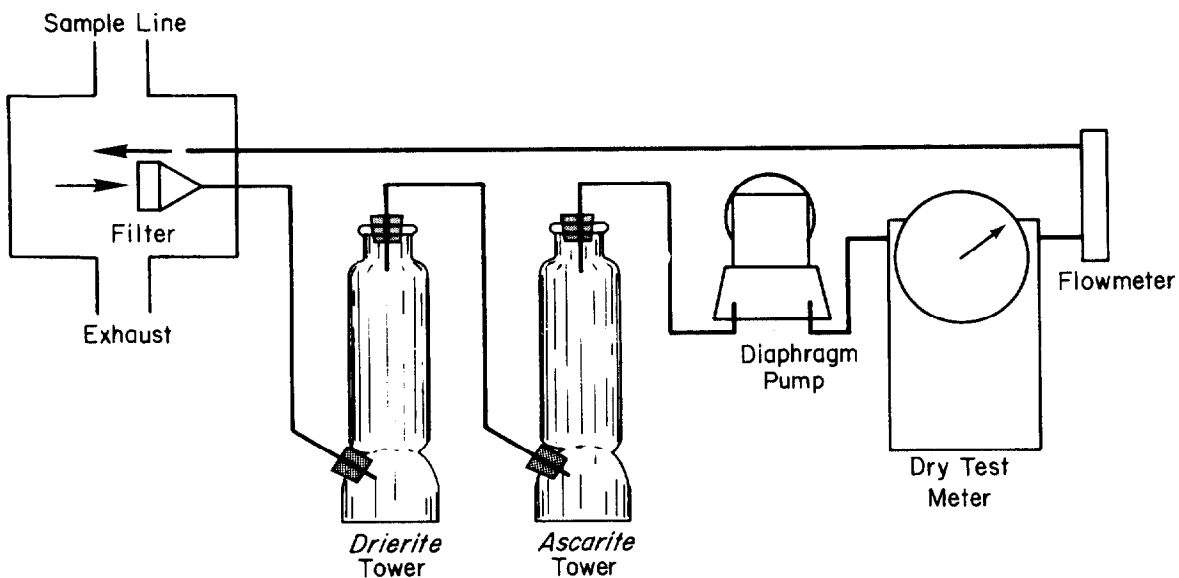


FIGURE 2
ARRANGEMENT OF SAMPLE COLLECTION EQUIPMENT

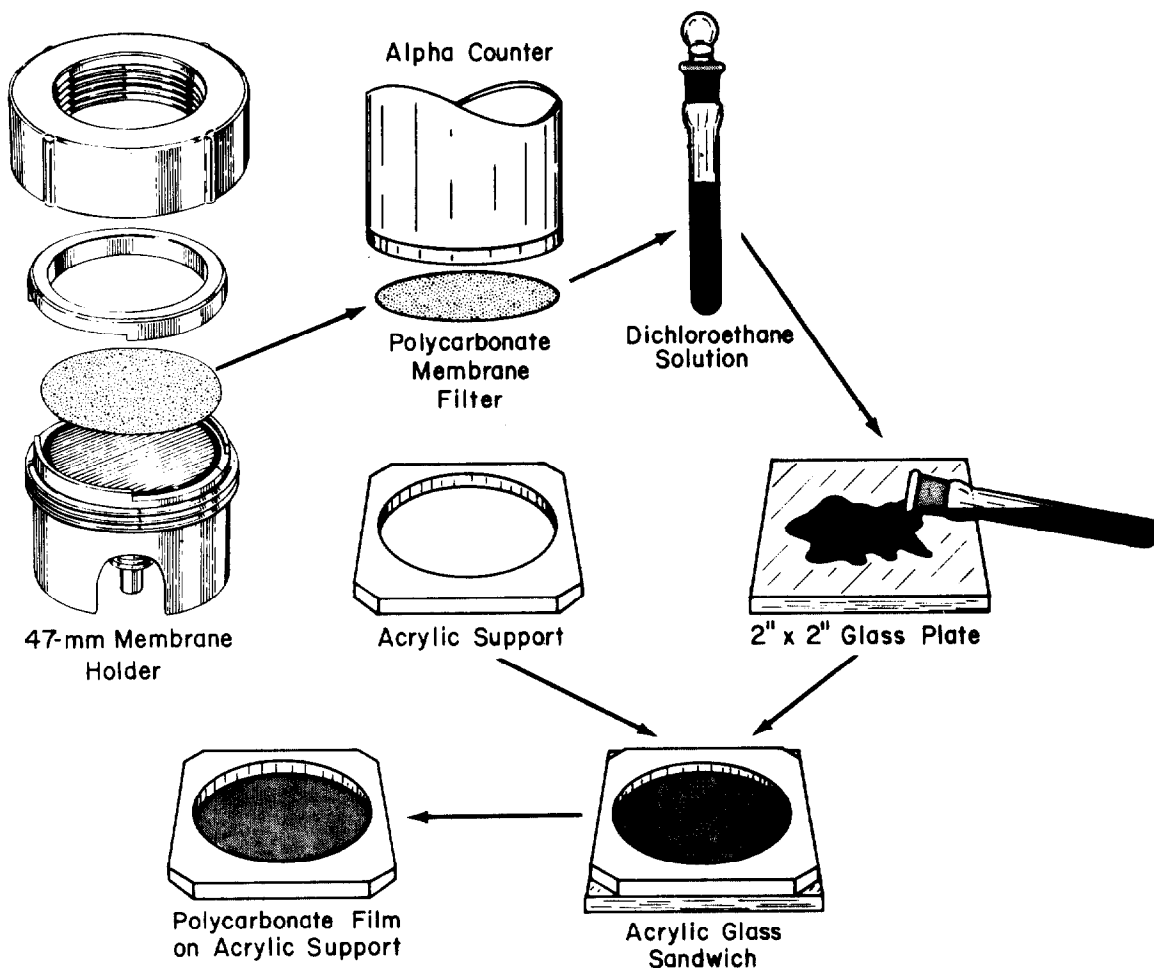


FIGURE 3
PROCEDURE FOR PREPARING POLYCARBONATE FILMS

15th DOE NUCLEAR AIR CLEANING CONFERENCE

Ascarite, in turn, absorbed nitrogen dioxide to protect the pump and the dry test meter. A small flowmeter was mounted on the exhaust side of the dry test meter to give an indication of the instantaneous flow rate through the system. Air from the meter was fed back into the exhaust system to prevent its release to the service area.

Film Preparation

Figure 3 shows the procedure for converting the particle-containing filter membrane to a polycarbonate film. After air was sampled, the radioactivity retained on each filter was measured before it was handled in the laboratory. Each filter was then dissolved in a 40% (v/v) solution of 1,2-dichloroethane in dichloromethane.

The clear polycarbonate solution containing the particles was poured onto a clean, 50-mm (two-inch) square glass plate. One edge of a second 50-mm square glass plate was used to spread the solution evenly over the surface of the first plate. A 50-mm square acrylic support with a 45-mm diameter hole was placed on top of the wet film. The support and plate combinations were placed in covered petri dishes for 16 hours while the films continued to dry.

The glass plates were then removed by dipping the support and plate combinations in distilled water and prying the supports from the glass with tweezers.

Fission Fragment Track Production

The cast polycarbonate film was irradiated in a thermal neutron fluence of about 9×10^{14} neutrons per cm^2 . Films were arranged for irradiation by stacking the supports on top of each other thus sandwiching each film between two supports. Wrapped with each stack were preweighed Type 302 stainless steel disks. The induced radioactivity from 27-day ^{51}Cr in these disks was later measured to determine the thermal neutron fluence to which the particles were exposed.

The packaged stacks were irradiated in a light water-cooled, enriched uranium-fueled standard pile with graphite reflectors.⁴

To make the fission fragment tracks visible with an optical microscope, the polycarbonate film was etched for ten minutes in 6N NaOH at 52 to 55°C.

Alpha Track Production

To identify the fissionable material in each particle, the alpha particle emission rate was measured by coating the polycarbonate film with Kodak Type NTB nuclear-track emulsion (Kodak catalog number 164 4425). Under darkroom lighting, a 4-oz jar of emulsion was immersed in a water bath maintained at 40°C until the emulsion melted. The polycarbonate films were coated with emulsion by holding the supports containing the films vertically by one corner and dipping them into the clear molten emulsion for about one second. The coated films were then maintained at 28°C and about 80% relative humidity until the emulsion cooled and gelled (about 30 minutes).

To determine the alpha particle emission rate for each aerosol particle, the polycarbonate films were stored for one week before being developed. Spun

15th DOE NUCLEAR AIR CLEANING CONFERENCE

aluminum *Desiccators** containing 60 grams of indicating *Drierite* were used to contain the films during this exposure. These were stored in a refrigerator between 4 and 5°C.

At the end of the exposure period, the alpha particle tracks in the emulsion were developed and all substances other than tracks were removed from the emulsion.

The film was prepared for track counting by placing the acrylic support on a 50-mm square, 1.0-mm thick polycarbonate block. Those particles having tracks were located under a microscope using a magnification of 105X. When found, the fission fragment and alpha particle tracks were counted using a magnification of 1000X.

This identification procedure was used to distinguish particle-bound plutonium from uranium. Highly enriched uranium mixtures will give a number of fission fragment tracks comparable to that of the plutonium mixtures. Even if there should be enough uranium to produce fission fragment tracks, mixtures of these isotopes would not produce alpha particle tracks. One femtocurie (fCi) of ^{239}Pu will produce about 22 alpha particles in a week and, when irradiated with a fluence of 8.64×10^{14} thermal neutrons/cm², will produce about 40 fission fragments. In a mixture of low-irradiation plutonium, the number of fission fragments produced will be increased to 53 with between 28 and 33 alpha particles depending on the age of the mixture. Only about half of these particles will produce tracks, yet this radiographic technique is much more sensitive than electron microprobe analysis, which is not sensitive to less than 10 fCi¹.

Particle Isolation

After a particle had been identified and the tracks counted, the particle was excised from the film in a polycarbonate square. At a magnification of 105X, two parallel cuts were made through the emulsion-coated film on either side of the particle using an ultra microlance. The film was then rotated through 90° and two more cuts made forming a square (see Figure 4a). The cut square was then probed in one corner by a tungsten needle, lifted from the film, and placed on a glass microscope slide (see Figures 4b, 4c, and 4d).

The emulsion layers were then removed from the polycarbonate square by placing a cover glass on top of the square. Water was introduced between the cover glass and slide using a glass microbrush. The emulsion was then removed by gently moving the cover glass a few mm from side to side (see Figure 4e); this rolled the swollen emulsion from the surface of the film, but not from the fission fragment tracks themselves. The cover glass was carefully lifted from the glass microscope slide, taking care not to lose the polycarbonate square containing the particle.

Particle Mounting

To mount a particle, the polycarbonate square was placed in a selected grid location on a beryllium sample mounting block** (Figure 4f). These sample mounting blocks were 25 mm in diameter and 13 mm thick and fit the standard electron microprobe sample holders, which grip the sides and provide the necessary electrical contact. The top surface of the block was highly polished and contains a grid

* Trademark of Fisher Scientific Company.

** Walter C. McCrone Associates, Inc. catalog number XIII-403.3.

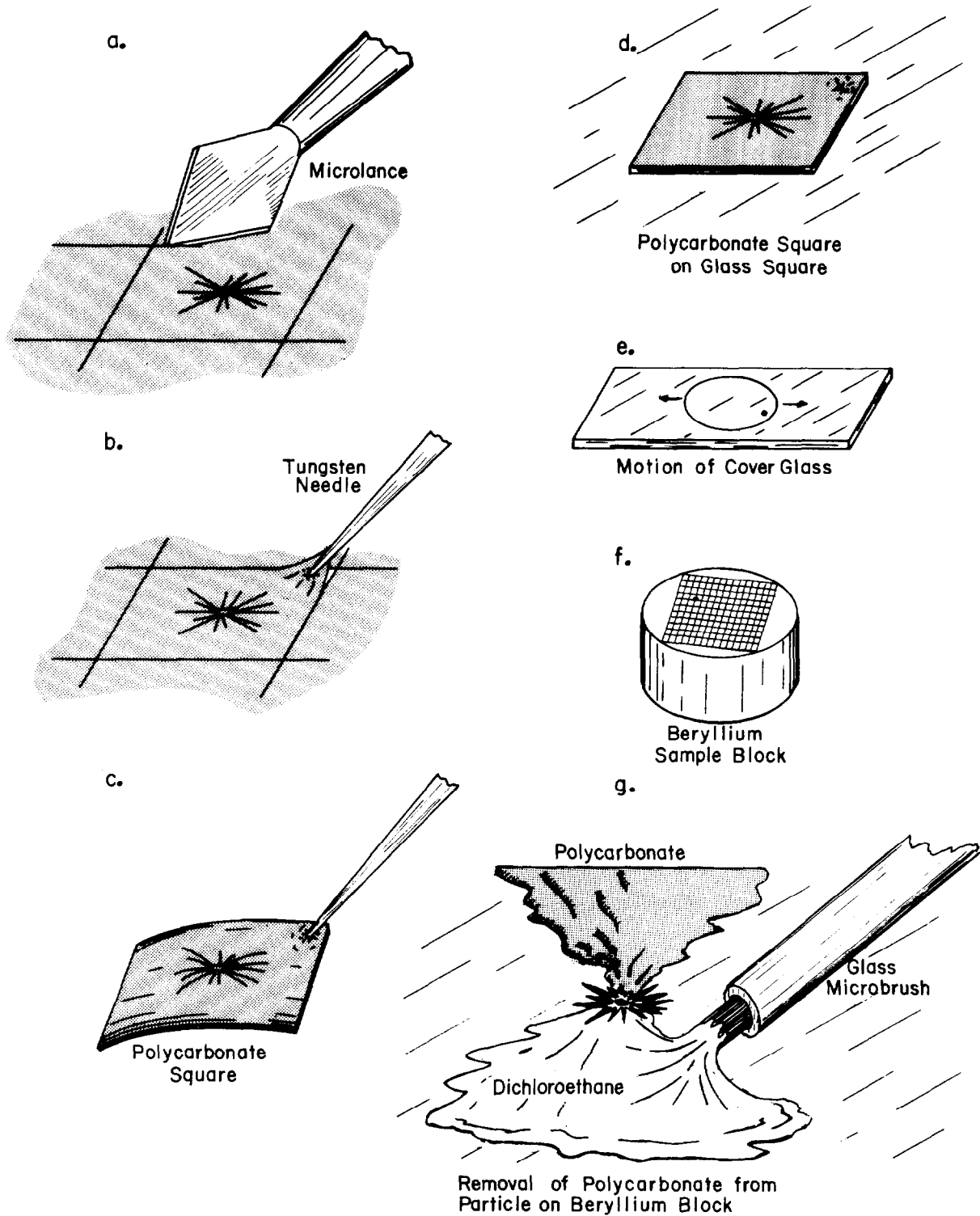


FIGURE 4
PROCEDURE FOR MOUNTING PARTICLE FOR FISSIONABLE MATERIAL IDENTIFICATION

15th DOE NUCLEAR AIR CLEANING CONFERENCE

network of 1-mm squares inscribed on the surface. The squares were numbered in mirror image fashion both vertically and horizontally through the center.

The polycarbonate square was then dissolved and washed back from the particle using dichloroethane from a glass microbrush. Dichloroethane from the brush was dispensed on the beryllium block just in front of the polycarbonate square until the square was engulfed in the solution. The microbrush was then used to push the solution back from the particle. Gelatin replicas of the fission fragment tracks remained with the particles.

A Polaroid picture of each particle was made at a magnification of 556X to identify the particles after the gelatin had been removed.

The gelatin with each particle was oxidized by exposure to an oxygen plasma for three hours in a low-temperature asher.*

To maintain control of particles after the gelatin track replicas were oxidized, each particle was located and photographed again using Polaroid film and a magnification of 556X. An arrow was marked on the film pointing to the particle, so there would be no mistake in what was intended for analysis.

The size of each particle was estimated from these Polaroid pictures taken after oxidation of the completely denuded particles. An average of the smallest and largest dimensions of the photographed particle were measured in mm and divided by the magnification.

Analysis

The plutonium-bearing particles, mounted on beryllium blocks, were analyzed with an electron microprobe. The analyses were made at Arizona State University in Tempe, Arizona, with a Cemeca MS46 electron microprobe equipped with four crystal, wave-length-dispersive spectrometers (take-off angle of 18°) and an energy-dispersive analyzer.

Analytical data included measurements of x-ray intensities and estimates of particle size and shape. These data, along with estimated average densities, were used in the FRAME computer program⁵ as modified for particles work by Armstrong.⁶ These calculations gave the composition of each particle in both elements and oxide weight percents. Oxygen was not measured as such; elements were simply assumed to be present in the oxide form.

Grouping of Data by Enrichment Factors

The results were expressed in terms of "enrichment factors" (dimensionless ratios of elemental concentrations), which enabled the intercomparison of the compositions of plutonium-bearing particles with other atmospheric aerosols and the intracomparison among particles collected from different sampling points. A definition of enrichment factors and an explanation of their development and application in this work is given in the Appendix to this report.

To compare the chemical composition of the particles collected from Systems I and II with each other and with the average for global crustal aerosol, the

* Manufactured by International Plasma Corporation.

15th DOE NUCLEAR AIR CLEANING CONFERENCE

particle analyses were grouped according to the level of the enrichment factors. Four groups were established for each element using the elemental concentration data in Table A-1 of the Appendix. The first group contained those particles which contained no detectable amounts of the element sought. The second group contained detectable amounts with enrichment factors less than one standard deviation below the geometric mean enrichment factor, \overline{EF}_g/s_g . The third group contained particles with enrichment factors between the lower and upper limits of one standard deviation from the geometric mean enrichment factor, \overline{EF}_g/s_g and $\overline{EF}_g \cdot s_g$, respectively. The fourth group contained enrichment factors greater than one standard geometric mean enrichment factor, $\overline{EF}_g \cdot s_g$. The third column of Table I gives the percent of the particles analyzed which gave positive analyses for each element. The fourth, fifth, and sixth columns of Table I contain the percent of those having positive analyses which had enrichment factors less than, between, and more than the lower and upper limits of the geometric standard deviation.

To compare the chemical composition of particles collected at the various sample points in System II with each other and global crustal aerosol (Table A-I), this process was repeated and the results are listed in Table II.

Particles having no detectable amounts of an element were not counted with those with enrichment factors less than the lower limit for the geometric standard deviation (s_g) because there can be no zero or negative concentration of enrichment factor values in log-normal frequency distributions. Thus, the size of the three groups are expressed as the percent of the particles giving positive analyses, rather than the percent of the total number of particles.

Particle Evaluation by Size

In this study, particles were selected for analysis on the basis of their being recognizable by their radiating fission fragment tracks under a 160 X dissecting microscope used for their excision from the polycarbonate film. The film was first scanned and the location of the particles marked. A proportion of the particles were then excised without regard for the number fission fragment tracks present. Thus, there was some bias against particles having less than five tracks. The selection of particles for analysis, however, was not biased by physical size. The size of the particles was not measured until after the particles had been mounted and the polycarbonate film containing the tracks dissolved. Since the distribution of the number of tracks per particle appears to be log normal, the size distribution of the analyzed particles is indicative of the size distribution of particles in the aerosol carrying most of the plutonium.

Cumulative frequency plots were constructed for particles from Systems I and II. Particles in each system were first ranked in order of their approximate diameter in μm from the smallest to the largest. A list of the number of particles having successively larger diameters was made. A cumulative total of the number of particles at increasing diameter segments was calculated and then normalized by dividing by the total number of particles from each system. This gave the fraction of the particles having a diameter equal to or smaller than any particular diameter. Table III lists the particle diameters in μm ; and, in Columns 2, 3, 4, 5, and 6, the fraction of the particles having diameters equal to or less than each diameter measured in System I and Sampling Points A, B, C, and D in System II, respectively. These fractions are also plotted on the logarithmic probability graph given in Figure 5.

For comparison, a cumulative frequency plot was also made of the size distribution of particles in natural atmospheric aerosols.

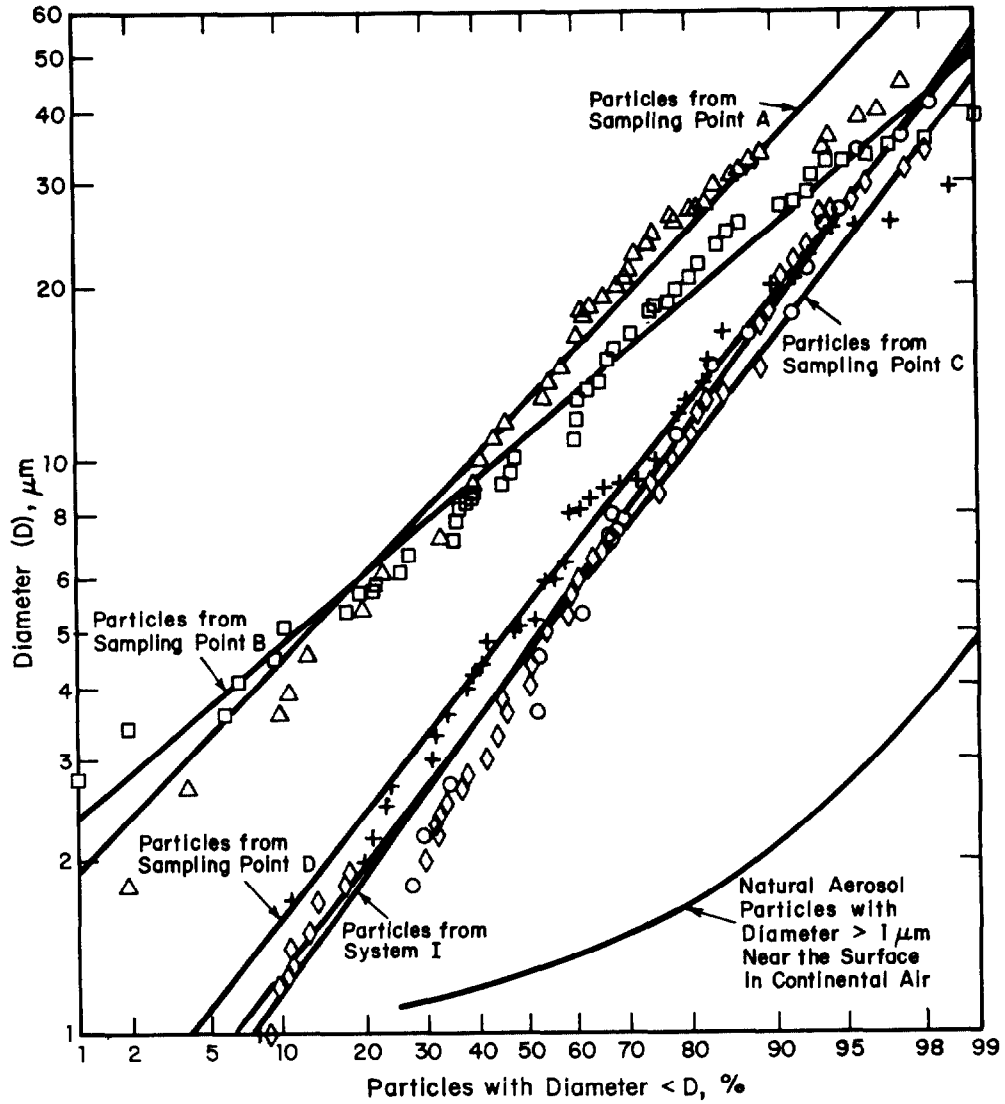


FIGURE 5
 SIZE DISTRIBUTION PLOTS FOR NATURAL AND COLLECTED PARTICLES

15th DOE NUCLEAR AIR CLEANING CONFERENCE

Table I. Comparison of Analyses of Particles From Systems I and II.

Element	System	Positive Analyses, %	% of Positive Analyses ^a		
			Less Than ^b	Within ^c	Greater Than ^d
Si	I	100	47	24	29
	II	99	29	30	41
Al	I	84	0	100	0
	II	88	0	100	0
Fe	I	93	14	35	51
	II	79	36	33	31
Ca	I	70	53	30	17
	II	52	41	40	19
Na	I	70	13	72	15
	II	54	8	81	10
K	I	90	56	30	14
	II	63	35	41	24
Mg	I	51	24	59	17
	II	39	38	52	10
Ti	I	74	20	17	65
	II	31	12	13	76
P	II	1	0	17	83
Mn	I	10	0	0	100
	II	12	4	8	88
Ba	II	0.5	0	0	100
S	I	17	47	47	5
	II	70	28	60	13
Cl	I	34	13	67	21
	II	40	2	82	16
Cr	I	53	0	18	82
	II	29	0	9	91
Ni	I	56	2	25	73
	II	9	0	3	97
Zn	I	64	4	41	55
	II	45	5	52	43
Co	II	1	0	0	100
Sc	II	0.2	0	0	100
Cu	I	36	12	37	51
	II	7	6	29	65
W	I	1	0	0	100
	II	0.5	0	0	100
Cd	II	0.2	0	0	100

a. The percent of the positive analyses less than, within, and greater than one geometric standard deviation of the global geometric mean enrichment factor.

b. $EF < \overline{EF}_g / s_g$.

c. $\overline{EF}_g / s_g \leq EF \leq \overline{EF}_g \cdot s_g$.

d. $EF > \overline{EF}_g \cdot s_g$.

15th DOE NUCLEAR AIR CLEANING CONFERENCE

Table II. Comparison of Analyses of Particles From Sampling Points A, B, C, and D of System II.

Element	Sampling Point	Positive Analyses, %	% of Positive Analyses ^a		
			Less Than ^b	Within ^c	Greater Than ^d
Si	A	99	35	33	32
	B	98	8	24	69
	C	100	36	31	33
	D	99	40	31	29
Al	A	79	0	100	0
	B	94	0	100	0
	C	89	0	100	0
	D	96	0	100	0
Fe	A	98	31	22	46
	B	100	40	39	21
	C	58	33	41	21
	D	49	46	34	20
Ca	A	56	20	44	36
	B	77	54	38	9
	C	41	45	40	15
	D	27	53	32	16
Na	A	55	18	60	22
	B	90	4	94	2
	C	39	5	82	14
	D	24	6	94	0
K	A	76	20	48	31
	B	73	46	44	10
	C	55	35	32	33
	D	37	54	27	19
Mg	A	63	33	58	9
	B	48	35	55	10
	C	17	47	42	11
	D	21	60	27	13
Ti	A	42	12	6	83
	B	27	10	24	66
	C	30	14	11	74
	D	15	9	18	73
P	A	2	0	50	50
	C	3	0	0	100
	D	1	0	0	100
Mn	A	7	13	0	88
	B	30	3	9	88
	C	5	0	0	100
	D	6	0	25	75
Ba	A	1	0	0	100
	B	1	0	0	100
S	A	58	30	54	17
	B	93	21	69	10
	C	66	24	61	15
	D	61	47	44	9

15th DOE NUCLEAR AIR CLEANING CONFERENCE

Table II., Continued

Element	Sampling Point	Positive Analyses, %	% of Positive Analyses ^a		
			Less Than ^b	Within ^c	Greater Than ^d
Cl	A	43	4	47	49
	B	72	1	99	0
	C	27	0	97	3
	D	10	14	86	0
Cr	A	27	0	6	94
	B	58	0	15	85
	C	13	0	0	100
	D	14	0	0	100
Ni	B	27	0	3	97
	C	4	0	0	100
	D	7	0	0	100
Zn	A	53	14	35	51
	B	88	0	69	31
	C	22	4	24	72
	D	6	0	75	25
Co	B	5	0	0	100
Sc	C	1	0	0	100
Cu	A	22	7	33	59
	B	3	0	0	100
	C	1	0	0	100
W	A	1	0	0	100
	B	1	0	0	100
Cd	D	1	0	0	100

a. The percent of the positive analyses less than, within, and greater than one geometric standard deviation of the global geometric mean enrichment factor.

b. $EF < \overline{EF}_g / s_g$.

c. $\overline{EF}_g / s_g \leq EF \leq \overline{EF}_g \cdot s_g$.

d. $EF > \overline{EF}_g \cdot s_g$.

15th DOE NUCLEAR AIR CLEANING CONFERENCE

Table III. Comparison of Size Distributions of Particles From Systems I and II With Natural Aerosols^a.

Diameter (D), μm	Fraction With Diameter $\leq D$					Natural Aerosol
	System I	Sampling Point A	Sampling Point B	Sampling Point C	Sampling Point D	
0.4	0.03			0.01	0.01	
0.5	0.04			0.02		
0.9	0.07			0.04	0.06	
1.1				0.09	0.08	0.25
1.2				0.10		0.42
1.4				0.11		0.64
1.7				0.14	0.11	
1.8	0.28	0.02		0.17		0.83
2.2	0.30			0.32	0.21	0.91
2.5				0.34	0.23	
2.7	0.35	0.04	0.01	0.37	0.24	0.949
3.0				0.42	0.31	
3.3				0.43	0.32	
3.6	0.53	0.10	0.06	0.46	0.34	0.979
3.9		0.11				0.983
4.0			0.07	0.51	0.38	
4.4				0.52	0.41	
4.5	0.54	0.13	0.10			0.989
5.0			0.11	0.55	0.48	
5.4	0.62	0.20	0.18	0.60		0.994
5.8			0.20	0.59		
6.1			0.22	0.61	0.56	
6.3		0.23	0.26			0.996
6.7			0.27	0.64	0.58	
7.0				0.67		
7.2	0.67	0.33	0.35	0.68		0.997
7.4				0.68		
7.8			0.36	0.70		
8.0	0.68	0.34	0.37	0.71	0.59	0.998
8.6			0.39		0.63	
9.0	0.75	0.40	0.46	0.74	0.69	0.999
10.0		0.41	0.48	0.78	0.75	
10.8	0.79	0.44	0.60	0.81		
11.7		0.46	0.61	0.82	0.79	
12.6	0.83	0.54	0.62	0.83	0.80	1.000
13.5		0.55	0.66		0.82	
14.4	0.84	0.58		0.89		
14.9			0.67		0.83	
16.2	0.88	0.61	0.71			
17.1		0.62		0.89	0.89	

15th DOE NUCLEAR AIR CLEANING CONFERENCE

Table III., Continued

Diameter (D), μm	Fraction With Diameter \leq D					Natural Aerosol
	System I	Sampling Point A	Sampling Point B	Sampling Point C	Sampling Point D	
18.0	0.92	0.64	0.75	0.90		
20.7		0.70	0.81	0.91	0.92	
21.6	0.93	0.71	0.82			
23.4		0.74	0.85	0.930	0.930	
24.3		0.75	0.86			
25.2	0.94	0.78	0.87		0.972	
26.9	0.95	0.81	0.91	0.939		
27.9		0.83	0.92			
28.8			0.93	0.956	0.986	
30.6		0.86	0.935			
31.5		0.87		0.974		
32.4		0.88	0.944			
33.5		0.89	0.963			
34.2	0.959	0.94	0.972	0.982		
35.1				1.000	1.000	
36.0	0.975	0.944	0.981			
39.6		0.968	0.991			
41.4	0.983		1.000			
50.4	0.992					
53.9		0.992				
59.4	1.000					
62.9		1.000				

α . The percent of the positive analyses less than, within, and greater than one geometric standard deviation of the global geometric mean enrichment factor.

15th DOE NUCLEAR AIR CLEANING CONFERENCE

A very simple function that has been used extensively in atmospheric research to express particle size distribution in both natural and polluted atmospheres is

$$\frac{dN}{dD} = aD^{-b} \quad (1)$$

where N is the number concentration or total number of particles per unit volume having diameters from the lower limit of definition of aerosols up to diameter D in μm . From the relationships

$$dD = D d(\ln D) \quad (2)$$

and

$$\ln D = \ln 10 \cdot \log D \quad (3)$$

the more useful expression

$$\frac{dN}{d(\log D)} = (\ln 10)aD^{-c} \quad (4)$$

is obtained where $c = b - 1$, and $dN/d(\log D)$ is called the number distribution. Junge⁷ found c to be about 3 over the size range $-0.7 < \log D < 1.5$ or $0.2 < D < 32 \mu\text{m}$. Integrating the first equation between D_0 and D ($D_0 < D$) gives

$$N = \left[\frac{aD^{-c}}{c} \right]_{D_0}^D = \frac{a}{3} \left[\frac{1}{D_0^3} - \frac{1}{D^3} \right] \quad (5)$$

Instead of expressing the distribution as the number of particles per unit volume, it can be expressed as a fraction, F , of the total number of particles or

$$F = \frac{N}{N_T} = 1 - \left[\frac{D_0}{D} \right]^3 \quad (6)$$

where N_T is the total number of particles when $D = \infty$, and $N_T = a/3D_0^3$. To obtain a reasonable distribution, only those particles which could be easily seen with an optical microscope were included. Thus D_0 was assumed to be $1 \mu\text{m}$, and Equation 6 can be expressed as

$$F = 1 - \frac{1}{D^3} \quad (7)$$

The frequency distribution for natural aerosols with particles diameters between $1 \mu\text{m}$ and D , calculated from this expression, is given in Column 7 of Table III and plotted in Figure 5.

To see how closely the distribution of particle diameters resembles a log-normal distribution, the assumption was made that the observed diameters represent a sample of a population having a log-normal distribution. The geometric mean diameter, \bar{D}_g , and geometric standard deviation, s_g , were calculated from these data using equations similar to those given earlier for the geometric mean enrichment factor and geometric standard deviation. These values are given in Table IV. Values for the upper 68.27% limit for the diameters were calculated from the product of \bar{D}_g and s_g . The best fit log-normal probability curves were plotted on the

15th DOE NUCLEAR AIR CLEANING CONFERENCE

logarithmic probability graph in Figure 5 by drawing straight lines through coordinates for \bar{D}_g and $\bar{D}_g \cdot s_g$ on the 50.00 and 84.14* cumulative percent abscissae, respectively.

To determine the degree of asymetry, the skewness (SK) of these frequency distributions was calculated using the relationship

$$SK = 3 \left(\frac{\ln \bar{D}_g - \ln d_{med}}{\ln s_g} \right) \quad (8)$$

where D_{med} = the median diameter. A perfect log-normal distribution has a skewness of zero. If a distribution has a higher tail to the right than to the left, it is positively skewed.

Table IV. Distribution of Particle Diameters in Systems I and II.

<u>System</u>	<u>Sample Location</u>	<u>Data Points, N</u>	<u>Geom Mean Diameter, Dg</u>	<u>Geom Std Deviation, Sg</u>	<u>Skewness, SK</u>
I		121	4.64	2.92	0.71
II	A	125	12.27	2.24	0.04
II	B	107	10.82	1.93	0.34
II	C	114	4.48	2.75	0.37
II	D	71	5.43	2.69	0.23

Particle Evaluation by Plutonium Content

Another characteristic studied was the distribution of plutonium among the particles as indicated by the observed number of fission-fragment tracks in the surrounding polycarbonate.

The track distribution among particles from both systems was evaluated in the same way as the particle diameters. The fraction of the particles with the number of tracks equal to or less than a selected number, T, are given for Sampling Points A, B, C, and D in Table V. Figure 6 is a logarithmic probability plot of cumulative percent of particles from each of these sampling points. Figure 7 is a similar plot for particles from four locations in System I. The calculated geometric mean for the number of fission-fragment tracks per particle. The geometric standard deviation, and the skewness for particles from each sampling point are given in Table VI. Best fit log-normal probability curves for each distribution are plotted in Figures 6 and 7. For the comparison of the track distributions for particles from the various sampling points in System I with those from System II, the probability curve for the track distribution for particles from Sampling Point A in System II is plotted with the distributions from System I in Figure 7.

* $50.00 + \frac{68.27}{2}$.

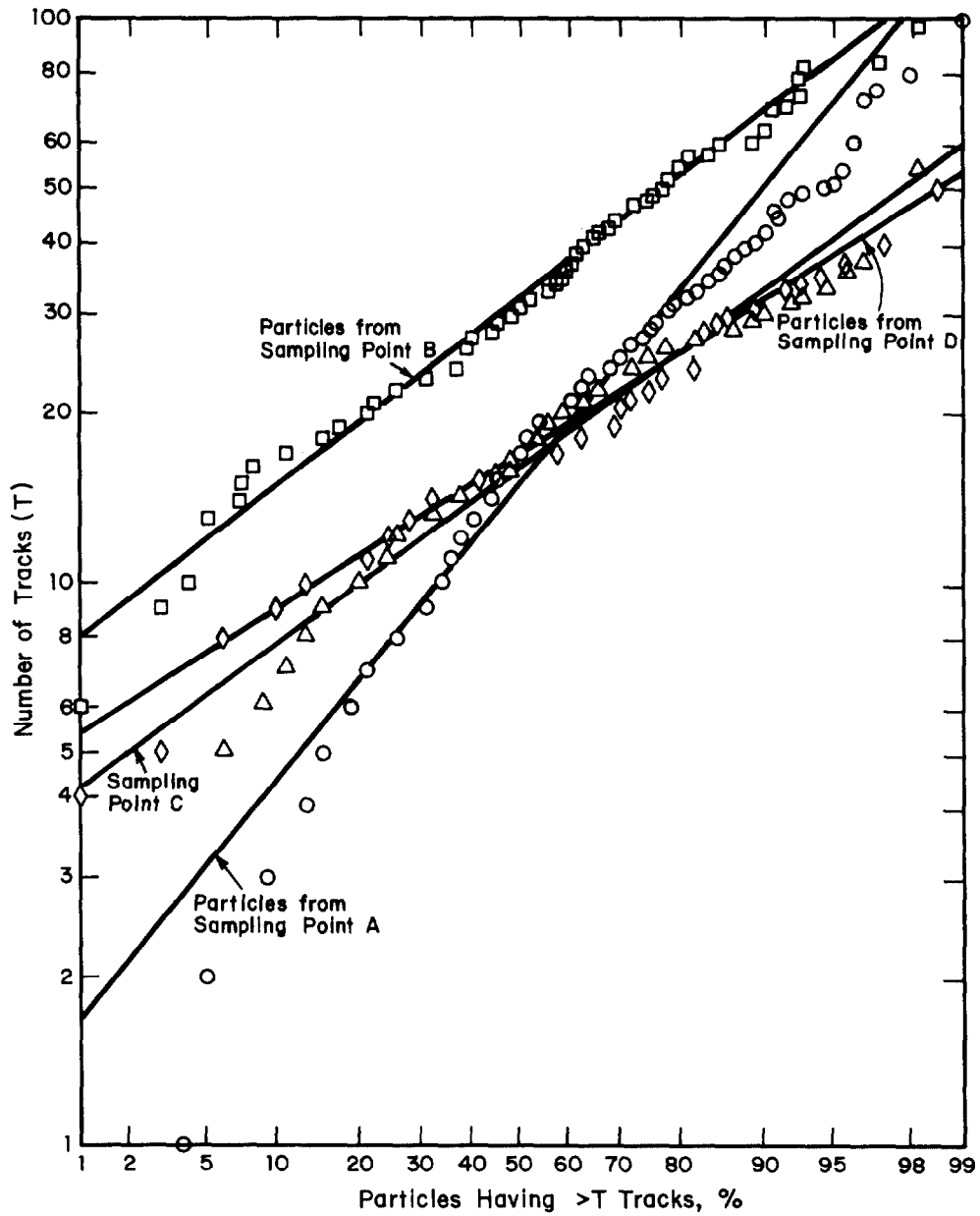


FIGURE 6
 DISTRIBUTION OF THE NUMBER OF TRACKS PER PARTICLE FOR
 PARTICLES COLLECTED FROM SAMPLING POINT A, B, C, AND D IN SYSTEM II

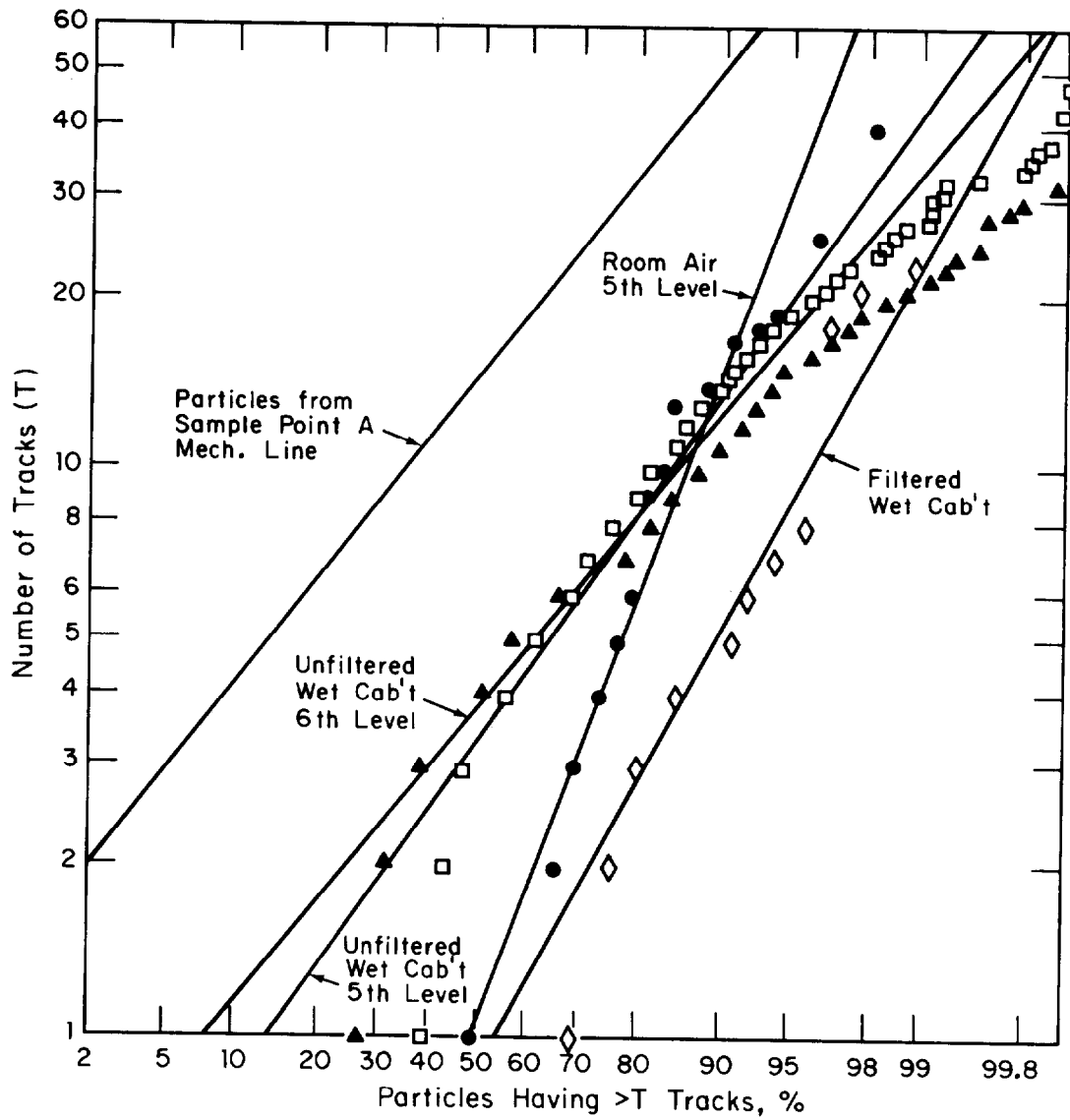


FIGURE 7
 DISTRIBUTION OF THE NUMBER OF TRACKS PER PARTICLE
 FOR PARTICLES COLLECTED FROM THE MECHANICAL LINE
 (SAMPLING POINT A), WET CABINETS, AND ROOM AIR

15th DOE NUCLEAR AIR CLEANING CONFERENCE

Table V. Distribution of Fission Tracks Among Plutonium-Bearing Particles Collected From Sampling Points A, B, C, and D.

Number of Tracks	Fraction With Tracks $\leq T$			
	Sample Point A	Sample Point B	Sample Point C	Sample Point D
1	0.04			
2	0.05			
3	0.09			
4	0.13			0.01
5	0.15		0.06	0.03
6	0.19	0.01	0.09	
7	0.21		0.11	
8	0.26		0.13	0.06
9	0.31	0.03	0.15	0.10
10	0.34	0.04	0.20	0.13
11	0.36		0.24	0.21
12	0.38		0.26	0.25
13	0.40	0.05	0.32	0.28
14	0.44	0.07	0.38	0.32
15	0.45	0.07	0.44	0.42
16	0.47	0.08	0.48	0.46
17	0.50	0.11	0.49	0.58
18	0.51	0.15	0.54	0.63
19	0.54	0.17	0.56	0.69
20	0.59	0.21	0.59	0.70
21	0.60	0.22	0.63	0.72
22	0.63	0.26	0.66	0.75
23	0.64	0.31	0.70	0.77
24	0.68	0.37	0.72	0.82
25	0.70		0.75	
26	0.72	0.39	0.78	
27	0.74	0.40	0.82	
28	0.75	0.44	0.87	0.83
29	0.76	0.45	0.89	0.85
30	0.78	0.48	0.90	0.86
31	0.79	0.50	0.92	0.89
32	0.81	0.52	0.93	
33	0.82	0.56	0.947	0.92
34	0.84	0.58		0.93
35	0.85	0.59		0.944
36	0.86	0.60	0.956	
37		0.61	0.965	0.958
38	0.87	0.62		
39	0.88			
40	0.89	0.63		0.972

15th DOE NUCLEAR AIR CLEANING CONFERENCE

Table V., Continued

Number of Tracks	Fraction With Tracks $\leq T$			
	Sample Point A	Sample Point B	Sample Point C	Sample Point D
41		0.65		
42	0.90	0.66		
43		0.68		
44	0.91	0.69		
46	0.91			
47		0.73		
48	0.92	0.75		
49	0.93	0.76		
50	0.945	0.77		0.986
51	0.950			
52		0.78		
54	0.955		0.991	
55		0.80		
57		0.81		
58		0.84		
59		0.85		
60	0.960	0.89		
63		0.90		
65			1.000	
68		0.91		
70		0.92		
72	0.965			
73		0.93		
75	0.970			
80	0.980	0.93		1.000
82		0.953		
84		0.972		
98		0.981		
100	0.990	0.991		
150	0.995	1.000		
200	1.000			

15th DOE NUCLEAR AIR CLEANING CONFERENCE

Table VI. Distribution of Fission Tracks Among Plutonium-Bearing Particles from Various Sources in Systems I and II.

Source	Data Points, N	Geom Mean of No. of Fission Tracks, \bar{T}_g	Geom Std Deviation, s_g	Skewness, SK	Geom Mean Activity Particle, fCi
<u>System I</u>					
Unfiltered 5th Level Wet-Cabinet Air	15,987	3.76	2.56	-0.20	0.09
Unfiltered 6th Level Wet-Cabinet Air	7,042	3.32	2.99	-0.51	0.08
5th Level Room Air ^{α}	53	1.00	8.40	-0.98	0.02
Filtered Wet-Cabinet Air ^{α}	98	0.87	4.14	-0.29	0.02
<u>System II</u>					
Sampling Point A Air	200	14.74	2.69	-0.43	0.36
Sampling Point B Air	107	32.38	1.78	0.23	0.79
Sampling Point C Air	114	16.50	1.75	-0.22	0.40
Sampling Point D Air	71	17.01	1.65	0.24	0.41

α . Values determined graphically.

Discussion

The most abundant elements in average crustal rock (and soil) are oxygen (46.60%), silicon (27.72%), aluminum (8.13%), iron (5.00%), calcium (3.63), sodium (2.83%), potassium (2.59%), magnesium (2.09), and titanium (0.44%).⁸ With the exception of oxygen, which was not detected by electron microprobe analyses, these elements are also found in most inorganic particles (Tables I and A-I). This supports the idea that most plutonium-bearing particles are airborne crustal material to which minute quantities of plutonium have become attached.

Of particular interest is the quantity of ^{239}Pu contained on these particles. One femtocurie (1 fCi = 10^{-15} Ci) of ^{239}Pu irradiated under the conditions described here should produce 41 fission-fragment tracks. The minimum detection limit for electron microprobe analysis of plutonium is about 0.2 picograms or about 10 fCi of ^{239}Pu ,¹ which is equivalent to 410 fission-fragment tracks. Because of this relatively low sensitivity of electron microprobe analysis, plutonium could be detected by this method in only one of the 558 particles selected for analysis, even though all the particles produced fission-fragment tracks. This single particle was a small, 1- μm -diameter particle, collected from unfiltered wet-cabinet exhaust. It contained 73% PuO_2 by weight (equivalent to 170 fCi of ^{239}Pu) in combination with Fe_2O_3 and mica.

15th DOE NUCLEAR AIR CLEANING CONFERENCE

Of the major crustal elements listed in Table I, silicon and iron were the most ubiquitous being found in most particles. The enrichment factor distribution for these elements, however, does not fall within the log-normal distribution for crustal material. For the enrichment factors of an element to match the log-normal distribution of crustal material in aerosols, there should be about 16% of the enrichment factors of less than one geometric standard deviation, 68% within one geometric standard deviation of the mean, and another 16% above one geometric standard deviation. This lack of conformity may result from the low values for the geometric standard deviations of the enrichment factors for these elements in aerosols.

Only the enrichment factors for sodium and chlorine fall within the log-normal distribution for crustal material. This may be due to the relative high solubility of compounds of these elements and, in the case of chlorine, the high value for the geometric standard deviation.

Particles from System I contain a greater variety of elements than those from System II and thus all but four elements are contained on a higher proportion of particles from System I than from System II. The most striking example was nickel. While 56% of the particles from System I contained nickel, only 9% of those in System II did. The major crustal elements (those in Table A-I comprising 0.4% or more of crustal material) are contained on over half the particles from System I and with the exception of magnesium in particles from sampling Points C and D and titanium are also contained on over half the particles from System II. Some of the minor elements (those comprising 0.1% or less of crustal material) are present in over half the particles, viz, nickel, chromium, and zinc in particles from System I and sulfur, chromium, and zinc in particles from sampling point B of System II. The chromium and nickel may have come from the 304L stainless steel alloy of cabinets and exhaust ducts or the *Hastelloy**-C alloy in the wet cabinets. However, few of the particles contained the proper ratio of chromium-to-nickel found in either alloy. Also, if *Hastelloy*-C contributed the nickel in the particles, some molybdenum should also have been detected.

Of the elements which are present on less than 10% of the particles, all but copper on particles from System II have high enrichment factors. This indicates that the minor constituents of crustal material are not uniformly distributed among particles but are concentrated on a few particles where they represent a major constituent.

The plutonium-bearing particles were larger than natural aerosol particles collected at relatively low altitude (<2.3 km) as seen in Figure 5. Those particles collected from sampling points A and B of System II were larger than those from System I, with geometric mean diameters two or three times those of particles from other locations.

15th DOE NUCLEAR AIR CLEANING CONFERENCE

Particles from all parts of System II also contained on the average more plutonium per particle than those from System I. As seen in Table VI, the geometric mean of the activity in System I, containing only HEPA filters, was a factor of 10 to 100 less than that of System II, which uses a large sand filter before the air is exhausted to the atmosphere. The geometric mean of measured activity per particle released to the atmosphere was 0.4 fCi.

A comparison of the mean diameters of particles collected from different sampling points, given in Table IV, with the mean number of fission fragment tracks for particles from the same location, given in Table VI, indicate a possible relationship between particle size and plutonium content. Correlation coefficients between the cube of the particle diameter and the number of fission fragment tracks from each particle from sampling Points B, C, and D were calculated. These are given in Table VII. These coefficients differ significantly from that expected from a random sample from a population of paired variables having a correlation coefficient of zero. Thus, even though the points on a plot of particle diameter cubed versus number of fission fragment tracks appears scattered, there is a significant correlation between the quantity of plutonium in particles collected from Sampling Points B, C, and D in System II and the particle volume. (Tracks with particles collected at other sampling points, where only ^{239}Pu could be found, were counted but not recorded for each particle. Only where a ratio of alpha particle to fission fragment tracks was needed to distinguish plutonium bearing particles from those having other fissionable materials were the track counts recorded).

Table VII. Correlation and Coefficient of Alienation for the Cube of the Diameter and the Number of Fission Fragment Tracks for Particles From Sampling Points B, C, and D of System II.

<u>Sampling Point</u>	<u>Number of Particles</u>	<u>Correlation Coefficient</u>
B	107	0.69
C	114	0.29
D	71	0.36

Summary

Plutonium-bearing particles collected from a nuclear reprocessing plant exhaust were found to be aggregates of crustal material. High enrichment factors for metals were evidence of the anthropogenic nature of some particles. The radioactivity of the plutonium associated with individual particles was very small (~ 0.4 fCi).

The results of this work indicate the need for further study of the behavior of these plutonium-bearing particles following their release to the atmosphere and subsequent interaction with the environment.

Acknowledgment

The author gratefully acknowledges the assistance of E. F. Holdsworth and J. T. Armstrong of the Chemistry Department of the Arizona State University in Tempe, Arizona, who performed the electron microprobe analyses.

15th DOE NUCLEAR AIR CLEANING CONFERENCE

Appendix: Use of Elemental Enrichment Factors to Express Particle Compositions

Background

Two recent developments in aerosol studies have provided valuable tools for the analysis of particle composition data. The first is the use of ratios of elemental concentrations called "enrichment factors" to compare aerosol compositions. Begun in the early seventies, this technique has gained wide acceptance in the last few years⁹⁻¹³. The second development is the availability of data on the composition of natural aerosols. Rahn⁹ published a compilation of 104 data sets of trace elements in aerosols along with the geometric mean and geometric standard deviation of the enrichment factors for each of the elements. These data sets were from sampling sites ranging from highly industrialized temperature zones to the tropics and poles, and represent all continents except South America, as well as various marine locations. As a framework from which to view much of the order in atmospheric aerosols, Rahn used the concept of aerosol-crust enrichment factors for the elements. This concept has been applied to analyzing data collected in this study to provide for (a) the intercomparison of the compositions of plutonium-bearing particles with atmospheric aerosols compiled by Rahn and (b) the intracomparison among particles collected from different sampling points.

Microprobe Analyses of Particles

To be comparable, results of microprobe analyses must be expressed as elemental ratios. The reason for this is that not all elements which may be present in an aerosol are detected by microprobe analysis. The microprobe used in this study is quantitative only for elements with atomic numbers greater than 10. It is only semi-quantitative for oxygen (the most abundant element in crustal material) as well as other major elements of low atomic number such as hydrogen, fluorine, and carbon. Atmospheric aerosols are known to contain in addition to elements and oxides, carbonaceous material such as sooty carbon and organics and water-soluble ionic material such as sulfate, nitrate, and ammonium ions. Thus elemental weight percents, normalized to 100 based on the elements detected cannot be compared. Even the addition of a hypothetical oxygen concentration, calculated on the supposition that all elements are present as oxides of known valence, will still not account for the organic fraction of particles. However, a ratio of the concentrations of one element to another will normally be relatively unaffected by the concentrations of other elements which may be present and thus can be used for comparisons even when a complete analysis of all the elements in an aerosol or single particle is not available.

Enrichment Factors

A dimensionless ratio of elemental concentrations, called the enrichment factor, has been defined as

$$EF(X) = \frac{(X/Ref)_{\text{aerosol}}}{(X/Ref)_{\text{source}}} \quad (A-1)$$

where $EF(X)$ is the enrichment factor of element X in an aerosol relative to some source material. X/Ref is the ratio of the concentration of element X to the concentration of the reference element, Ref , in both the aerosol and the source material.

15th DOE NUCLEAR AIR CLEANING CONFERENCE

Source Material

Elemental ratios in aerosols or in single particles are normalized by dividing them by ratios of the same elements in a standard source material to obtain the enrichment factors. If a particle is composed of the same material as the source, the enrichment factor will be 1.00 for all elements. If the ratio of an element to the reference element is greater or less than the same ratio in the source material, the enrichment factors will be greater or less than 1.00, and the particle is said to be either enriched or depleted, respectively, in that element.

The most commonly-used crustal source material for continental enrichment-factor calculations is globally-averaged crustal rock. (For marine enrichment-factor calculations, sea salt is used.) Because the composition of plutonium-bearing particles are compared with data reported by Rahn,⁹ the same crustal-rock composition used by him (that reported by Mason)⁸ was selected as the source material composition for this work. Column 2 of Table A-I gives the elemental concentrations in globally-averaged crustal rock for those elements found in plutonium-bearing particles.

Reference Element

Of the various elements which seem to be reliably crust-derived in aerosols, aluminum is generally considered to be the most suitable reference elements. (When sea salt is the source material, the nearly universal choice is sodium.) Aluminum is a major element (81,300 ppm in rock), well-determined by a variety of analytical techniques, and has a minimum of specific pollution sources.

Thus for this work, enrichment factors for element X in most particles were calculated using

$$EF(X) = \frac{(X/Al)_{\text{particle}}}{(X/Al)_{\text{rock}}} \quad (A-2)$$

with aluminum as the reference element and average crustal rock as the source material. However, 18 particles from System I and 48 from System II contained no aluminum. Thus the enrichment factors had to be based on silicon rather than aluminum where

$$EF(X) = \frac{(X/Si)_{\text{particle}}}{(X/Si)_{\text{rock}}} \cdot \frac{(\overline{Si}/Al)_{\text{g aerosol}}}{(Si/Al)_{\text{rock}}} = 0.79 \frac{(X/Si)_{\text{particle}}}{(X/Si)_{\text{rock}}} \quad (A-3)$$

(The second set of ratios is the geometric mean of the global aerosol-crust enrichment factor explained in the next section.)

Using these two relationships, the enrichment factors were calculated from the elemental weight percents obtained for 115 particles in System I and 415 particles in System II. Six small (0.5 to 3.6 μm diameter) iron particles in System I and two particles [$\sim 15 \mu\text{m}$ diameter containing K, Cr, and Fe (1:3:3)] from Sample Point A of System II contained neither aluminum nor silicon and were thus not included in the study.

15th DOE NUCLEAR AIR CLEANING CONFERENCE

TABLE A-I. Elemental Concentrations in Average Crustal Rock and Geometric Mean Enrichment Factors of Various Aerosols

Element	Conc., ppm	Geometric Mean Enrichment Factors					
		Global \overline{EF}_g/s_g	Global \overline{EF}_g	Global $EF_g \cdot s_g$	Remote Marine \overline{EF}_g	Remote Conti- nental \overline{EF}_g	Urban \overline{EF}_g
Si	277,200	0.62	0.79	1.01	0.7	0.7	0.79
Al	81,300	1.00	1.00	1.00	1.0	1.0	1.00
Fe	50,000	1.05	2.06	4.06	2.5	1.5	2.2
Ca	36,000	1.15	2.84	7.04	8.0	1.5	2.9
Na	28,300	0.64	4.44	30.8	$10^2 - 10^3$	0.4	1.81
K	25,900	0.99	1.98	3.98	6.0	1.5	1.63
Mg	20,900	0.64	2.38	8.90	$10^1 - 10^2$	0.7	2.0
Ti	4,400	1.01	1.39	1.92	1.2	1.2	1.63
P	1,050	0.79	2.63	8.71	-	-	2.6
Mn	950	1.45	3.91	10.5	3.0	2	3.2
Ba	425	2.61	5.50	11.6	-	~2	4.8
S	260	228.0	608.0	1620.0	-	-	490.0
Cl	130	100.0	740.0	5470.0	$10^4 - 10^5$	40.0	300.0
Cr	100	2.50	8.11	26.3	20.0	6	6.2
Ni	75	8.74	31.9	116.0	100.0	50	10.8
Zn	70	79.7	257.0	832.0	400.0	80	300
Co	25	0.91	3.52	13.6	4.0	1.5	4.6
Sc	22	0.59	1.17	2.34	0.8	0.8	0.60
Cu	55	34.0	102.0	304.0	150.0	20.0	149
U	1.8	0.92	2.87	8.93	-	-	2.87
W	1.5	4.89	19.1	74.3	-	-	11.0
Cd	0.2	274.0	1920.0	13,400.0	5000.0	2000.0	940.0

Comparative Aerosol Data

To compare the elemental composition of plutonium-bearing particles with that of atmospheric aerosols, enrichment factors calculated for elements in these particles were grouped according to data supplied by Rahn⁹ for aerosols. In his report, trace element concentrations in aerosols from 104 published and unpublished data sets were used to calculate enrichment factors. From the enrichment factors in each data set, the geometric mean enrichment factor (\overline{EF}_g) and geometric standard deviation (s_g) of the logarithmic frequency distributions of enrichment factors were calculated for each element using the following formulae:

$$\overline{EF}_g = \exp \left[\frac{1}{N} \sum_{i=1}^N \ln EF_i \right] \quad (A-4)$$

and

$$s_g = \exp \left\{ \left[\frac{1}{N-1} \sum_{i=1}^N (\ln EF_i - \ln \overline{EF}_g)^2 \right]^{\frac{1}{2}} \right\}$$

where N = the number of data points

EF_i = the enrichment factor of the *i*th point.

The geometric mean enrichment factors obtained by Rahn⁹ for 19 elements are given in Table A-I for global, remote marine, remote continental, and urban aerosols. The geometric means of the global aerosol enrichment factors include data from all points and may be weighted too heavily toward cities, but they can serve as a useful first approximation to a general aerosol. The urban enrichment factors are geometric means for 29 cities. The enrichment factors for remote continental and remote marine areas were read from the enrichment-factor plots and are therefore somewhat subjective.

To obtain the lower and upper limits for 68.27% of the enrichment factors closest to the geometric mean, values for \overline{EF}_g/s_g and $\overline{EF}_g \cdot s_g$, respectively, were calculated using global values. (When describing concentrations at selected statistical levels remote from a mean, the s_g is a multiplier or divider of the \overline{EF}_g , whereas its counterpart Gaussian standard deviation functions as an increment to the arithmetic mean. This is a consequence of the fact that multiplying and dividing values is equivalent to adding and subtracting their logarithms.) The results from these calculations are also given in Table A-I.

15th DOE NUCLEAR AIR CLEANING CONFERENCE

References

1. S. Marshall Sanders, Jr. "Composition of airborne plutonium-bearing particles from a plutonium finishing operation." USERDA Report DP-1445, E. I. du Pont de Nemours and Co., Savannah River Laboratory, Aiken, South Carolina (November 1976).
2. S. Marshall Sanders, Jr. "Characterization of airborne plutonium-bearing particles from a nuclear fuel reprocessing plant." USERDA Report DP-1470, E. I. du Pont de Nemours and Co., Savannah River Laboratory, Aiken, South Carolina (September 1977).
3. Kvetoslav R. Spurny, Jampes P. Lodge, Jr., Evelyn R. Frank, and David C. Sheesley. "Aerosol filtration by means of nuclepore filters: structural and filtration properties." Environ. Sci. Technol. 3 (5) 453-464 (1969).
4. R. C. Axtmann, L. A. Heinrich, R. C. Robinson, O. A. Towler, and J. W. Wade. "Initial operation of the standard pile." USAEC Report DP-32, E. I. du Pont de Nemours and Co., Savannah River Laboratory, Aiken, South Carolina (1953).
5. H. Yakowitz, R. L. Myklebust, and K. F. J. Heinrich. "FRAME: An on-line correction procedure for quantitative electron probe microanalysis." National Bureau of Standards Technical Note 796, National Bureau of Standards, Washington, DC (1973).
6. John T. Armstrong and Peter R. Buseck. "Quantitative chemical analysis of individual microparticles using the electron microprobe: Theoretical." Anal. Chem. 47, 2178-2192 (1975).
7. C. E. Junge. "Handbook of geophysics and space environments." pp 5-23. S. L. Valley, editor. Air Force Cambridge Research Laboratories, Office of Aerospace Research, US Air Force, Cambridge, MA (1965).
8. B. Mason. "Principles of geochemistry," 3rd ed., p 45. John Wiley and Sons, New York, NY (1966).
9. Kenneth A. Rahn. "The chemical composition of the atmospheric aerosol." Technical Report, Graduate School of Oceanography, University of Rhode Island, Kingston, RI (1976).
10. Kenneth A. Rahn. "Sources of trace elements in aerosols - an approach to clean air. Ph.D. Thesis, University of Michigan, Ann Arbor, MI (1971). Xeros University Microfilms (Order No. 72-4956).
11. William H. Zoller, E. S. Gladney, and Robert A. Duce. "Atmospheric concentrations and sources of trace metals at the south pole." Science 183, 198 (1974).
12. Robert A. Duce, Gerald L. Hoffman, and William H. Zoller. "Atmospheric trace metals at remote northern and southern hemisphere sites: pollution or natural?" Science 187, 59 (1975).
13. H. E. Neustadter, J. S. Fordyce, and R. B. King. "Elemental composition of airborne particulates and source identification: data analysis techniques." Air Pollution Control Assoc. 26 (11), 1079 (1976).

15th DOE NUCLEAR AIR CLEANING CONFERENCE

AGGLOMERATION CHARACTERISTICS OF FAST REACTOR HCDA AEROSOLS*

G. W. Parker, G. E. Creek, and A. L. Sutton, Jr.
Chemical Technology Division, Oak Ridge National Laboratory
Oak Ridge, Tennessee 37830

Abstract

The behavior of vaporized mixed oxide fuel aerosols postulated to result from fast reactor core disruptive accidents is a subject which is intensely evaluated in fast reactor safety analysis, containment design, and site selection licensing procedure.

In this program, surrogate uranium oxide aerosols produced by vapor condensation of super-heated liquid UO_2 have been produced in a variety of ways and have been intercompared with respect to particle morphology, number concentration, deposition behavior, surface area, oxygen content, and diffusion, sedimentation, and agglomeration rates. It has been established that, within a relatively narrow range, the primary particles are nearly identical when examined for initial shape, and size distribution, and effective density. However, primary particles in those aerosols produced by the most rapid heating methods followed by nearly instantaneous cooling are smaller in size and generally spherical, while those produced by slower processes in combination with delayed cooling give rise to a large proportion of crystalline particles which result in more tightly bound agglomerates. Deposition behavior is not significantly affected by this difference.

Stokes diameters, which can be rather accurately calculated from the rate of settling, compare favorably with aerodynamic mean diameters measured with inertial devices. Agglomerate sizes appear to follow the cube root of the maximum initial concentration.

The HAARM-2 version of the HAA-3 aerosol code has been used to obtain detailed time-dependent predicted behavior on a reference closed volume. The interrelations observed suggest that, in a given system, many of the characteristics can be calculated after only a few cases have been experimentally measured.

I. Introduction

A relatively long-standing program in the study of uranium oxide vapor-condensation aerosols has been conducted intermittently at ORNL since 1960, when the initial interest was in the safety analysis of the proposed air-craft nuclear propulsion reactor. This project, although short-lived, served to place some initial values on the partitioning of volatile fission products elements from molten UO_2 .

Continuing through the 1960s as part of the AEC-LWR Nuclear Safety Studies, a long series of fission product release experiments

*Research sponsored by Office of Nuclear Regulatory Research, U. S. Nuclear Regulatory Commission under Interagency Agreements 44-551-75 and 40-552-75 with the U. S. Department of Energy under contract W-7405-eng-26 with the Union Carbide Corporation.

15th DOE NUCLEAR AIR CLEANING CONFERENCE

were conducted. These included both high-temperature annealing and melting experiments in which the vaporization of UO_2 was relatively minor. The real emphasis on reactor fuel vaporization was initiated by the Division of Reactor Safety Research in support of the larger LMFBR Aerosol Release and Transport (ART) Program. The overall goal of this total program was to provide the analytical techniques and experimental data necessary to assess the transient behavior and the radionuclide release from breeder reactor cores as a result of postulated events of varying severity, up to and including severe hypothetical core disruptive accidents (HCDAs).

II. Experimental Program

The generation of UO_2 and U_3O_8 vapor-condensation aerosols has been investigated by a number of different techniques in order to simulate specific environmental factors and to provide a basis for the evaluation of various separate effects, particularly specific energy input on primary size distribution, and the comparative agglomeration behavior vs aerosol mass concentration from both instantaneous and continuous generating sources. Five different aerosol generation processes have been used in the various experiments:

1. instantaneous UO_2 vaporization by the arc-imaging (solar-type) furnace,
2. instantaneous UO_2 vaporization by capacitor discharge in premelted UO_2 ,
3. continuous U_3O_8 vaporization by the pyrophoric oxidation of molten uranium metal sparged with oxygen,
4. continuous UO_2 vaporization by superheating molten UO_2 in a dc electric arc cold-hearth furnace, and
5. continuous UO_2 vaporization incidental to melting UO_2 in tungsten crucibles heated by RF induction.

Four of these methods are described here in varying details with illustrations of typical results. Only the UO_2 vaporization incidental to UO_2 melting is not discussed further. Details are given elsewhere.⁽¹⁾

Instantaneous Vaporization of UO_2 by the ADL Arc-Imaging Furnace

While this method is not literally "instantaneous," it has the essential characteristics of the process in that only a very small hot zone is produced, similar to the laser method, and the resultant vapor is almost instantly quenched. The sample of UO_2 was placed at the secondary focus of the reimaging mirror (Fig. 1) and was heated to partial melting for 1 to 2 min.

Vaporized uranium oxide particles that collected on Millipore filters during the melting were examined in the electron microscope. The replication method was used to observe particles from specimens melted in air and in helium. It was confirmed by the transmission

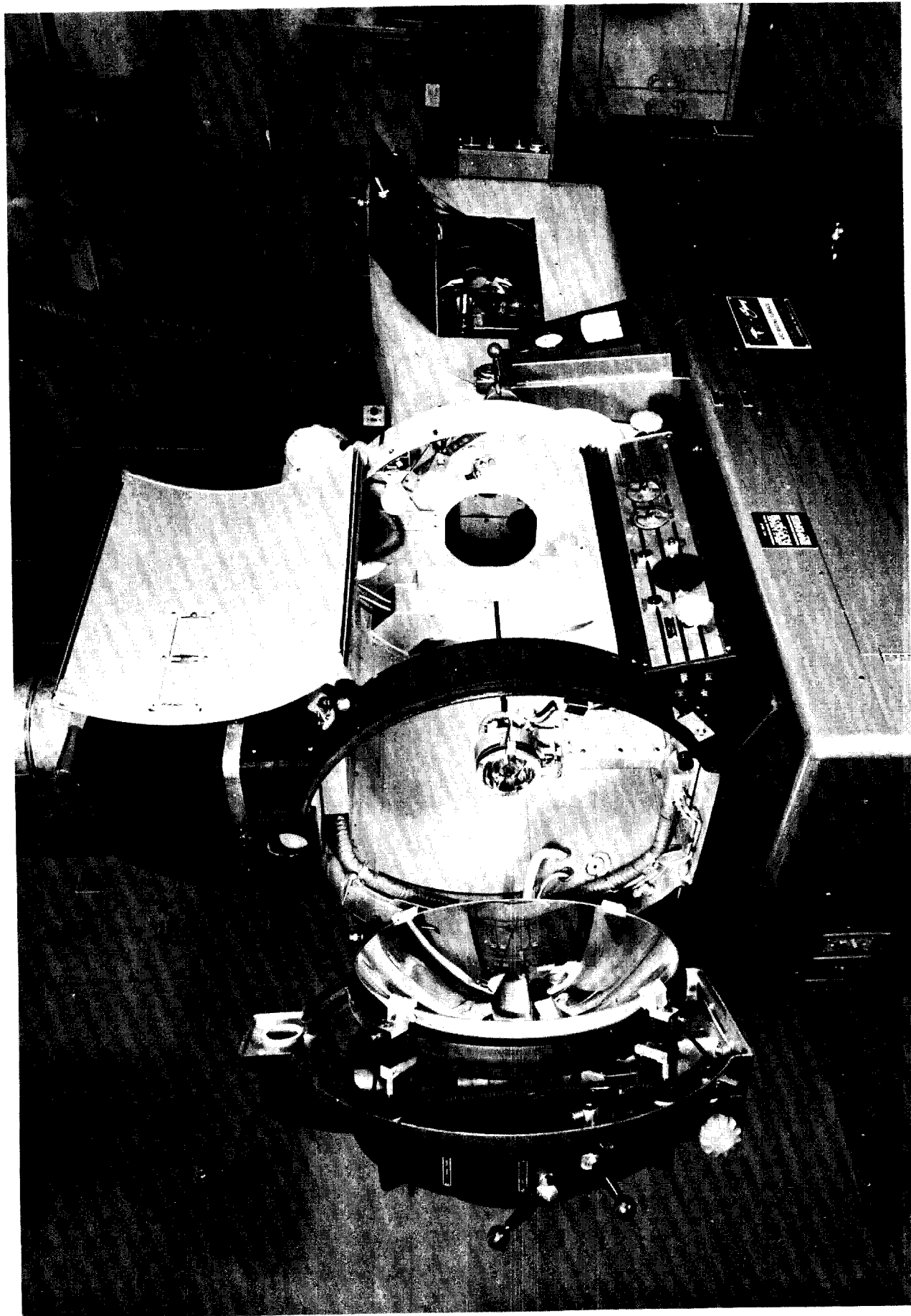


Fig. 1. ADL Carbon Arc-Imaging Furnace

electron diffraction technique that the oxide collected from melting UO_2 in air is composed of crystalline U_3O_8 (Fig. 2a), while that collected from melting in helium consists of somewhat spherical shapes of UO_2 (Fig. 2b). Ninety-seven percent of the crystalline U_3O_8 particles had a diameter greater than 0.025μ . The average diameter of the U_3O_8 particles was about 0.1μ , while the UO_2 in helium measured between 0.0075 and 0.03μ (averaging 0.01μ). The more rapid cooling that would occur in helium possibly accounts for the smaller spherical shapes. The unusual characteristics of the U_3O_8 particles as seen, completely dispersed, reflect the almost instantaneous collection on a filter before any detectable agglomeration had occurred.

Instantaneous UO_2 Vaporization by High-Energy Capacitor Discharge in Pre-melted UO_2

Development of the capacitor discharge vaporization (CDV) system⁽²⁾ was patterned after the early work at Karlsruhe by Schaikarski and coworkers.⁽³⁾ The approach at ORNL was enhanced by incorporating the suggestions offered by Dr. Schaikarski, which included the direct electric heating of a UO_2 column to nearly complete melting prior to capacitor discharge.

With the CDV technique, ceramic fuel can be put into HCDA-like mean energy states of up to 3000 J/g , which is sufficient to effect prompt disassembly of a fuel pin and flash a significant portion of the superheated liquid fuel to vapor. The efficiency of the energy deposition, which was initially quite low, has been gradually improved by optimizing both the electrical circuitry and the physical configuration of the specimen until most of the power is expended in the vaporization process. The range of time intervals for disassembly can be adjusted to match HCDA theory within about 1 msec .

The aerosol experiments with this method of generation were conducted in a small vessel of about 0.5-m^3 capacity. The installation is shown in Fig. 3.

Some earlier experiments performed at the Arnold Engineering Center's Von Karman Facility were also limited to about the same scale vessel. An example of the rate-of-change data for the CDV-CRI-III is given in Fig. 4.

Continuous U_3O_8 Vaporization by the Pyrophoric Oxidation of Molten Uranium Metal with Oxygen

The initial aerosol generation method used in the Containment Research Installation Vessel (CRI-II) was the rapid oxidation of molten metallic uranium by sparging the melt with gaseous oxygen. The generated aerosol was mainly U_3O_8 , and the yield was limited by the high-temperature attack of the melt on the quartz furnace (Fig. 5). The maximum concentration of U_3O_8 aerosol obtained was little more than 1 g/m^3 , and the method was not considered practical to scale up. Comparative results of these experiments are summarized in Table I.

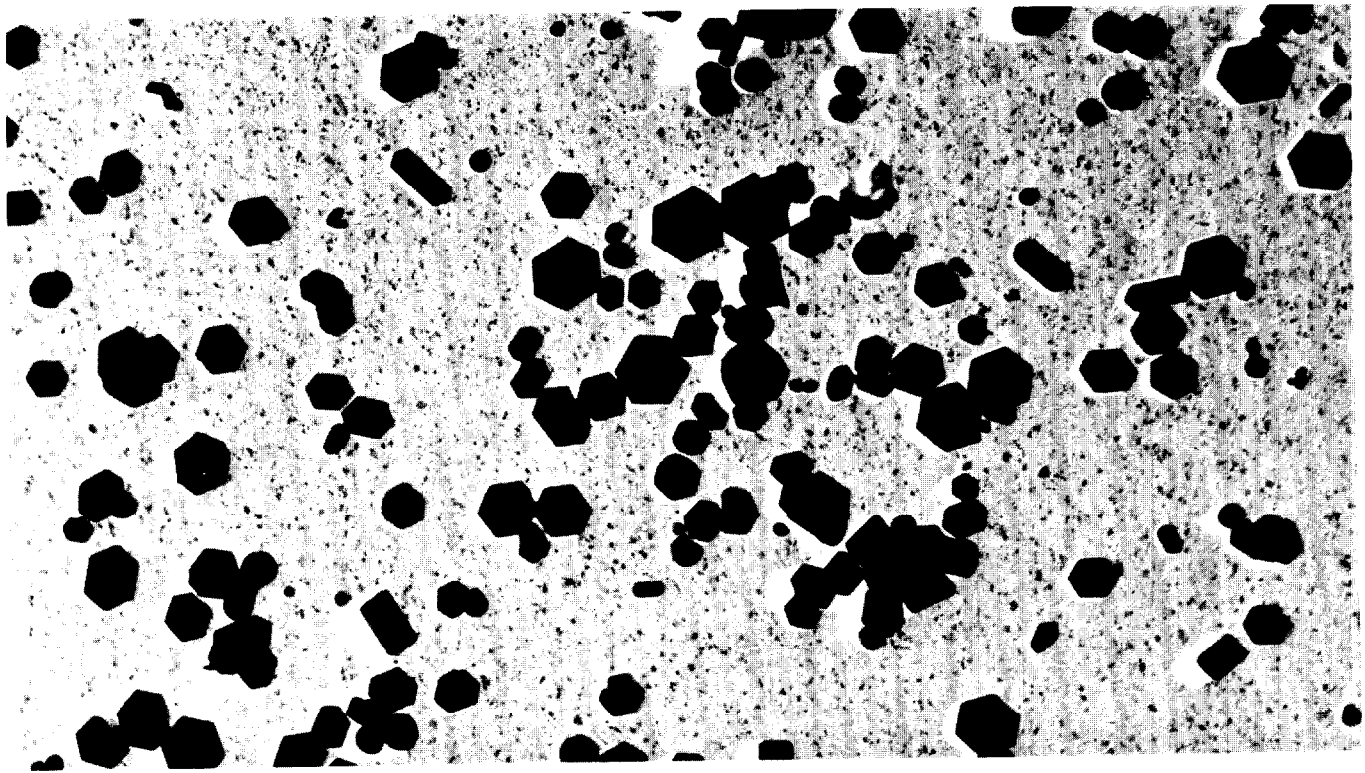


Fig. 2a. Replica of crystalline U_3O_8 particles vaporized from UO_2 melted in air. 40,000X.

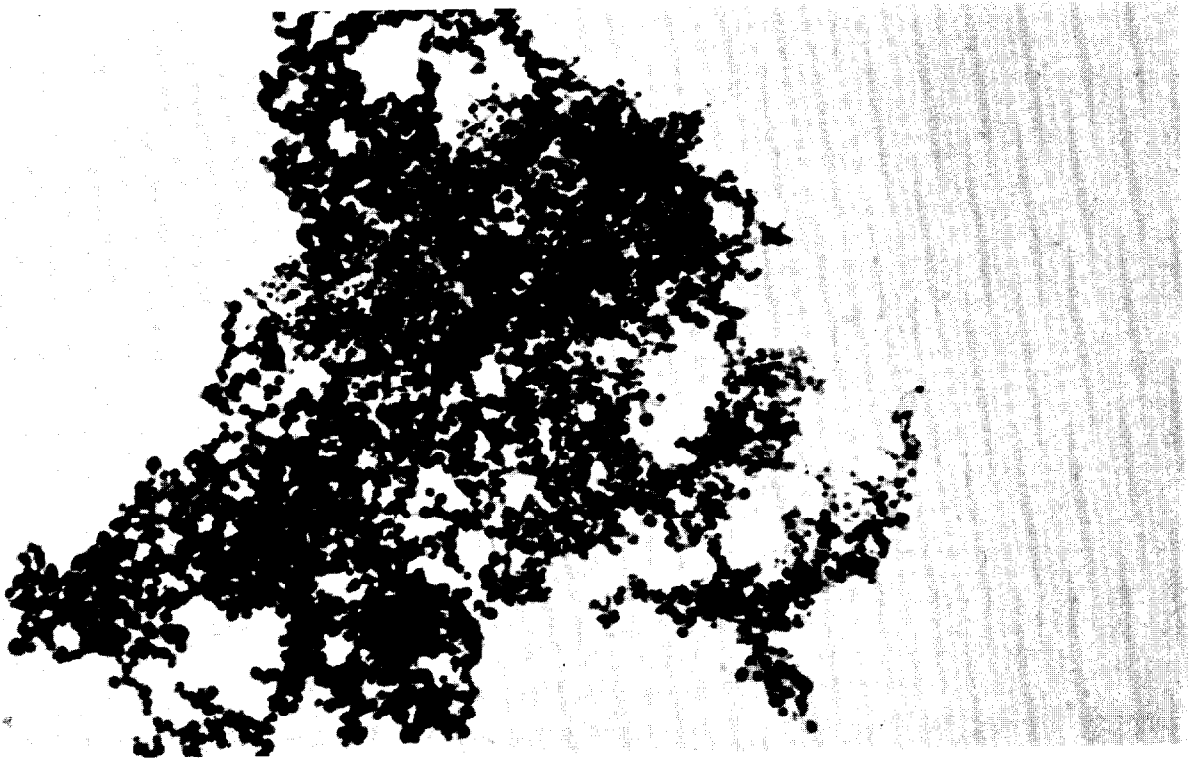


Fig. 2b. Replica of spherical particles of uranium oxide vaporized on melting UO_2 in helium. 69,200X.

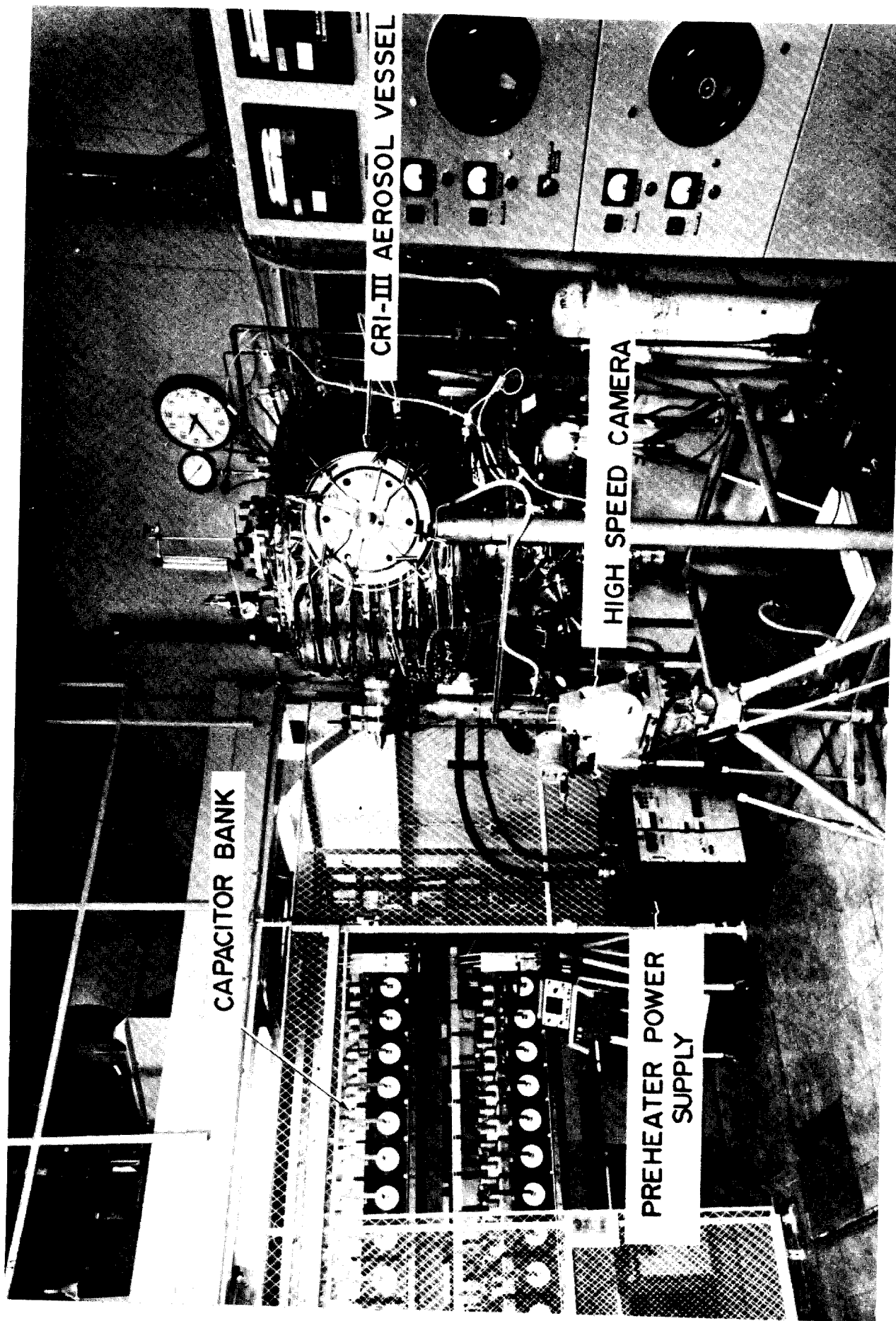


Fig. 3. Overall view of the operational area where ORNL capacitor discharge vaporization experiments are conducted.

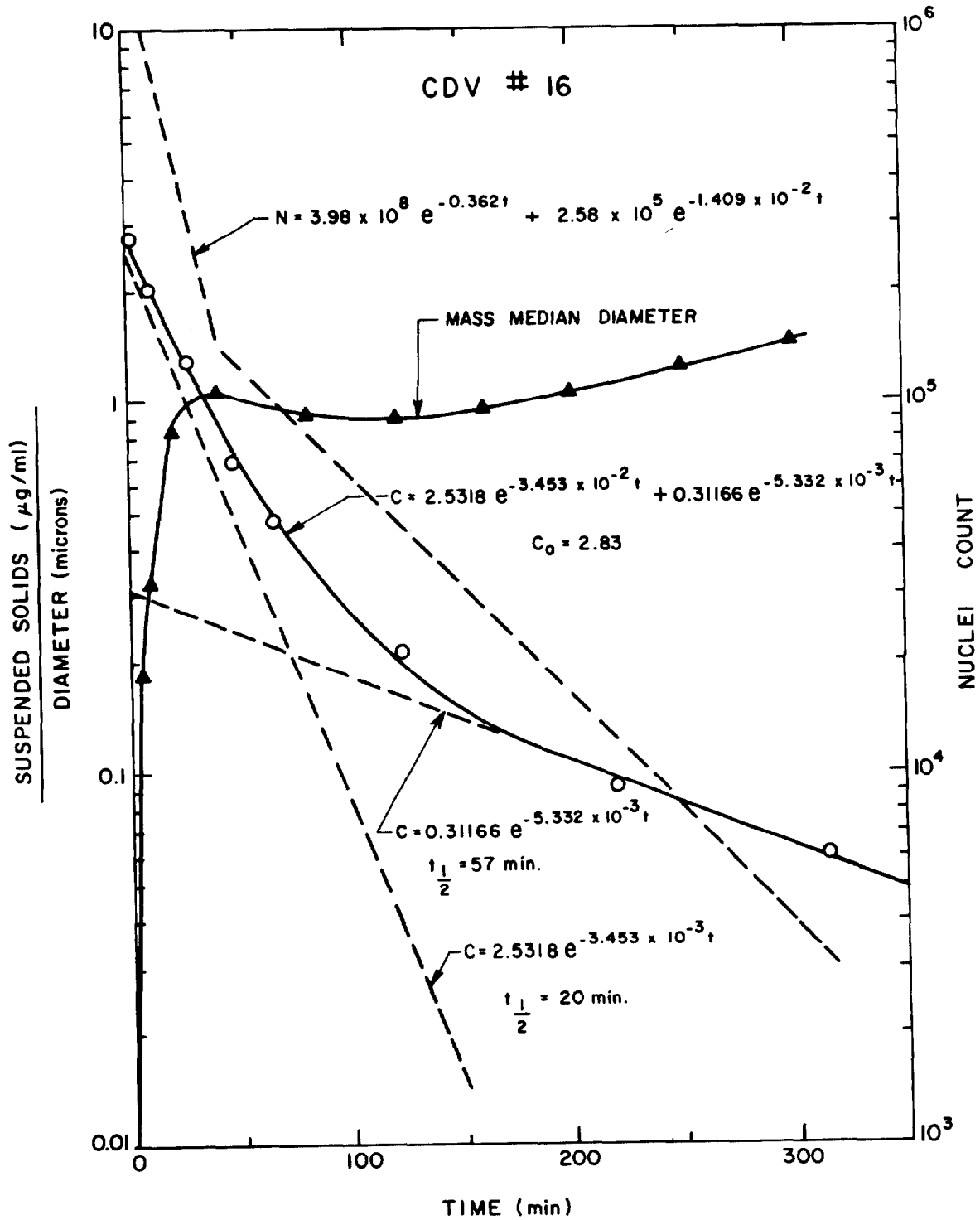


Fig. 4. Histograms for CDV Run 16 showing rate of change in concentration and nuclei count and calculated mass median diameters of agglomerates.

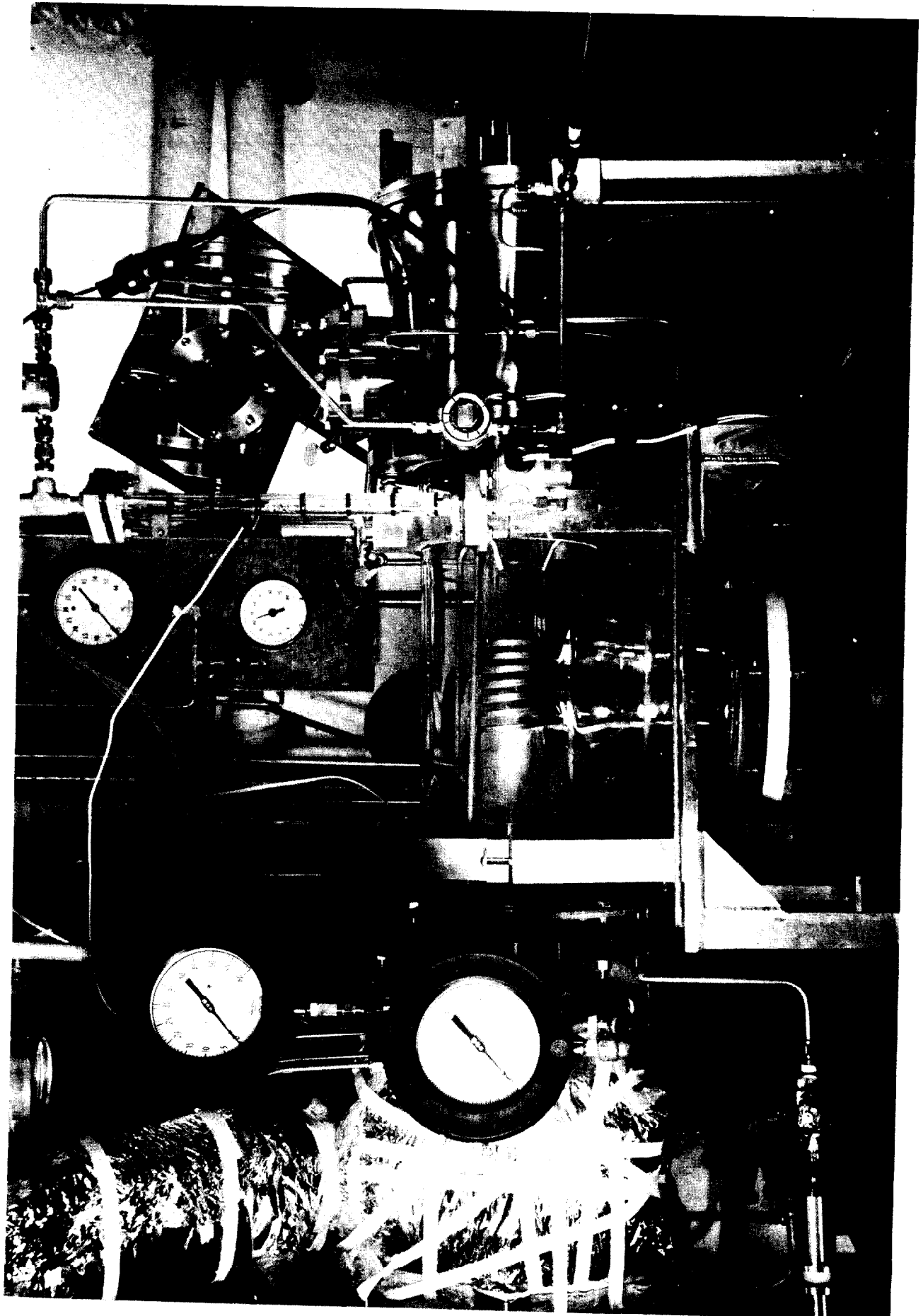


Fig. 5. Furnace for induction heating of metallic uranium.

Table I. Summary of TEM primary particle size determinations.

Photo No. (T)	Magnification (X)	Geometric Mean Diameter (μ)	Arithmetic Mean Diameter (μ)	Standard Deviation (σ)	Source of Microscope Grid Sample	Time of Sample (min)
1660	165,000	0.030	0.036	1.78	CRI 5-15-75 Grid 2	9 ^a
CRI-II U-pyrophoric oxidation						
2196	125,000	0.031	0.036	1.68	AF-6, ESU No. 4	75
CRI-II arc-furnace vaporization						
Arnold Engineering Development Center capacitor discharge						
1691	213,000	0.020	0.026	1.64	AEDC 7/2/75 11-34	a
ORNL-CRI-III capacitor discharge						
2132	300,000	0.013	0.014	1.58	CDV 24-2, ESU No. 2	50

^aContinuous plateout.

The dc Electric Arc Cold-Hearth Vaporization of UO₂

The second method of aerosol generation which was employed in CRI-II was a dc cold-hearth furnace (Figs. 6 and 7) which produces a predominantly UO₂ form of oxide. The actual composition of the aerosol varies somewhat according to the quality of the argon fill gas in the CRI-II vessel. It also varies with the frequency at which new uranium oxide pellets are added to the furnace since the initial melting process releases some surplus oxygen. This method of vaporization could probably be adapted to produce either UO₂ or U₃O₈ by controlling the oxygen content of the carrier gas or by introducing oxygen in the transfer pipe before the vaporized UO₂ cools below the ignition temperature of UO₂, that is, about 300 to 500°C.

Maximum yields obtained thus far have been about 10 g/m³; however, minor improvements, including increasing the flushing rate of the beehive chamber or inserting a tungsten liner over the copper hearth, should result in a considerable increase in yield. This aerosol source is distinctly not "instantaneous," but can be used as a "continuous" source and made to reach steady-state conditions at relatively high concentrations. A typical example of the deposition behavior and rate-of-concentration change is shown in Fig. 8.

The CRI-II is a 4.52-m³ stainless steel vessel with cylindrical walls, a dished flanged head, and a conical bottom. It was designed, constructed, and operated in the 1960s for use in safety studies of the LWR type in support of the NRTS LOFT program and was reactivated in 1974 in support of the LMFBR-RSR program by NRC. It is housed in a semienclosed, specially shielded, and ventilated area in the ORNL radiochemical hot laboratory. It is presently equipped with two unique fuel aerosol generators designed for attaining high concentrations of UO₂, U₃O₈, or Na₂O_x mixed aerosols. One of the generators is the 100-kW dc electric arc cold-hearth furnace (mentioned above) in which molten UO₂ is literally boiled off as vapor. It is capable of vaporizing about 50 g of UO₂ per minute. The other generator (not yet operational) employs a 40-kW dc plasma arc to ignite a mixture of powdered uranium metal and oxygen and is expected to produce even higher concentrations of vapor-condensation oxides.

III. Comparative Sizes of UO₂ and U₃O₈ Primary Particles and Agglomerates

A brief comparison has been made of the primary and agglomerated particle sizes from each of the four separate fuel aerosol behavior projects conducted over the past two years in the Breeder Reactor Transient Release Program. Approximately 41 separate TEM photomicrographs were subjected to individual particle-size determinations for the primary particle evaluation. The average geometric mean primary particle diameter was found to be 0.034 μ for both the uranium-metal pyrophoric oxidation process and the UO₂ arc-furnace process (see Table I for typical examples of each). The particle size of the Arnold Engineering Development Center (AEDC) capacitor-vaporized aerosol averaged 0.025 μ, while that of the ORNL-CDV aerosol averaged only 0.014 μ. These differences are understandable since the first two processes subject the primary particles to a "hot zone" growth

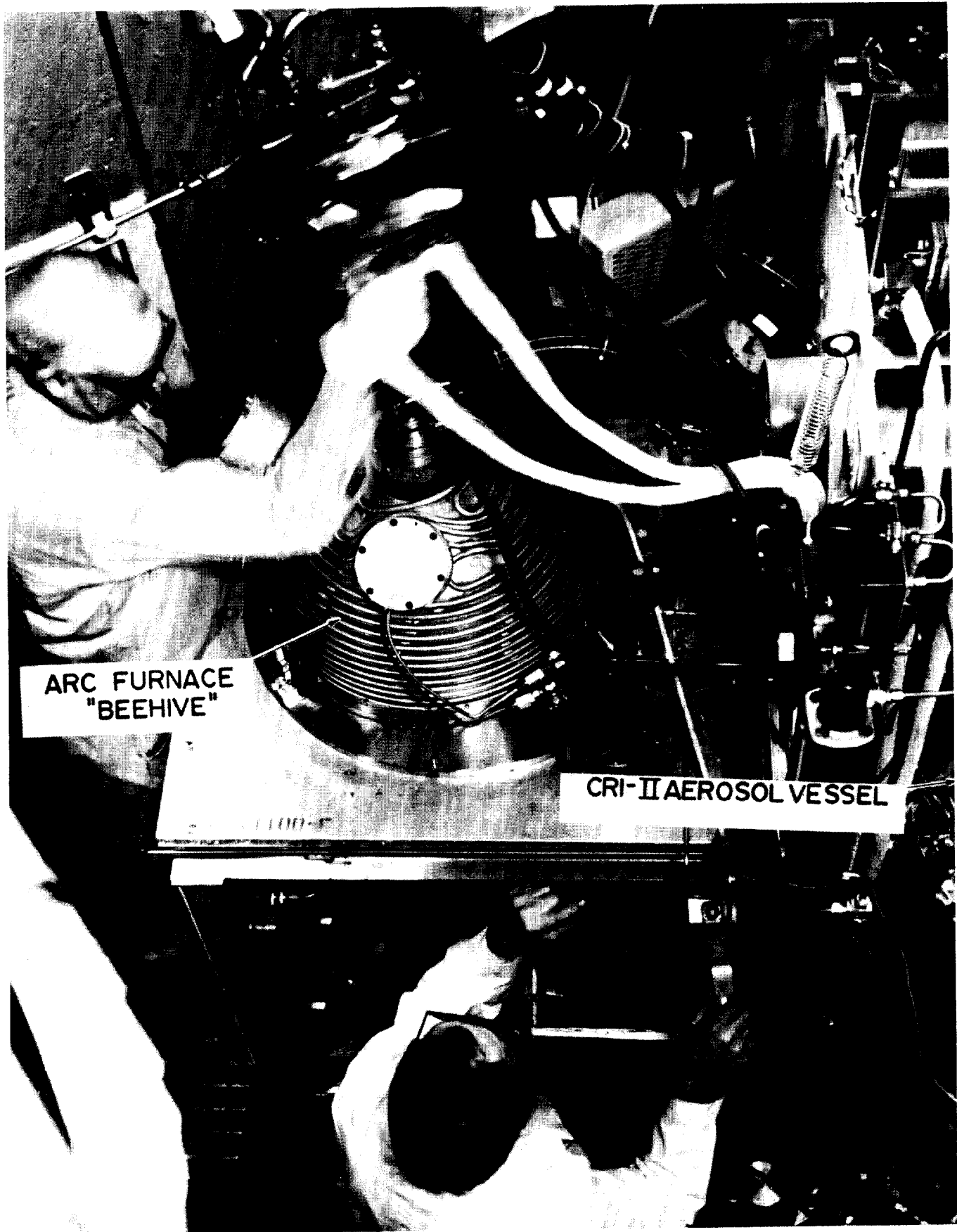


Fig. 6. Electric arc furnace in operation

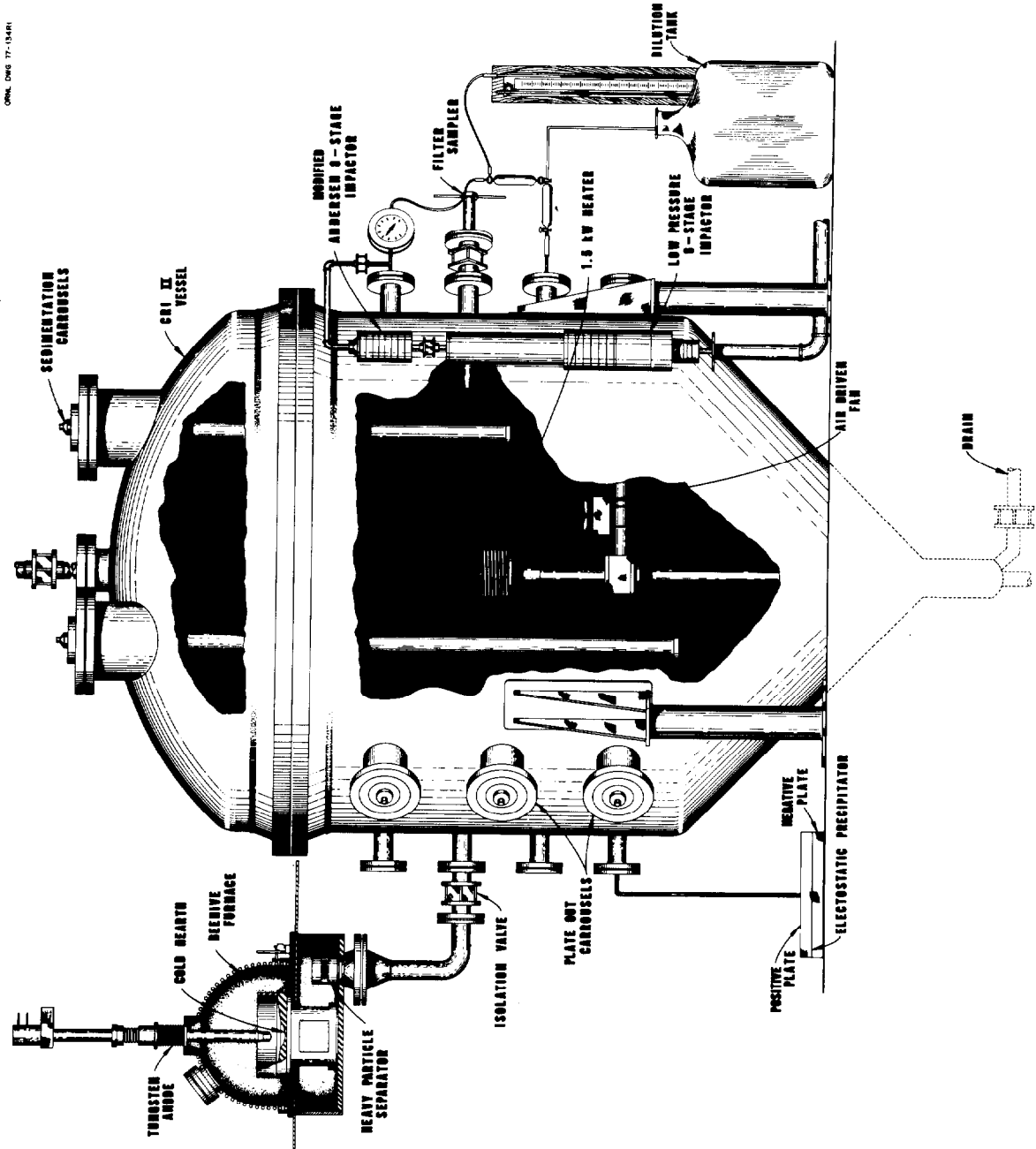


Fig. 7. CRI-II vessel, aerosol sampling equipment and electric Arc Hearth Furnace.

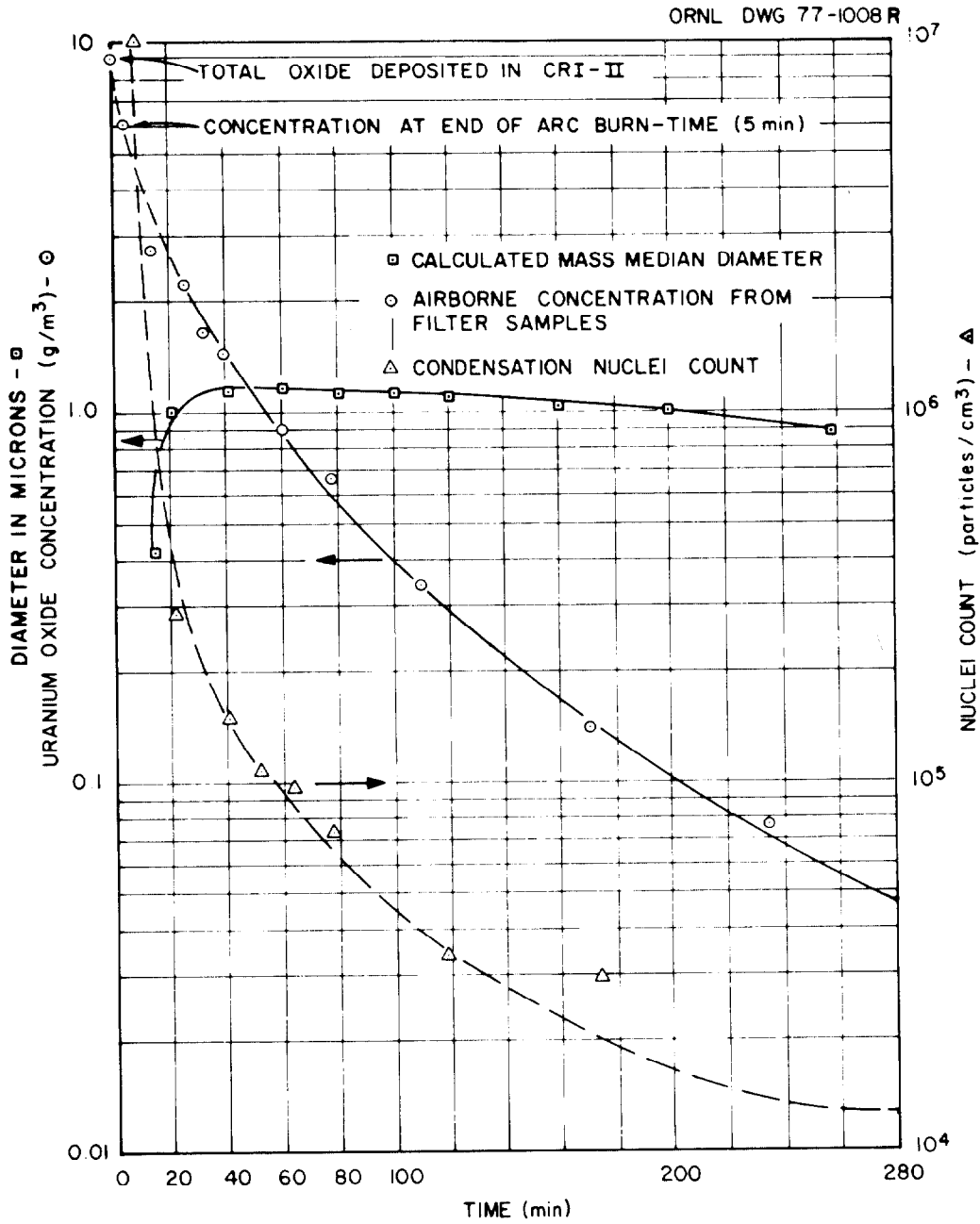


Fig. 8. Histogram of rate of change in airborne UO₂ concentration and condensation nuclei count for Run AF-6.

15th DOE NUCLEAR AIR CLEANING CONFERENCE

process, which is revealed in their high degree of crystallinity (Fig. 9a). The rapidly quenched vapor from the superheated liquid in the capacitor discharge processes should yield a smaller, unenhanced primary particle size (Fig. 9b). The minor difference between the two may be explained by the different voltages and time constants of the electrical pulse.

The differences observed in the primary size distribution are due to the inherent rate of cooling of the vapor. The capacitor-discharge type of aerosol is generated instantaneously compared with the aerosol generated either by the arc furnace or by pyrophoric oxidation. Both of the latter methods have cooling rates several orders of magnitude slower, permitting crystal growth by vapor condensation.

Efforts to determine differences in the behavior of the branched-chain agglomerates of UO_2 and U_3O_8 aerosols have not revealed a clear contrast, although the theoretical densities of these two oxides are 10.9 and 8.3 g/cm^3 , respectively. Figures 10a and 10b are typical of the arc-furnace and CDV types of UO_2 agglomerates.

IV. Stokes Diameters from Concentration Changes and Impactor Analysis

An additional effort was made to compare the Stokes diameters as calculated from concentration changes with the mass mean diameters (MMDs) determined experimentally by the multistage cascade impactors. These comparisons, with few exceptions, indicate that the calculated maximum Stokes diameters are somewhat greater ($\sim 1.5 \mu$) than the impactor data ($\sim 1.0 \mu$) for most of the arc-furnace (AF) runs. These results are shown in Table II and Fig. 11.

Table II. Comparison of impactor results with calculated Stokes diameters.

Run No.	<u>Andersen impactor data</u>		Standard Deviation (σ)	Calculated Stokes Diameter (μ)	Maximum Concentration (g/m^3)
	Time of Sample (min)	Mass Median Diameter (μ)			
CRI U-pyrophoric oxidation					
10	16-18	0.72	2.04	1.15	1.97
CRI-II arc-furnace vaporization					
6	27.5-29.4	1.1	2.4	1.62	6.0
Arnold Engineering Development Center Capacitor discharge					
35S	a	a	a	0.63	0.88
ORNL-CRI-III capacitor discharge					
7	71	1.46	2.2	1.54	2.04

^aNo impactor samples taken.

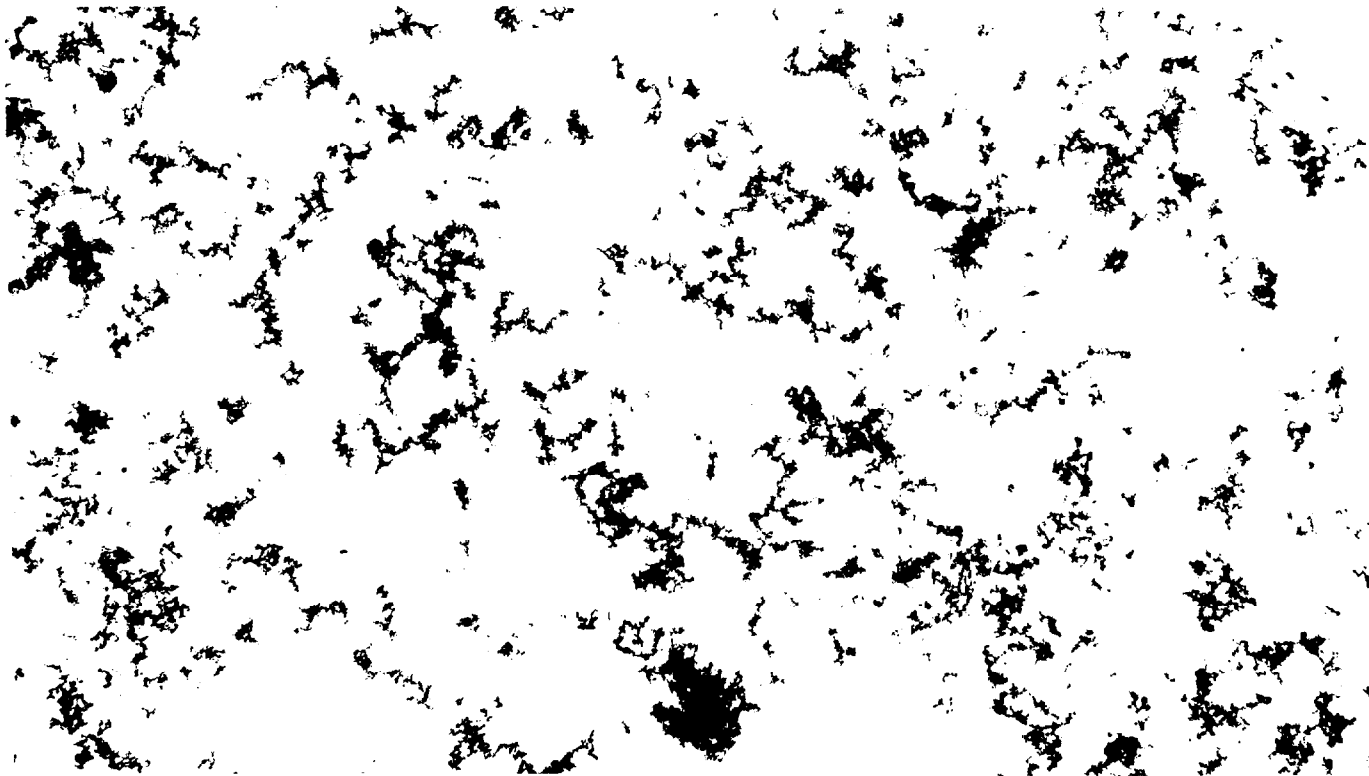


Fig. 9a. Photomicrograph of arc furnace UO_2 aerosol agglomerates at 5000X.



Fig. 9b. Photomicrograph of CDV UO_2 aerosol agglomerates at 5000X showing primary particles slightly smaller than AF particles.

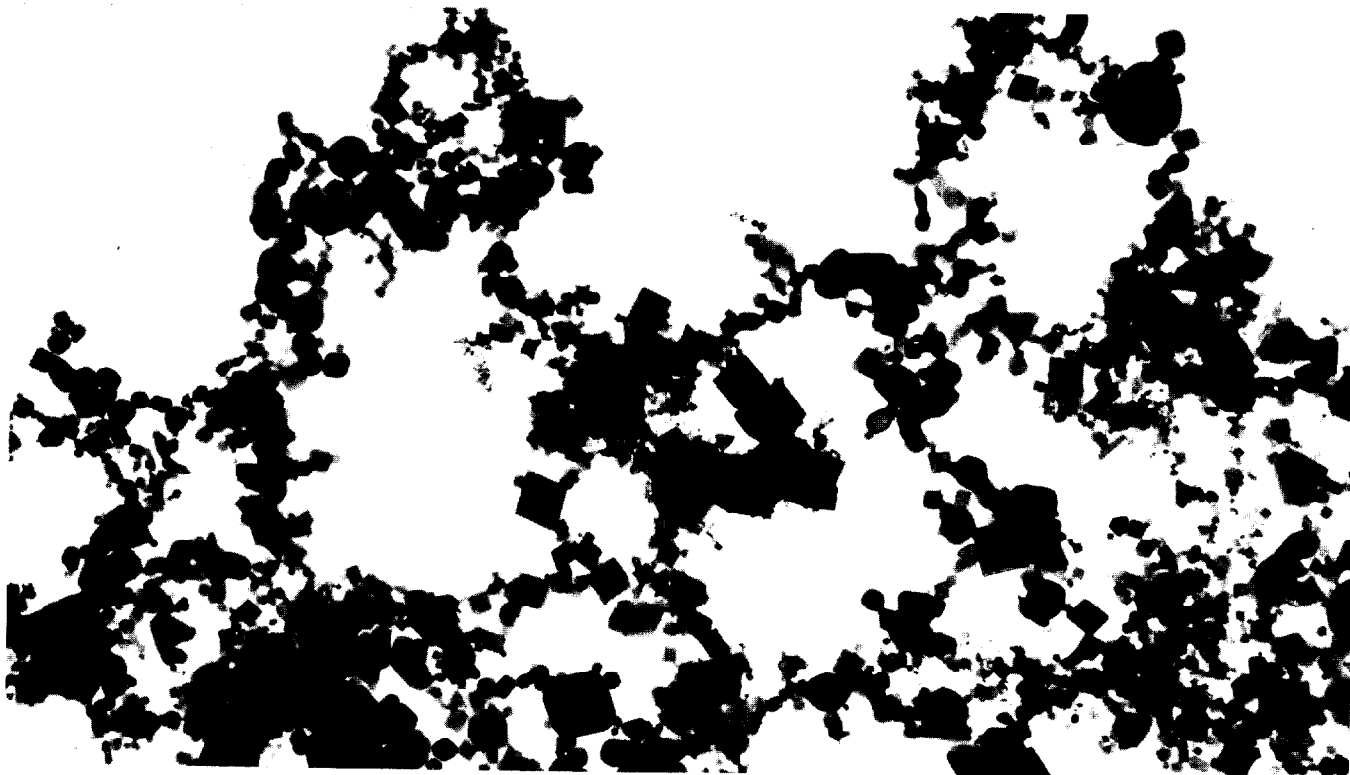


Fig. 10a. Photomicrograph of arc furnace UO_2 aerosol showing high degree of crystallinity of primary particles.

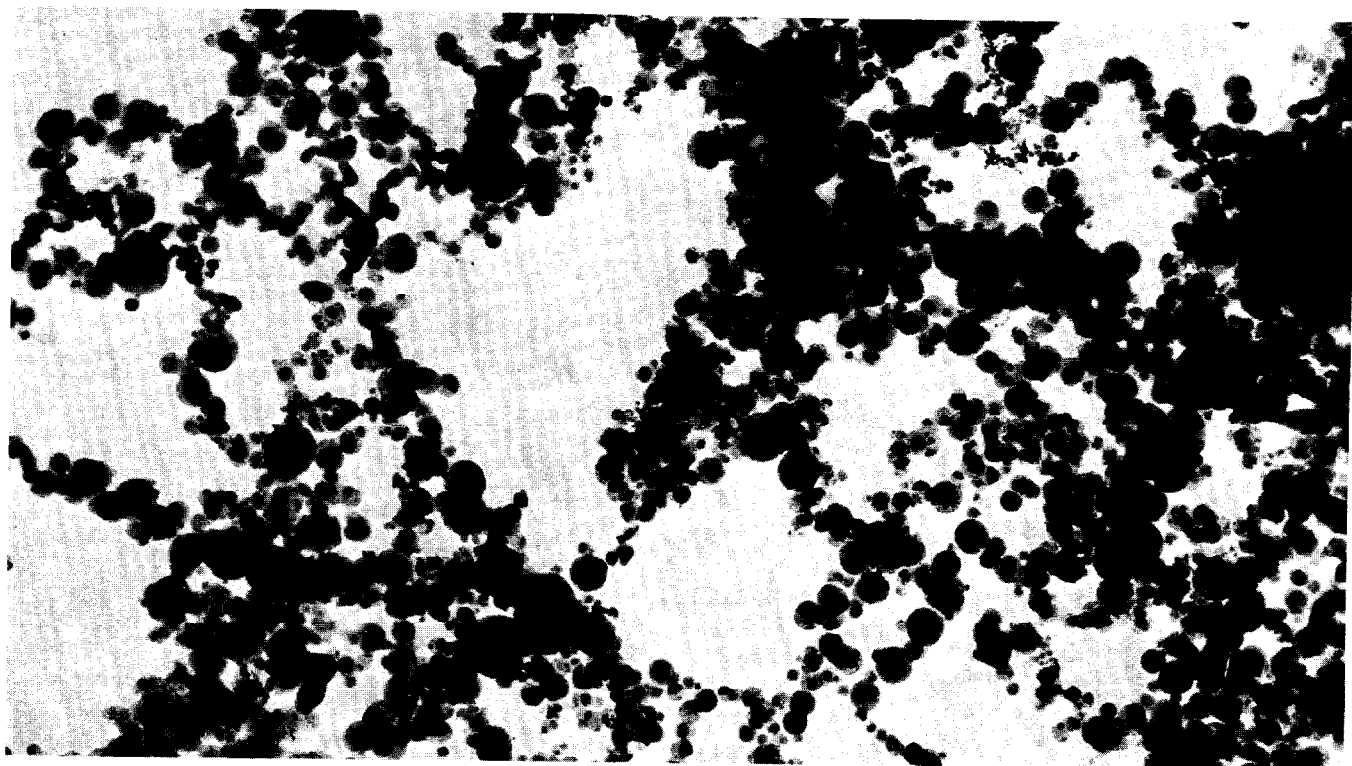


Fig. 10b. Photomicrograph of CDV UO_2 aerosol showing spherical primary particles.

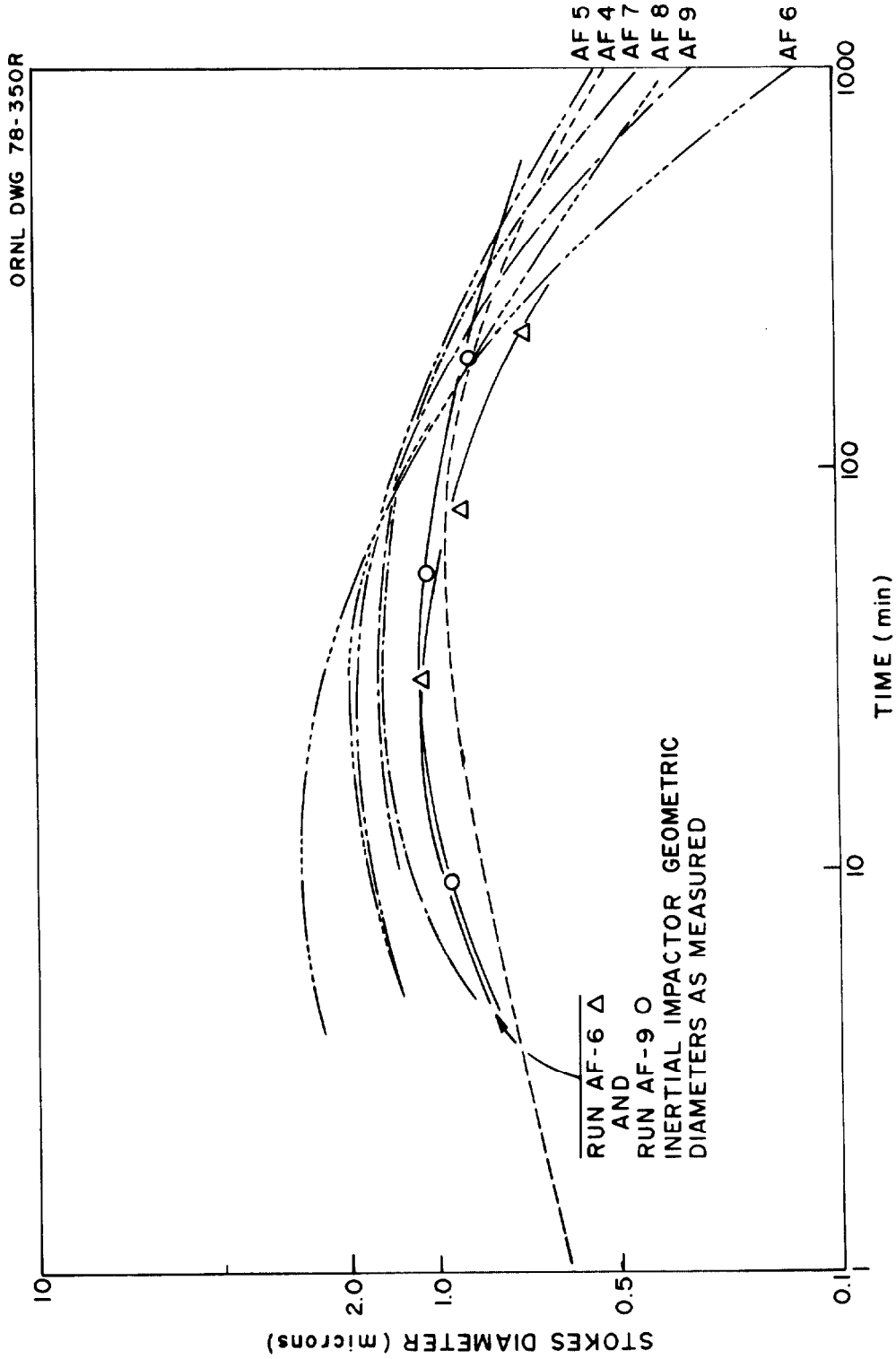


Fig. 11. Stokes diameters computed from airborne UO_2 measurements using plateau corrections derived from deposition sampler data.

15th DOE NUCLEAR AIR CLEANING CONFERENCE

The deposition and plateout samplers expose sample plates to the CRI-II atmosphere for various periods. From these results, the amount of material deposited on the walls and floor of the tank can be estimated by dividing the average amount of plateout or deposition by the total material deposited and by normalizing with respect to the appropriate surface area ratio. Results of these calculations for Run AF-3 are shown in Tables III and IV.

Table III. Results of calculations for Run AF-3.

Exposure Time (min)		Deposition (ug)			Plateout (ug)			Settling Fraction, floor	Plateout Fraction, wall
From	To	Long ^a	Short ^a	Av	High ^a	Low ^a	Av		
0	5	240	820	530	220	200	210	0.419	0.581
5	25	620	470	545	26	19	22.5	0.87	0.126
25	58	400	600	500	18	21	19.5	0.88	0.12
58	92	400	510	455	20	7	13.5	0.906	0.094
92	161	530	320	425	27	5	16	0.883	0.117
161	265	320	290	305	13	27	20	0.813	0.187
265	613	270	130	300	22	5	13.5	0.809	0.191
613	1453	280	190	235	23	27	25	0.728	0.272

^aLong, short, high, and low designate sampler locations at 196, 94, 81, and 157 cm from the tank top, respectively.

The Stokes diameters of particles satisfy the following conditions when airborne concentrations are not adjusted to account for plateout:

$$D_s = \left(\frac{18V\eta}{\rho g} \right)^{1/2} \tag{1}$$

$$C_2/C_1 = e^{-Vt/h}, \text{ or } V = \frac{-h}{t} \ln(C_2/C_1), \tag{2}$$

where

- D_s = Stokes diameter (cm),
- V = particle velocity (cm/sec),
- η = viscosity of air = $1.87 \times 10^{-4} \rho$,
- ρ = particle density (g/cm³),
- g = gravitational constant (980 cm/sec²),
- C_2 = concentration at time t_2 ,
- C_1 = concentration at time t_1 ,
- t = exposure time in sec ($t_2 - t_1$),
- h = tank height (200 cm).

Combining Eqs. (1) and (2) gives

$$D_s = \sqrt{\frac{-6.3 \times 10^{-5} \ln (C_1/C_2)}{t}}$$

Using the start of an exposure time for t_1 and C_1 and the end of the exposure for t_2 and C_2 , Stokes diameters were computed for Run AF-3 where airborne concentrations have been adjusted for plate-out. The results of these calculations are given in Table IV.

Table IV. Stokes diameters for Run AF-3 with corresponding airborne concentrations adjusted for plateout effect.

Exposure time (min)		C_1 ($\mu\text{g}/\text{cm}^3$)	C_2^a ($\mu\text{g}/\text{cm}^3$)	Stokes Diameter (μ)
t_1	t_2			
0	5	1.539	1.498	0.75
5	25	1.44	1.15	1.09
25	58	1.11	0.77	1.07
58	92	0.728	0.506	1.06
92	161	0.483	0.258	0.98
161	265	0.229	0.123	0.80
265	613	0.0978	0.0378	0.54
613	1453	0.0236	0.0078	0.37

^aValues adjusted for plateout.

The concentration of airborne solids (no plateout correction) can be computed from

$$C_i = 1.389^{-0.864} \times 10^{-4} t_i + 0.15^{-0.1818} \times 10^{-5} t_i, \quad (3)$$

which is an empirical fit to the data (t is in seconds, $i = 1, 2$). The plateout effect is accounted for by multiplying the airborne concentration difference [$C_2 - C_1$, as obtained from Eq. (3)] over an exposure time by the settling fraction (Table II) and subtracting this product from C_1 to obtain C_2 , the apparent concentration after the time interval if gravitational settling were solely responsible for the decrease.

Figure 12 is a graph of diameter vs time for Runs AF-1 and AF-3.

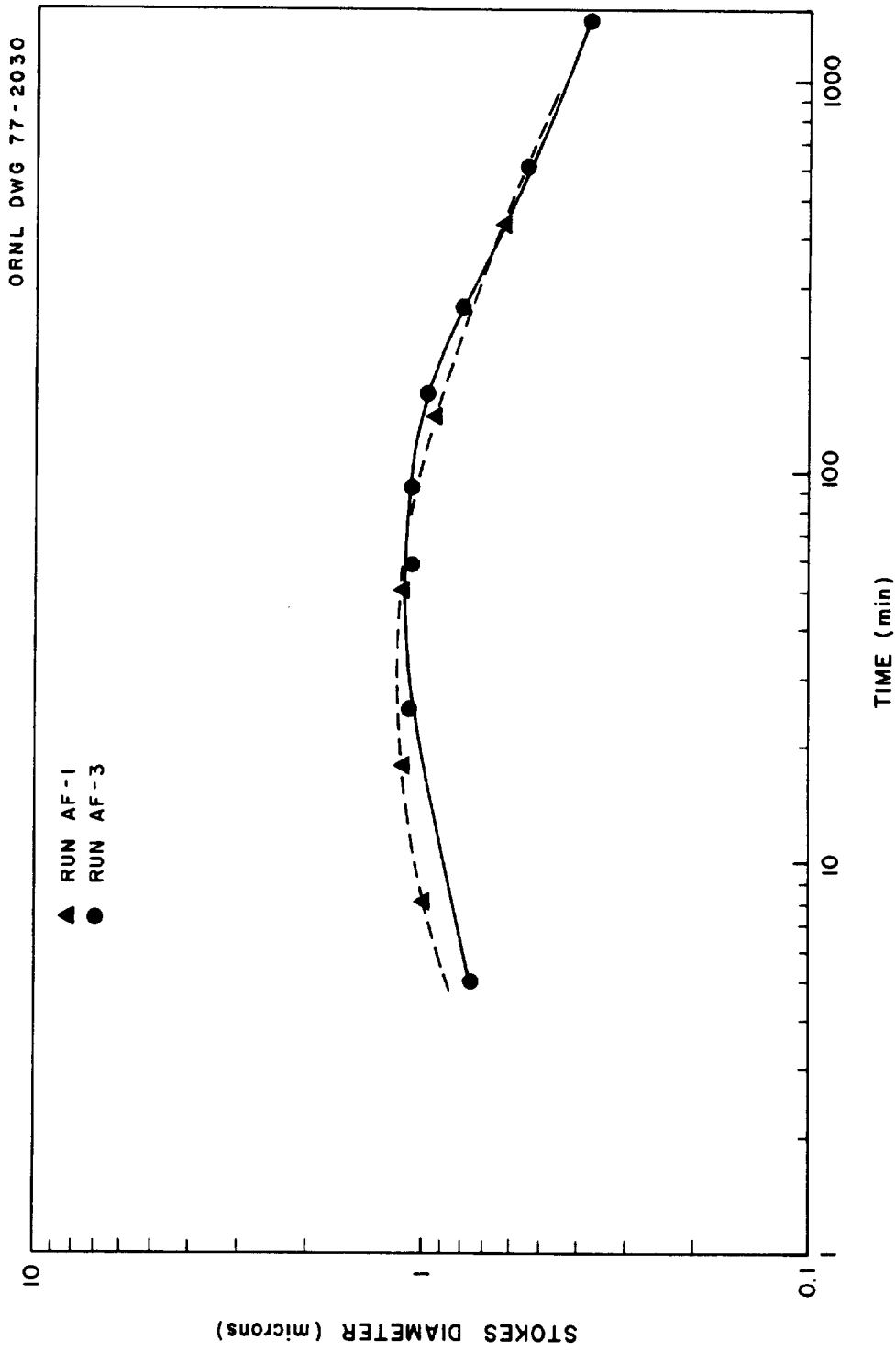


Fig. 12. Stokes diameters for UO_2 agglomerates as calculated from airborne concentration changes due to settling.

15th DOE NUCLEAR AIR CLEANING CONFERENCE

The relative importance of sedimentation, or fallout, compared with plateout is illustrated in Fig. 13 for Run AF-3. The plateout fraction is a nearly instantaneous process accompanying the initial agglomeration step and is probably dominated by Brownian motion of the small primary particles. This is particularly true when the aerosol is settled under room-temperature conditions, as was the case in these two runs. In Run AF-3, the maximum concentration was about 1.4 g/m^3 . The plateout fraction was about 30% of the total, even though Fig. 13 shows that the mass deposited per unit area on the floor was about an order of magnitude higher than that on the walls (because the total wall area is about three times that of the floor).

As a part of the effort to characterize the UO_2 agglomerated chains and clusters and the changes with respect to time, we have installed microscope grids on the fallout carousel between the fallout plates. The results of collecting such particles for Run 8 are illustrated for four time periods in Fig. 14. The photographs appear to confirm a self-preserving size concept during these periods, as does the Stokes calculations.

V. Correlation of Experimental Results with Aerosol Agglomeration Codes

The reference code most widely used in the LMFBR-RSR programs is a Battelle modification of the AI's HAA-3, which is called HAARM-2.⁽⁴⁾ HAARM-2, now being supplemented by HAARM-3, has been used with some success in predicting the relative behavior of aerosols when only one or two parameters are varied.

An example of the use of HAARM-2 is illustrated in Fig. 15, in which the sensitivity of the particle diameter (agglomerate size) is varied in order to find the fraction of material expected to plate out. The total deposition is also derived from the code and compared with the experimental observations for Runs AF-6 and AF-3. Both the match to AF-6 by the $1.0\text{-}\mu$ -diam input and the 16% plateout fraction are in good agreement with actual data.

Another example of the use of HAARM-2 in predicting fuel aerosol behavior is given in Fig. 16, where the expected range in particle diameters as a function of maximum initial concentration is plotted in terms of elapsed time, assuming an instantaneous source. The predicted maximum radius in Curve III converted to geometric mean diameter, and corrected to a theoretical density of 10.9, is 1.05μ . This value agrees closely with the 1.0μ trial diameter and plateout fraction in Fig. 15.

An example of the further correlation with both HAARM-2 and BNL Trap⁽⁵⁾ codes is shown in Fig. 17. This correlation of deposition rates also serves to illustrate the small but distinct differences between UO_2 and U_3O_8 , which are probably due to the density difference expected in the two oxides.

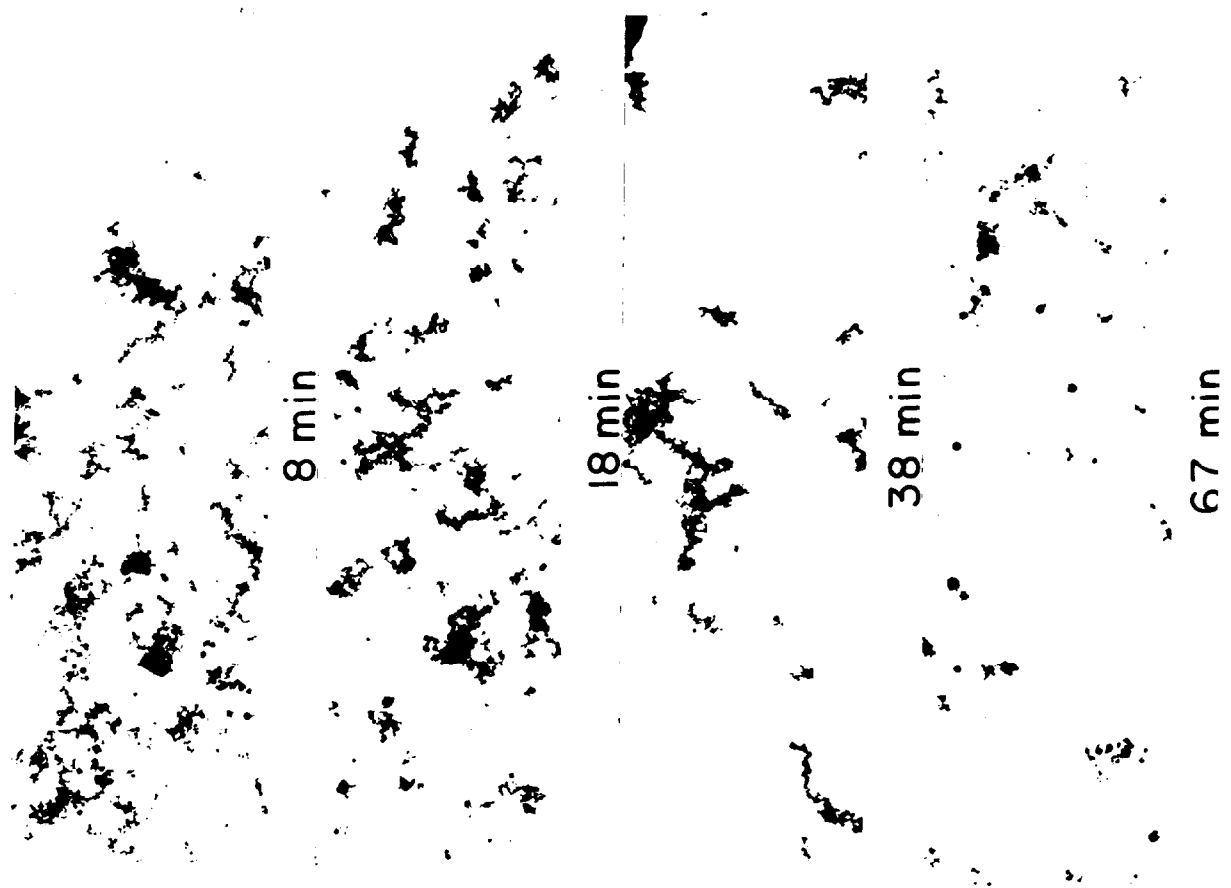


Fig. 14: UO₂ agglomerates settled on microscope grids at different time intervals (5000X).

ORNL DWG 77-2029

AF 3

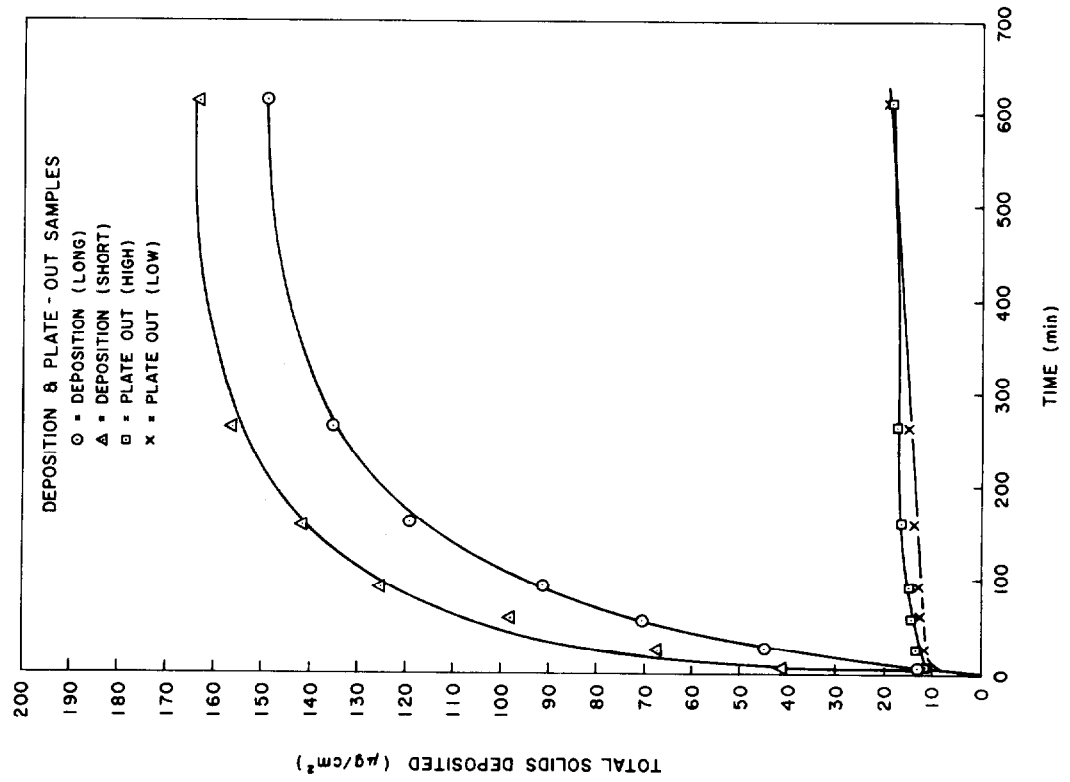


Fig. 13. Accumulated fallout and plateout fractions of UO₂ aerosol, Run AF-3.

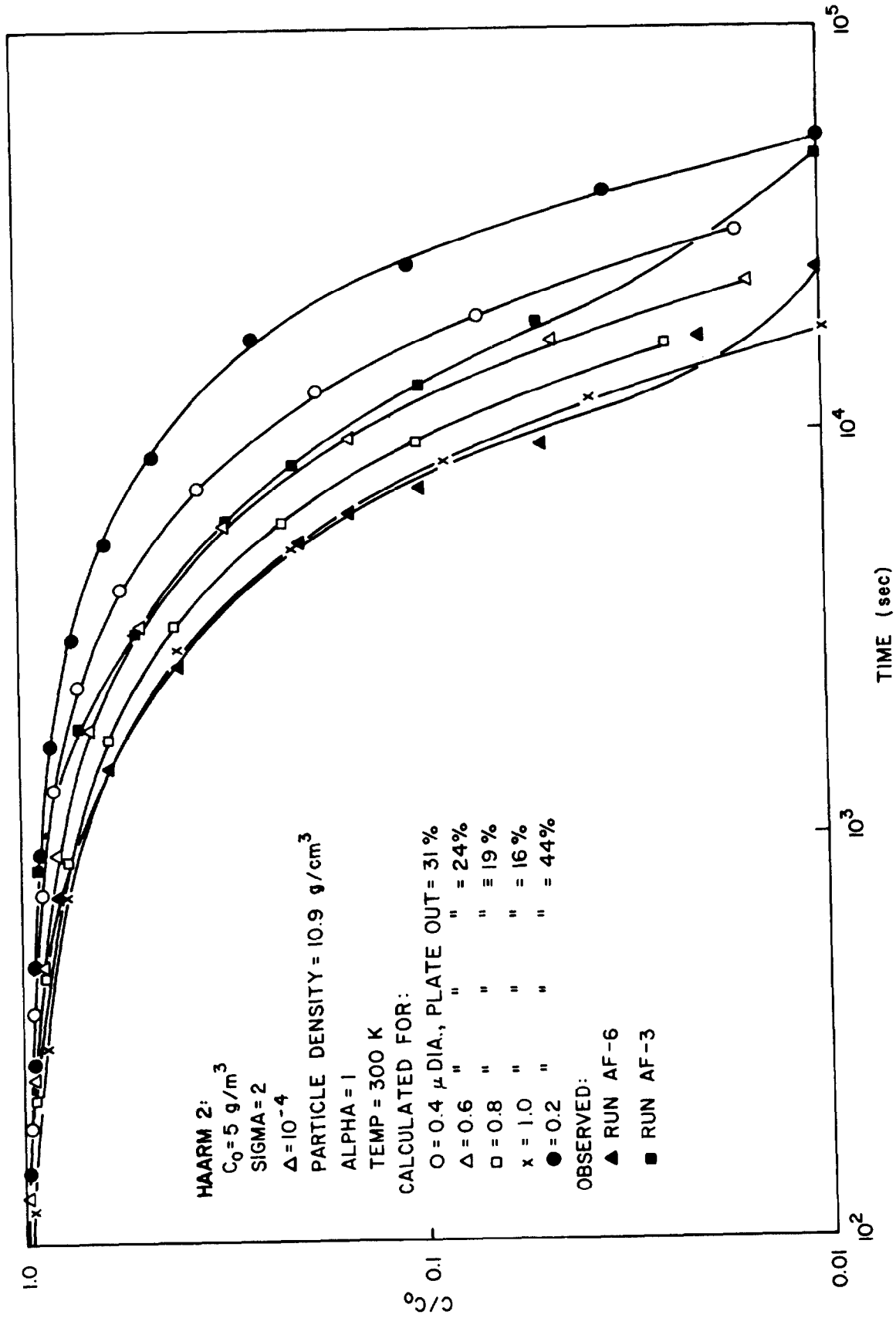


Fig. 15. Correlation of particle diameter with deposition rate as calculated by HAARM-2 and as observed in CRI-II.

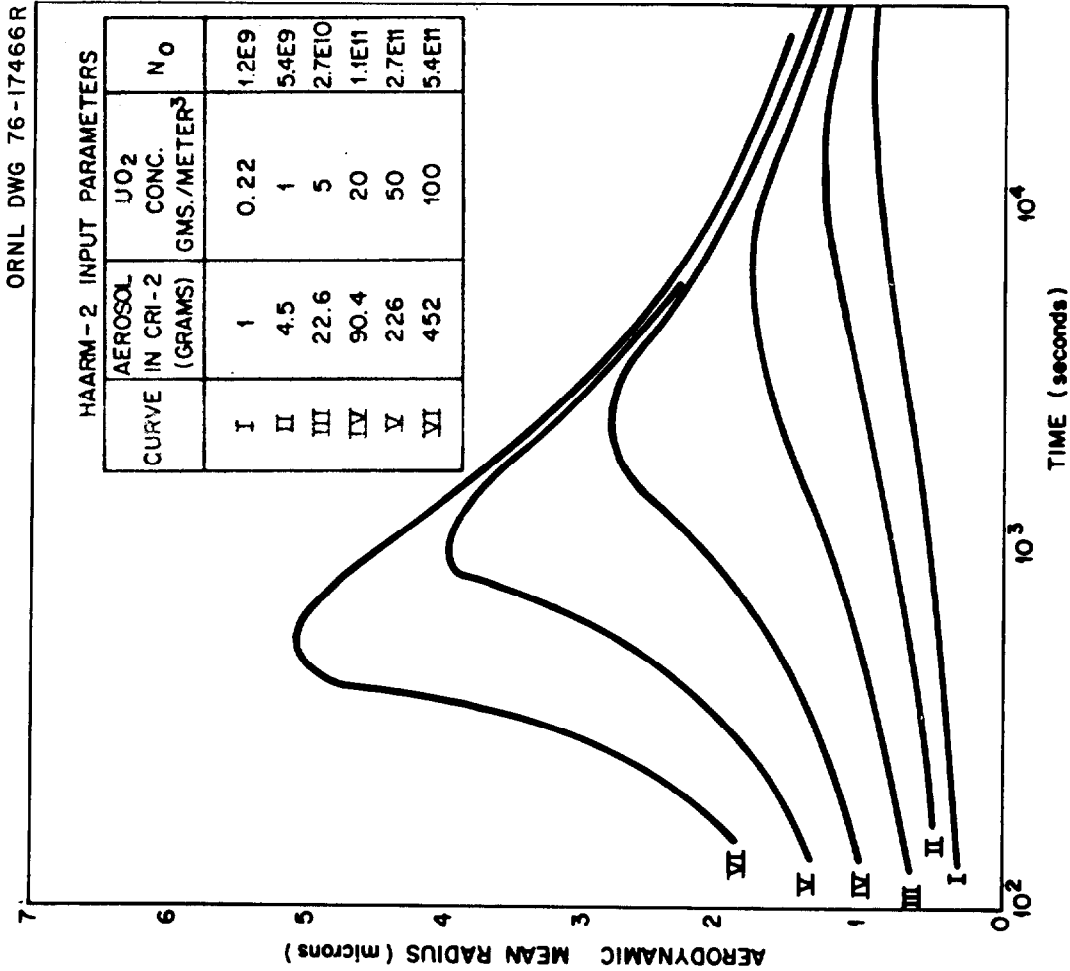


Fig. 16. Predicted time for maximum particle growth vs concentration.

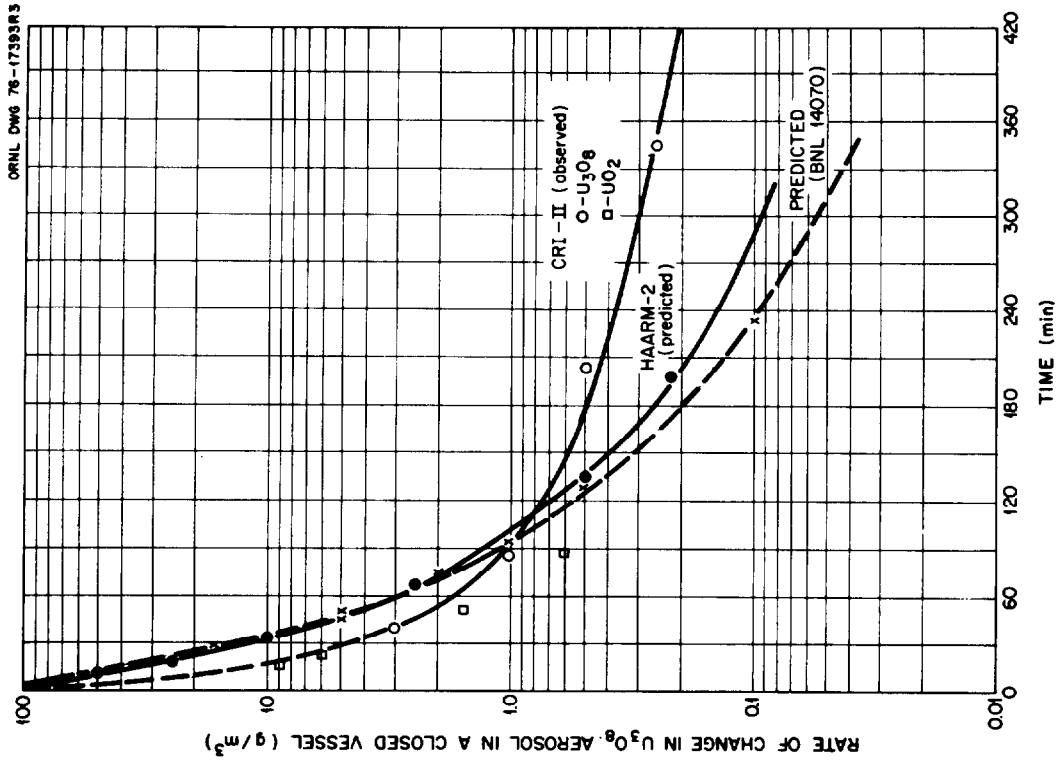


Fig. 17. Deposition rates for airborne concentration change for UO₂ and U₃O₈ in CRI-II as calculated by HAARM-2 and as observed.

VI. BET Surface Area as a Measure of
Primary Particle Size

Whenever a sufficient amount of aerosol has been available (~ 1 g), it has been used to determine the total surface area available for gas adsorption. This area is also a measure of the individual particle surface area and therefore the particle diameter.

In the arc-furnace experiments, where 50 to 100 g of aerosol are generated and deposited both inside the furnace and on the floor of the CRI-II vessel, samples are easily collected and measured for total surface area. The surface area measured between 5 and 7 m^2/g for most of the tests. The smaller area is typical of the material plated out in the furnace; the larger area is typical of the settled oxide. The corresponding individual particle diameter calculated for 7 m^2/g is 0.08 μ , or about twice that determined by electron microscopy. This difference may be indicative of partially connected primary particles or of the presence of a few large particles that settled on the floor after being ejected from the furnace and thus were never a part of the aerosol. A better technique for collecting the massive aerosol sample by delayed filtration should avoid this contaminant.

VII. Summary and Conclusions

The HAARM and HAA aerosol codes correlate fairly well with our experiments involving single component fuel particles at the limited level of concentrations presently being studied. The codes are useful in demonstrating sensitivity to a selected variable but require careful restriction of the other variables in order to correlate satisfactorily with experimental data. In general, the codes are relatively conservative compared to experimental observations.

The more highly concentrated breeder reactor fuel aerosols that are postulated may be expected to vary considerably in physical characteristics according to the specific hydrodynamic and thermal environment following an HCDA. Extensive variations in the primary particle sizes produced and in the stability of the chains and agglomerates may occur after these aerosols escape into the containment.

Attenuation rates (i.e., rates of change from initial concentration) in a closed vessel initially vary in proportion to the mass concentration for both fuel aerosols alone or fuel and coolant aerosols, since the higher concentrations produce equally heavier agglomerates and more rapid settling rates. Demonstration experiments at the higher levels and more realistic environments will be needed to bound the uncertainties.

15th DOE NUCLEAR AIR CLEANING CONFERENCE

VIII. References

1. G. W. Parker, G. E. Creek, W. J. Martin, C. J. Barton, and R. A. Lorenz, Out-of-Pile Studies of Fission Product Release from Overheated Reactor Fuel, ORNL-3981 (July 1976).
2. M. J. Kelly, G. W. Parker, and J. M. Rochelle, Development of the Capacitor Discharge Vaporization Technique to Produce Aerosols Formed Under Conditions Postulated For Hypothetical Core Disruptive Accidents, ORNL/NUREG/TM-160 (in press).
3. W. Schaikarski, The Karlsruhe Research Program on Nuclear Aerosols and Its Relation to the Plutonium Hazard of Fast Sodium Reactors, KFK-798 (July 1968).
4. L. D. Reed and J. A. Gieseke, HAARM-2 Users Manual, BMI-X-665 (Oct. 31, 1975).
5. A. W. Castleman, Jr., F. L. Horn, and G. C. Lindauer, "On the Behavior of Aerosols Under Fast Reactor Accident Conditions," in Proceedings of the International Congress on the Diffusion of Fission Products, Saclay, France, Nov. 2-4, 1969, CONF-691104 or BNL-14070.

DISCUSSION

TILLERY: Determination of stoke diameter from the aerodynamic diameter of branched chains, determined by the cascade impactor, requires some assumptions about the slip factor dynamic shape of the branched chains. Did you use the aerodynamic diameter given by the impactor calibration or did you use shape factor values such as those given by Stöber for fibers?

PARKER: We do a straight gravimetric determination of what is on the stage. For the calibration, we simply use the unit density calibration and the bulk density of the material. You just divide one over $\sqrt{\alpha\rho}$ or multiply by $\frac{1}{\sqrt{\alpha\rho}}$.

Not knowing any better you assume α is 1 and that leaves you with $\sqrt{10.9}$, which is 3.3. If you go back and forth from aerodynamic size or unit density size to mass median, you simply use that multiplier.

TILLERY: There is, of course, for the smaller particles a slip factor that has to be put in. Therefore, you have to make an assumption about the slip factor for the branched chains or for the long cylindrical particles if you wish to transpose to a Stokes diameter which is equivalent to a spherical particle of the same density as the particle of interest. I think that would tend to compensate somewhat for the oversize in the Stokes diameter which you get if you fail to include the slip correction factor.

PARKER: I think there are a number of things we could do. We are of the opinion that, at the concentration we are working, we just might "smear" that problem out. But, in all fairness, I would feel much better if we had the centrifuge data to go with it.

SHAW: Have you observed any break-up of aggregates in the first couple of

15th DOE NUCLEAR AIR CLEANING CONFERENCE

stages of the cascade impactor, especially in the large particle size range?

PARKER: Two years ago, we reported at the Aerosol Technology Conference that we had two sets of measurements which were contradictory. The instruments which had sonic jets were giving more particles by almost a factor of 10. For the atmospheric impactor, we presently do not have a way of stating unequivocally that it is not breaking up aggregates. Whenever we get Marvin Tillery's centrifuge, we think we will be able to determine this.

SHAW: Do you use any coating to prevent disaggregation?

PARKER: We use three things: silicone oil coatings, thick filters, and membrane filters. When we vary the amount of material collected on a plate, we get some odd distributions but we can always tell that the unsatisfactory measurements occur because of overloading the plate.

15th DOE NUCLEAR AIR CLEANING CONFERENCE

SODIUM OXIDE/HYDROXIDE AEROSOL PROPERTIES AND BEHAVIOR IN A LARGE VESSEL*

R. K. Hilliard, J. D. McCormack
J. A. Hassberger, A. K. Postma
Hanford Engineering Development Laboratory
Operated by Westinghouse Hanford Company
Richland, Washington 99352

Abstract

Two large-scale aerosol behavior tests were performed in the Containment Systems Test Facility (CSTF) using sodium pool fires as the aerosol source. The purpose was to characterize the properties and behavior of sodium aerosol particles formed and aged in a large containment vessel. The results will be used as baseline data for comparison with follow-on air cleaning tests. The 20-m high, 850-m³ CSTF containment vessel is approximately half scale of a commercial reactor containment building for parameters which affect agglomeration and gravitational settling. Thus, the test air cleaning systems will be challenged with an aerosol closely representative of that postulated for LMFBR accidents. The results of these tests also offer an excellent opportunity to evaluate computer models which have been developed for the purpose of predicting aerosol behavior during hypothetical accidents in sodium cooled reactor containment spaces.

The two tests differed only in that steam was injected in the second test to simulate the release of water vapor from heated concrete. The aerosol in the first test was a dry mixture of sodium peroxide, sodium hydroxide and sodium carbonate. In the second test it was predominantly wet sodium hydroxide. The addition of water vapor caused more rapid fallout during the aerosol release period, but lower settling rates afterward. The net results was a 25% lower potential for aerosol leakage in the wet test. Detailed analyses of computer model comparisons have not yet been performed, but preliminary HAA-3B code predictions were in good agreement with suspended mass concentration and the ratio of mass settled to plated on walls.

Air cleaning tests will next be performed in the same facility to demonstrate the effectiveness of various types of scrubbers, filters and novel devices for cleaning the very high mass concentration aerosol from the containment atmosphere.

I. Introduction

The aerosol likely to be formed during postulated accidents in sodium cooled reactors has been the subject of considerable study at many laboratories during the past decade⁽¹⁻¹⁰⁾. These studies have encompassed theoretical treatment, computer modeling and experimental measurements. Several areas remain where further information is

*Work performed under USDOE Contract EY-76-C-14-2170.

15th DOE NUCLEAR AIR CLEANING CONFERENCE

needed. The need for large-scale experiments to clarify the effects of vessel size and shape on airborne concentration has been pointed out⁽²⁾. Present experimental data are limited to vessels 9-m or less in height. Vessel height affects agglomeration time and probably the physical nature of the agglomerate particles. Many postulated accidents involve structures with concrete surfaces that release water vapor when heated⁽¹¹⁾. Water vapor adsorbed by aerosol particles may cause significant chemical and physical changes in the particles.

The CSTF was constructed and operated for the purpose of studying containment and air cleaning systems under light water reactor (LWR) accident conditions⁽¹²⁾. The capability of generating sodium aerosols has been added and an experimental program is under way to develop and demonstrate air cleaning systems under simulated sodium cooled reactor accident conditions⁽¹¹⁾. The CSTF program includes tests with aerosols generated by sodium pool fires and sodium sprays in air and inert atmospheres. In some tests steam and carbon dioxide will be added to simulate off gases from heated concrete. The present paper reports the results of the first two tests which used sodium pool fires in air atmospheres. No engineered air cleaning features were employed. Aerosol depletion was caused solely by passive processes.

II. Experimental Arrangement

Experimental Equipment

A schematic diagram of the experimental arrangement is shown in Figure 1. Table I gives the dimensions of the containment vessel, which was fabricated according to the ASME Section VIII Code (1962) with a design pressure of 0.517 MPa (75 psig) at 160°C (320°F). It is a carbon steel (SA 212-B) vessel with standard dished top and bottom heads. All interior surfaces are coated with a modified phenolic paint. The external surfaces are covered with a 25.4-mm thick layer of fiberglass insulation with a thermal conductivity of 0.0467 W/m°C at 100°C.

Sodium was heated in a 1.9-m³ 304SS vessel to the desired test temperature. At time zero a valve was opened and argon pressure forced the sodium through a 2-in. schedule 40 pipe (52.5-mm ID) into a carbon steel pan centered near the bottom of the containment vessel. The burn pan rested on insulating fire brick and the sides of the pan were insulated. The pan was equipped with a hinged, gasketed lid which permitted termination of the aerosol source on command.

Test Conditions

The two tests, AB1 and AB2, were performed with essentially the same initial conditions, but in the second test steam was injected at a rate equivalent to the release of water vapor from approximately 10-30 m² of hot concrete⁽¹³⁾. Although the aerosol and steam release rates and duration were arbitrary, they are within the range of accident conditions postulated in LMFBR safety analyses.

The initial containment atmosphere was air at normal temperature and humidity. Other test conditions are listed in Table I.

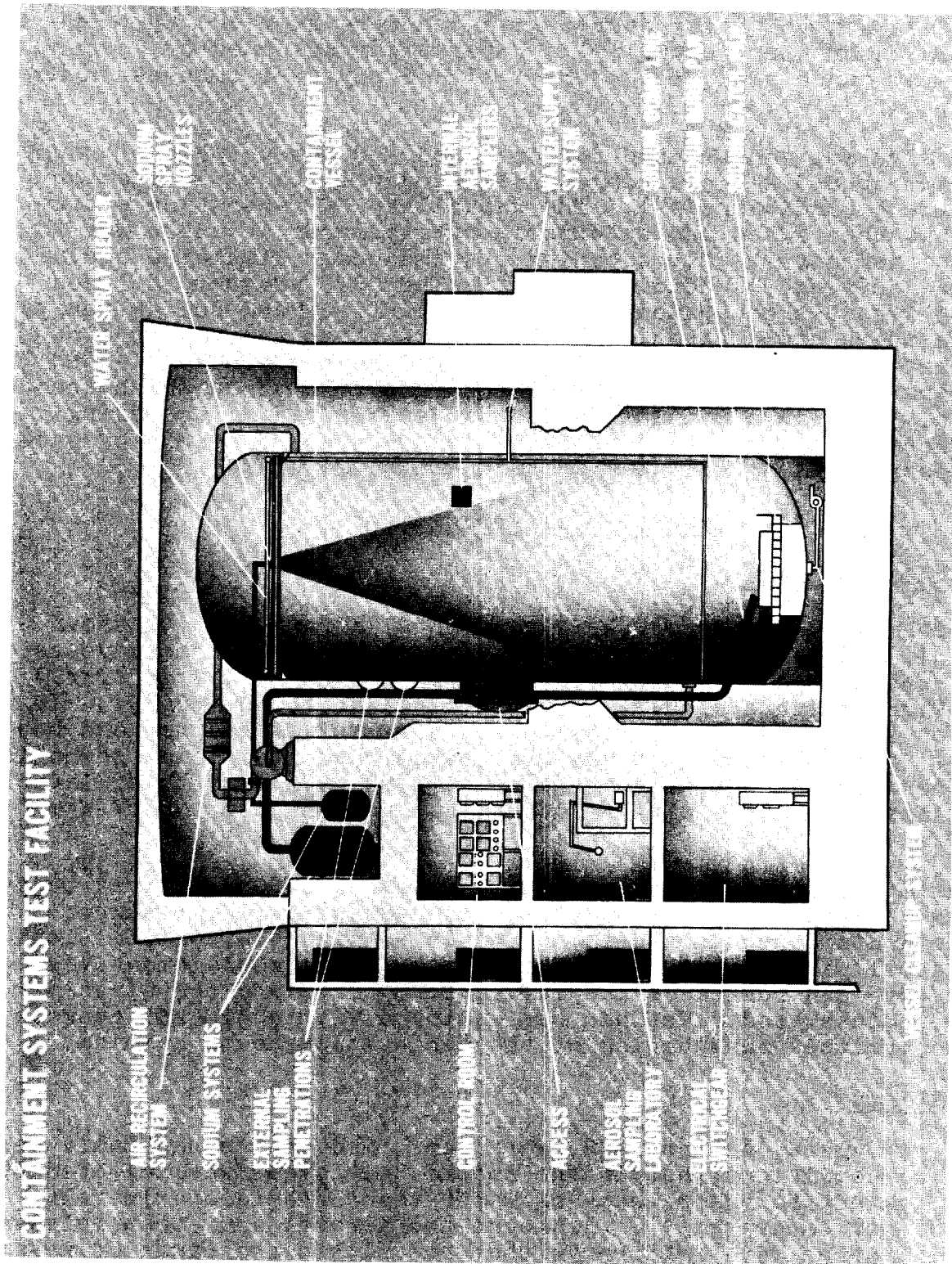


Figure 1. Schematic diagram of the Containment Systems Test Facility.

15th DOE NUCLEAR AIR CLEANING CONFERENCE

Table I. Test conditions for CSTF tests AB1 and AB2.

	<u>AB1</u>	<u>AB2</u>
<u>Containment Vessel</u>		
Diameter, m	7.62	7.62
Overall height, m	20.3	20.3
Volume, m ³	850	850
Total horizontal surface, m ²	88	88
Shell surface, m ²	520	520
Total internal surface, m ²	1000	1000
Vessel steel mass, kg	103,000	103,000
Leakage rate, %/d at 10 psig	2.0	2.6
<u>Sodium Spill</u>		
Mass sodium spilled, kg	410	472
Sodium burn pan surface, m ²	4.4	4.4
Initial sodium temperature, °C	600	600
Sodium fire duration, sec	3600	3600
Total sodium oxidized, kg	154	146
<u>Steam Addition</u>		
Flow started, sec after time zero	-	960
Flow stopped, sec after time zero	-	4560
Flow rate, kg/sec	0	0.019
<u>Initial Containment Atmosphere</u>		
Oxygen, vol %	19.8	20.9
Dew point, °C	10.0	7.6
Temperature, °C	26.5	20.5
Pressure, MPa (absolute)	0.125	0.128
<u>Containment Atmosphere During Test</u>		
Maximum temperature, °C	91	96
Maximum pressure, MPa (absolute)	0.142	0.153
Final oxygen, vol %	14.7	16.7
Final dew point, °C	-40	-1.5
<u>Aerosol Source</u>		
Type	Na pool fire	Na pool fire
Source duration, sec	3600	3600
Average source rate (as sodium), g/s	11.1	10.8
Total aerosol release (as sodium), kg	40.0	38.8
Fraction of oxidized sodium released	0.261	0.266

Test Procedure

The procedure used in each of the tests was to install and calibrate the equipment and instrumentation, dry the vessel to a constant, normal humidity, seal the vessel so that it was essentially leak tight and heat the sodium to 600°C in the auxiliary sodium tank. At a time defined as "time zero", t_0 , a valve was opened and the sodium flowed into the burn pan through the electrically heated delivery line. Figure 2 is a photograph taken through a viewing window near the bottom of the vessel. A dense plume of aerosol particles formed immediately and swirled upward until the aerosol was dispersed throughout the containment volume. The sodium flow lasted 80 seconds and then the sodium supply system was isolated from the containment vessel.

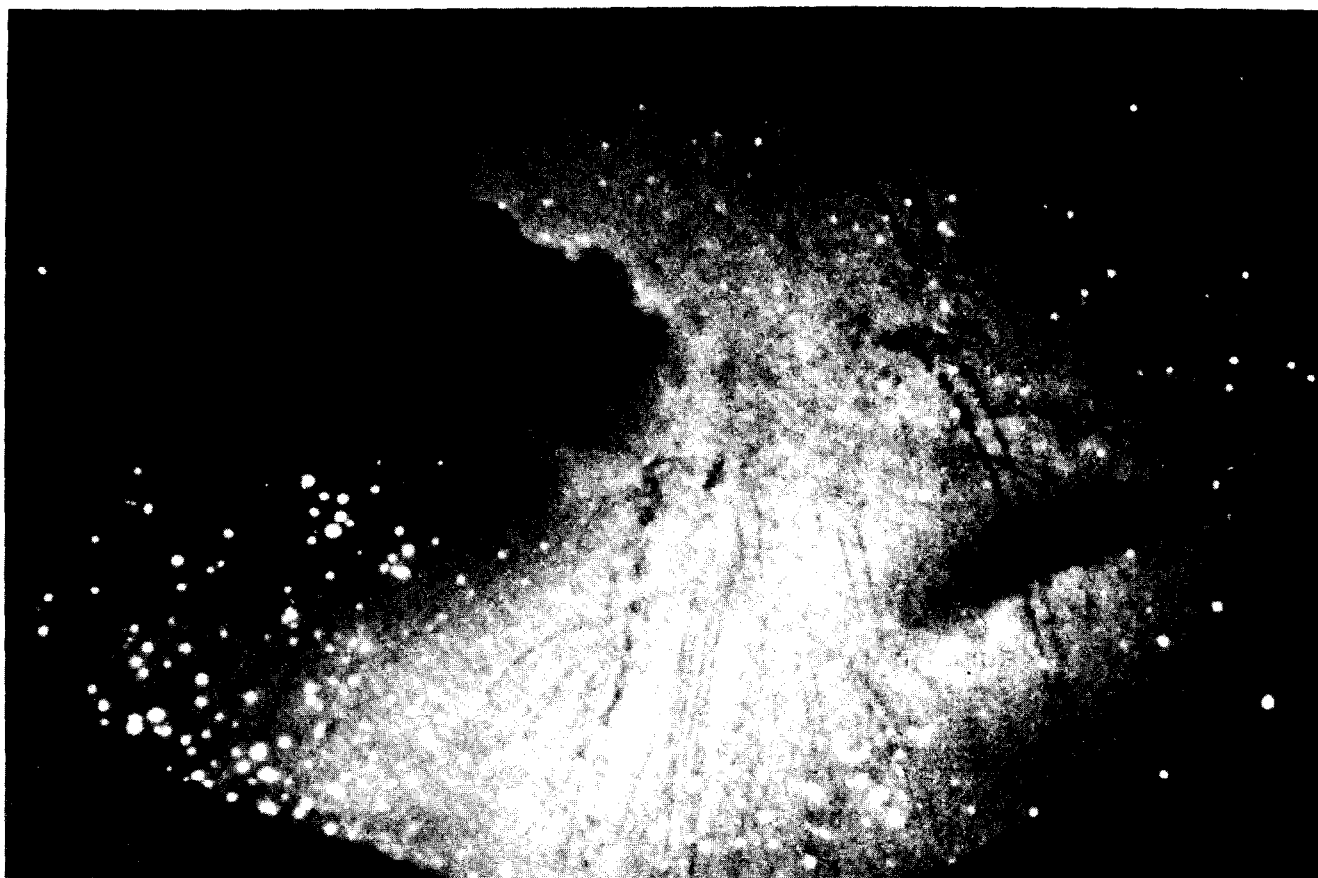


Figure 2. View of sodium spilling into ABl burn pan ten seconds after start of spill.

Temperature measurements were made continuously by 45 thermocouples. Containment atmosphere pressure and gaseous analysis was also continuous. Aerosol characterization was performed by periodic "grab" samples taken through air lock ports at four locations on the containment vessel wall. In addition, clusters of sampling filters with remote operated solenoid valves were located at ten different locations throughout the atmosphere. Besides the suspended mass concentration samples, measurements were made of particle size distribution (by cascade impactors), aerosol chemical composition, particle mobility,

15th DOE NUCLEAR AIR CLEANING CONFERENCE

and instantaneous settling rates (by deposition coupons). Electron microscope grids were exposed and convection current velocity was measured. Temperature, pressure and gas analysis data were recorded on stripchart recorders and on a 100-channel digital data logger.

The experimental aerosol measurements were made with decreasing frequency over a five-day period of time. Then a ventilation fan was started to prepare for personnel entry and the internal samplers and integral deposition trays were retrieved. Figure 3 is a view of the vessel interior at the time of first entry during AB1. Next, the burn pan with the partially oxidized sodium was removed, weighed, and its contents sampled. A patch of vertical wall surface was decontaminated and the washings analyzed for sodium content. The vessel was then washed by a series of water sprays, beginning with the bottom head, then the vertical walls, then the top head. Finally, steam was injected for several days to clear all crevices by condensation. The volume of each wash was measured and analyzed for sodium concentration to enable a sodium mass balance to be made.

The filter samples and electron microscope grids were protected from exposure to ambient atmosphere by special holders and techniques. The filter papers were weighed to obtain total mass and then analyzed for sodium content by acid titration or flame emission spectroscopy.

III. Experimental Results

Containment Response

The atmosphere within the containment vessel was reasonably well mixed at all times excluding, of course, the region near the surface of the sodium pool and in the plume where mixing occurred. This conclusion was reached by noting that the standard deviation from the mean bulk gas temperature was <5% of the mean and that the suspended mass concentration at ten locations agreed within $\pm 10\%$ during the sodium fire period and within $\pm 40\%$ at long times. The gas composition at two elevations 12 m apart also agreed closely. The oxygen concentration decreased by 5.1% in AB1, 4.2% in test AB2. The containment temperature and pressure are plotted in Figures 4 and 5 for tests AB1 and AB2, respectively.

An attempt was made to measure the convection current velocity near the wall by means of a thermopile-type anemometer inserted near the vessel mid-elevation. A maximum vertical velocity of 1.0 ± 0.3 m/s was measured in both tests at a distance of 25-50 mm from the wall. The highest velocities occurred approximately 20 minutes after the spill in test AB1 and near the end of the sodium fire period during the steam release test AB2. Difficulty was experienced in making this measurement due to deposition of aerosol on the anemometer probe. Very frequent cleaning was required.

Sodium Fire and Aerosol Generation

The post-test sodium mass balance is given in Table II. Sodium recovered in the water washes accounts for the deposited aerosol mass, since it is reasonably certain that no material escaped from the burn pan except as an aerosol. The sodium oxidation rate was nearly identical for the two tests, averaging 34 kg Na/hr m^2 . Likewise, the

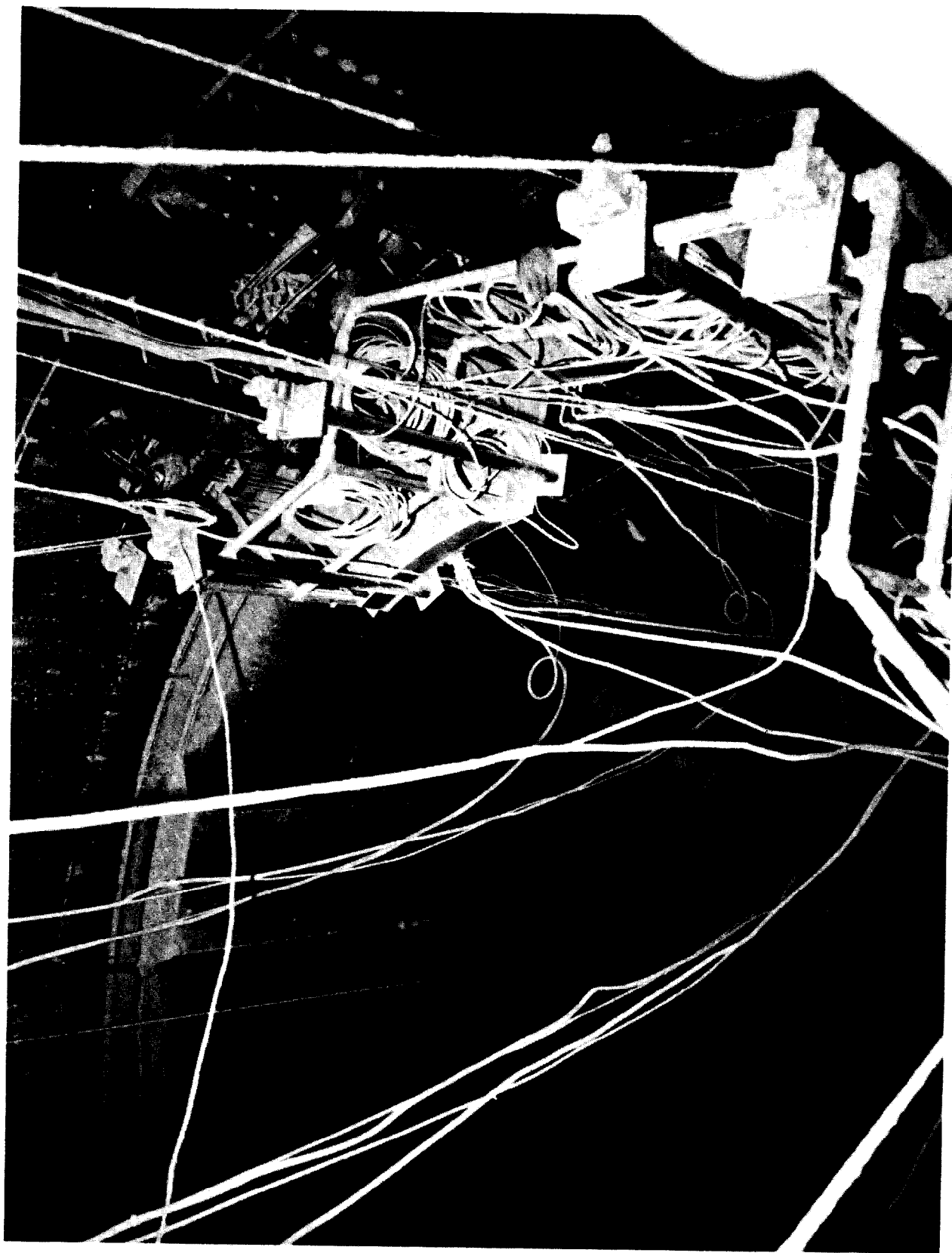


Figure 3. View of vessel interior showing deposited aerosol—test ABL.

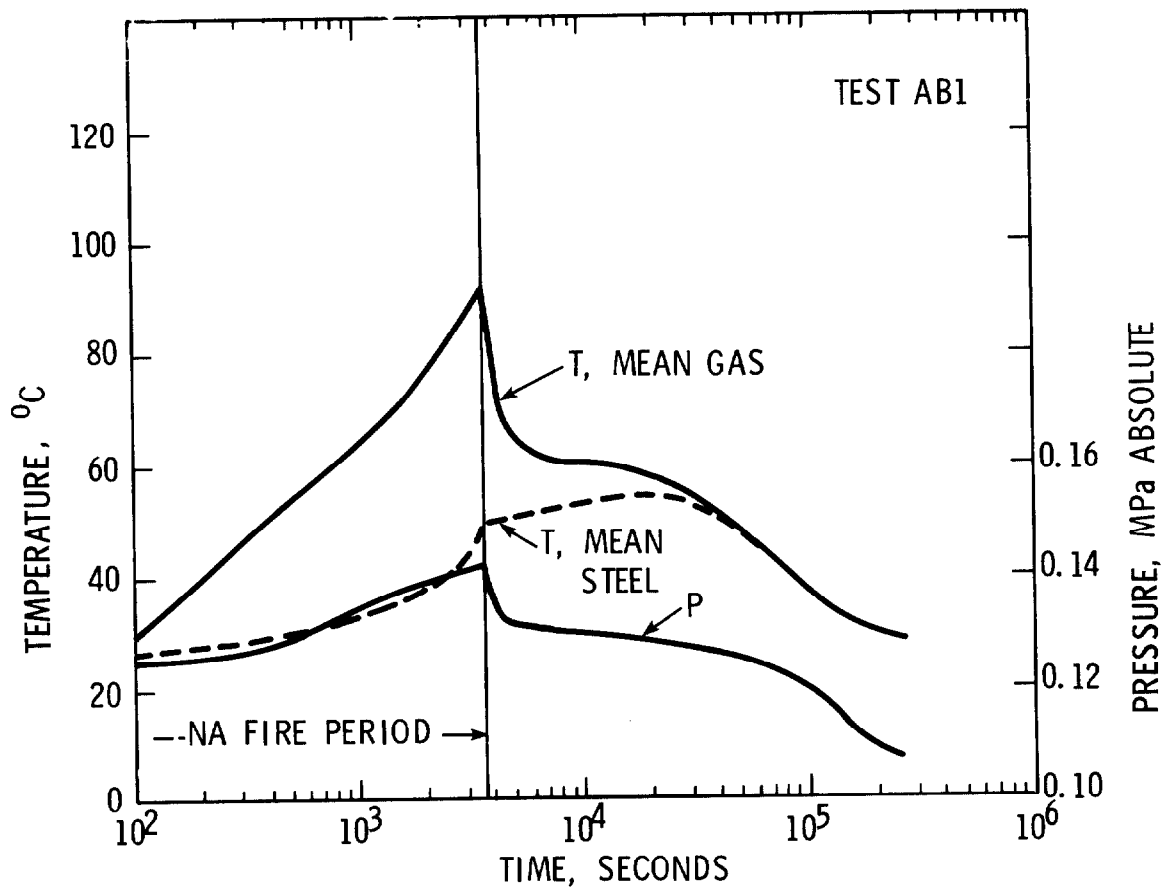


Figure 4. Containment temperature and pressure—test AB1.

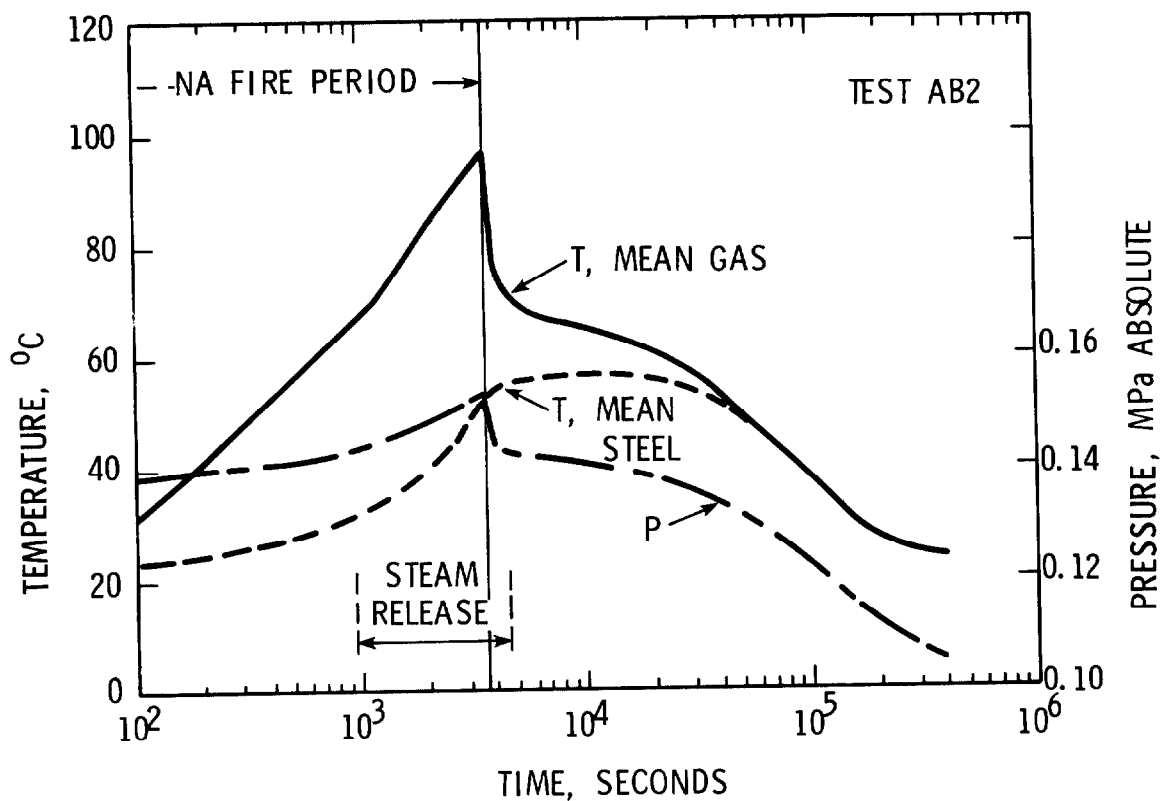


Figure 5. Containment temperature and pressure—test AB2.

15th DOE NUCLEAR AIR CLEANING CONFERENCE

Table II. Sodium mass balance.

	kg Na	
	Test AB1	Test AB2
<u>Delivered to CV</u>	409	472
<u>Accounted for in CV</u>		
Metallic Na in burn pan	256	326
Oxidized Na in burn pan	117	108
CV water washes	39.8	38.6
Samples	0.2	0.2
Leaked (estimate)	0.02	0.02
Total accounted for (+15%)	413.00	473.00

fractions of oxidized sodium released as an aerosol were nearly the same, averaging 0.26. These observations show that the presence of a source of water vapor in the atmosphere did not affect the sodium oxidation kinetics or the aerosol release fraction significantly. These observations are summarized in Table III.

Table III. Sodium oxidation and aerosol release.

	Test AB1	Test AB2
Mass of sodium reacted, kg	153	146
Average oxidation rate, kg Na/hr m ²	34.8	33.2
Total aerosol mass release, kg Na	40.0	38.8
Average aerosol release rate, kg Na/hr m ²	8.95	8.68
Average aerosol mass source, kg Na/s	0.0111	0.0108
Fraction of oxidized Na released as aerosol	0.261	0.266

Sodium recovery by selective post-test washing of the vessel surfaces showed that approximately 7.3% of the aerosol deposited on vertical surfaces, while 92.7% settled on horizontal surfaces in each test. All horizontal surfaces were effective for collecting aerosol by settling, even surfaces sheltered by overhanging ledges and platforms.

The visibility within the vessel was estimated by observations of visual range made through two viewing windows. The results, shown in Figure 6, are in good agreement with those reported by Reist and Hinds⁽¹⁴⁾ for sodium burning in a 90 m³ cell.

Aerosol Chemical Composition

Samples of the suspended aerosol were taken on Teflon membrane filters and protected from laboratory air until analyzed for chemical composition by a combination of x-ray diffractometry, infrared spectroscopy and wet chemistry. The chemical form of the aerosol in test AB1 is listed in Table IV for several times during the test and for the composite floor deposit. The chemical composition changed continually during the test as reactions occurred with the O₂, H₂O and CO₂ in the atmosphere. Shortly after the sodium spill the aerosol was predominantly NaOH, formed by reaction of sodium oxide aerosol particles with the ambient humidity in the atmosphere. The initial 10°C dew point atmosphere in test AB1 contained 9.0 kg of water vapor,

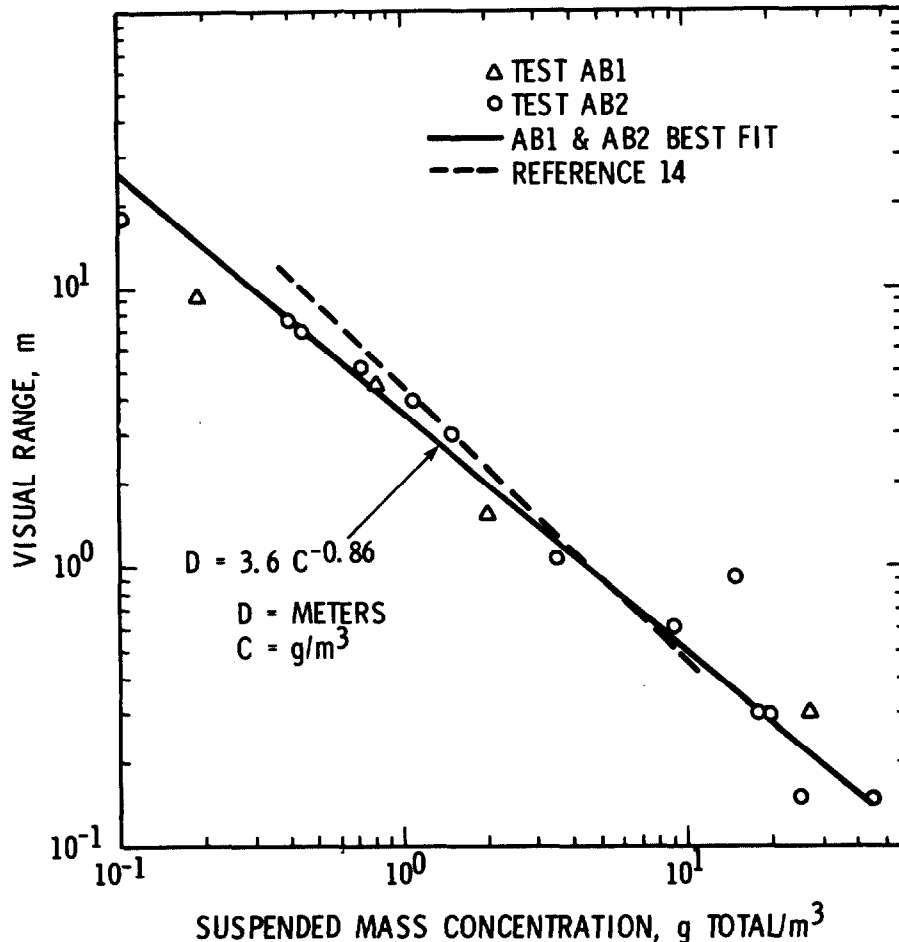


Figure 6. Visual range in a closed vessel during a sodium pool fire.

sufficient to convert half of the released sodium to NaOH. In test AB2 the aerosol was completely converted to NaOH with excess water of hydration and solution. The average composition of the AB2 aerosol was equivalent to a 60 wt% solution of NaOH.

Approximately 75 filter papers taken from four different locations during each test were protected from laboratory air until weighed to obtain total mass. The samples were then analyzed for sodium content and the mass fraction of sodium in the suspended aerosol was calculated and plotted as a function of time in Figure 7. The effect of reactions with the atmosphere is displayed clearly. Analysis for only sodium could lead to significant errors in total mass.

A 2-g sample of the composite settled "dry" aerosol was exposed to the laboratory air (35% relative humidity) and its weight and volume measured as a function of time. Within about 30 hr the weight had doubled and gas bubbles had formed. The color changed from yellow-tan to white. The bulk volume increased by a factor of approximately 15 due to the presence of the gas bubbles. Continued exposure to room air caused the sample to lose weight and form a hard crust of sodium carbonate.

15th DOE NUCLEAR AIR CLEANING CONFERENCE

Table IV. Aerosol chemical analysis - test AB1.

(a)	Mass Fraction				
	Suspended Aerosol ^(b)				Composite ^(c)
	Sample S1 t=16 min	S2 t=46 min	S3 t=190 min	S4 t=610 min	Sample S5 t=5d
Na ₂ O ₂	0.150	0.560	0.430	0.350	0.273
Na ₂ CO ₃	0.029	0.004	0.018	0.061	0.009
NaH	0.0001	0.007	0.0011	0.011	0.0008
NaOH	0.821	0.429	0.479	0.421	0.670
H ₂ O	0.0	0.0	0.072	0.097	0.047
Total	1.0000	1.0000	1.0000	1.0000	1.0000
Total Na	0.573	0.585	0.538	0.519	0.551
Total H	0.0205	0.011	0.020	0.023	0.022
Total C	0.0033	0.0005	0.0021	0.0069	0.0011

(a) Na₂O₂, Na₂CO₃, NaH and Total Na analyzed by wet chemistry and infrared spectroscopy. NaOH and H₂O calculated. Na₂O not detected by x-ray diffraction.

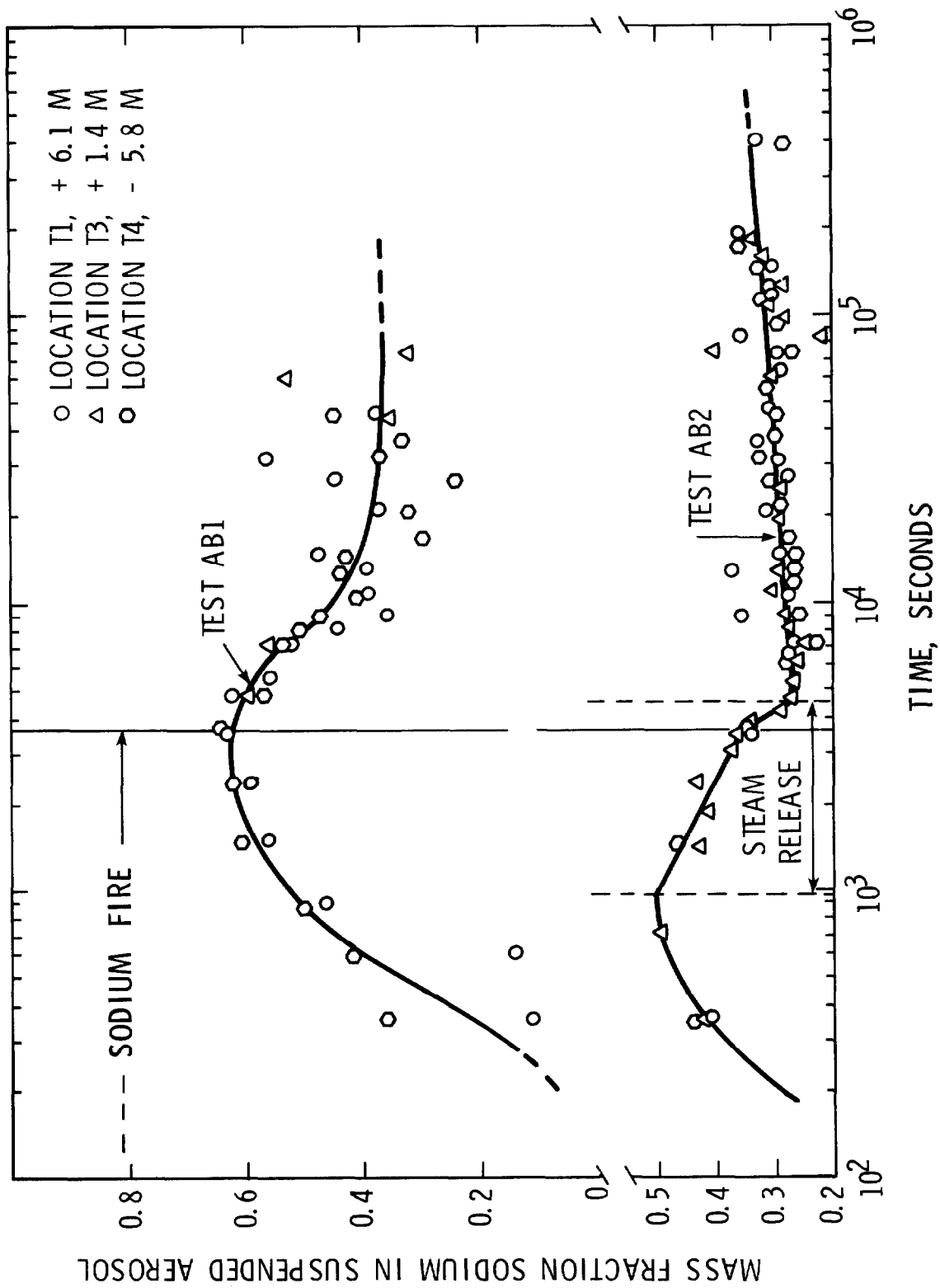
(b) Material collected on membrane filter at stated time.

(c) Floor deposit obtained at end of test.

Suspended Mass Concentration

The concentrations of suspended mass at various times are listed in Tables V and VI for tests AB1 and AB2, respectively. The figures in the tables are mean values of samples taken concurrently at four locations from high, low and central regions in the containment atmosphere. The standard deviation from the mean is also shown. Individual measurements are believed accurate to ± 15%. The concentrations are reported in two ways—as total mass and as sodium. The data of Tables V and VI are plotted as a function of time in Figures 8 and 9 for total mass. The maximum concentrations of suspended sodium were 15 and 12 g/m³ for tests AB1 and AB2, respectively. The maximum concentrations of total mass were 22 and 34 g/m³.

As soon as the burn pan lid was closed, stopping the aerosol release, the concentrations decreased rapidly with ever increasing half times. The concentration of dry aerosol in test AB1 decreased more rapidly than the wet AB2 aerosol after the source was terminated, but the wet aerosol was removed more rapidly during the source period. The overall result was that the attenuation factor for suspended sodium mass available for leakage was lower in the wet test than in the dry test. This is displayed graphically in Figure 10. The attenuation factor was calculated by integrating numerically the observed concentration over the time period of interest and dividing by the product of the release concentration and time. The attenuation factor is a multiplier in evaluating the mass available for leakage to the environs. Figure 10 shows that the addition of steam was beneficial, with 25% greater attenuation at 2 hr and 15% greater at 5 days. Although these differences are not great, it is important to know that the effect is beneficial rather than harmful because water vapor would be present to a significant extent in many postulated accidents.



HEDL 7806-14.6

Figure 7. Mass fraction of sodium in suspended aerosol.

15th DOE NUCLEAR AIR CLEANING CONFERENCE

Table V. Suspended mass concentration - test AB1.

Time (a) sec	Suspended mass concentration, g/m ³ (c)			
	Sodium		Total Mass	
3.6 (2)	5.62 (0)	± 9.0 (-1)	2.7 (1)	± 1.3 (1)
6.0 (2)	1.12 (1)	± 5.0 (0)	2.8 (1)	± 1.4 (1)
9.0 (2)	1.42 (1)	± 8.3 (-1)	2.8 (1)	± 3.5 (0)
1.5 (3)	1.32 (1)	± 2.1 (0)	2.3 (1)	± 4.0 (0)
1.8 (3)	1.30 (1)	± 2.2 (-1)	2.2 (1)	± 1.5 (0)
2.4 (3)	1.60 (1)	± 4.5 (0)	2.6 (1)	± 7.5 (0)
3.1 (3)	1.54 (1)	± 8.4 (-1)	2.5 (1)	± 2.1 (0)
3.6 (3)	1.82 (1)	± 4.4 (0)	2.9 (1)	± 7.3 (0)
4.2 (3)	8.25 (0)	± 2.7 (-1)	1.3 (1)	± 1.0 (0)
4.8 (3)	6.35 (0)	± 1.8 (0)	1.0 (1)	± 2.9 (0)
5.4 (3)	4.30 (0)	± 1.1 (0)	7.4 (0)	± 2.0 (0)
6.3 (3)	2.09 (0)	± 1.3 (-1)	3.7 (0)	± 3.5 (-1)
7.2 (3)	1.80 (0)	± 5.1 (-1)	3.4 (0)	± 1.0 (0)
8.1 (3)	1.02 (0)	± 2.7 (-1)	2.0 (0)	± 5.7 (-1)
9.0 (3)	7.16 (-1)	± 1.4 (-1)	1.5 (0)	± 3.3 (-1)
1.1 (4)	4.54 (-1)	± 5.9 (-2)	1.0 (0)	± 1.7 (-1)
1.3 (4)	3.17 (-1)	± 3.6 (-2)	7.5 (-1)	± 1.5 (-1)
1.5 (4)	2.17 (-1)	± 4.8 (-2)	5.3 (-1)	± 1.4 (-1)
1.6 (4)	1.52 (-1)	± 1.2 (-2)	3.8 (-1)	± 6.4 (-2)
1.75 (4)	1.55 (-1)	± 5.0 (-3)	4.0 (-1)	± 7.3 (-2)
1.93 (4)	8.95 (-2)	± 7.4 (-3)	2.3 (-1)	± 4.5 (-2)
2.09 (4)	9.89 (-2)	± 4.9 (-4)	2.6 (-1)	± 4.8 (-2)
2.60 (4)	5.60 (-2)	± 1.7 (-2)	1.5 (-1)	± 5.3 (-2)
3.20 (4)	2.78 (-2)	± 1.1 (-2)	7.5 (-2)	± 3.3 (-2)
3.80 (4)	2.48 (-2)	± 4.1 (-3)	6.7 (-2)	± 3.5 (-2)
4.60 (4)	1.50 (-2)	± 9.8 (-4)	4.0 (-2)	± 8.0 (-3)
6.09 (4)	7.46 (-3)	± 1.0 (-4)	2.1 (-2)	± 4.1 (-3)
7.38 (4)	5.97 (-3)	± 1.8 (-3)	1.7 (-2)	± 6.1 (-3)
8.70 (4)	2.52 (-3)	± 8.5 (-4)	7.0 (-3)	± 2.7 (-3)
1.03 (5)	2.19 (-3)	± 3.6 (-4)	6.1 (-3)	± 1.6 (-3)
1.08 (5)	1.55 (-3)	± 1.4 (-5)	4.3 (-3)	± 8.4 (-4)
1.19 (5)	1.33 (-3)	± 3.5 (-5)	3.7 (-3)	± 6.5 (-4)
1.27 (5)	1.14 (-3)	± 2.1 (-4)	3.2 (-3)	± 8.5 (-4)
1.35 (5)	1.11 (-3)	± 2.0 (-4)	3.1 (-3)	± 8.2 (-4)
1.49 (5)	7.74 (-4)	± 5.8 (-5)	2.2 (-3)	± 4.6 (-4)
1.82 (5)	5.80 (-4)	± 1.5 (-4)	1.6 (-3)	± 5.2 (-4)
4.17 (5)	6.45 (-5)	± 2.1 (-6)	1.8 (-4)	± 3.3 (-5)
4.27 (5)	1.78 (-2)	± 3.5 (-3)	4.9 (-2)	± 1.4 (-2)
4.42 (5) (b)	1.05 (-2)	± 3.0 (-3)	2.9 (-2)	± 1.0 (-2)

(a) Numbers in parentheses are exponents of base 10; e.g., read 1.05 (-2) as 1.05 x 10⁻².

(b) Ventilation fan started at 4.25 (5) sec.

(c) Mean of 4 sampling locations.

15th DOE NUCLEAR AIR CLEANING CONFERENCE

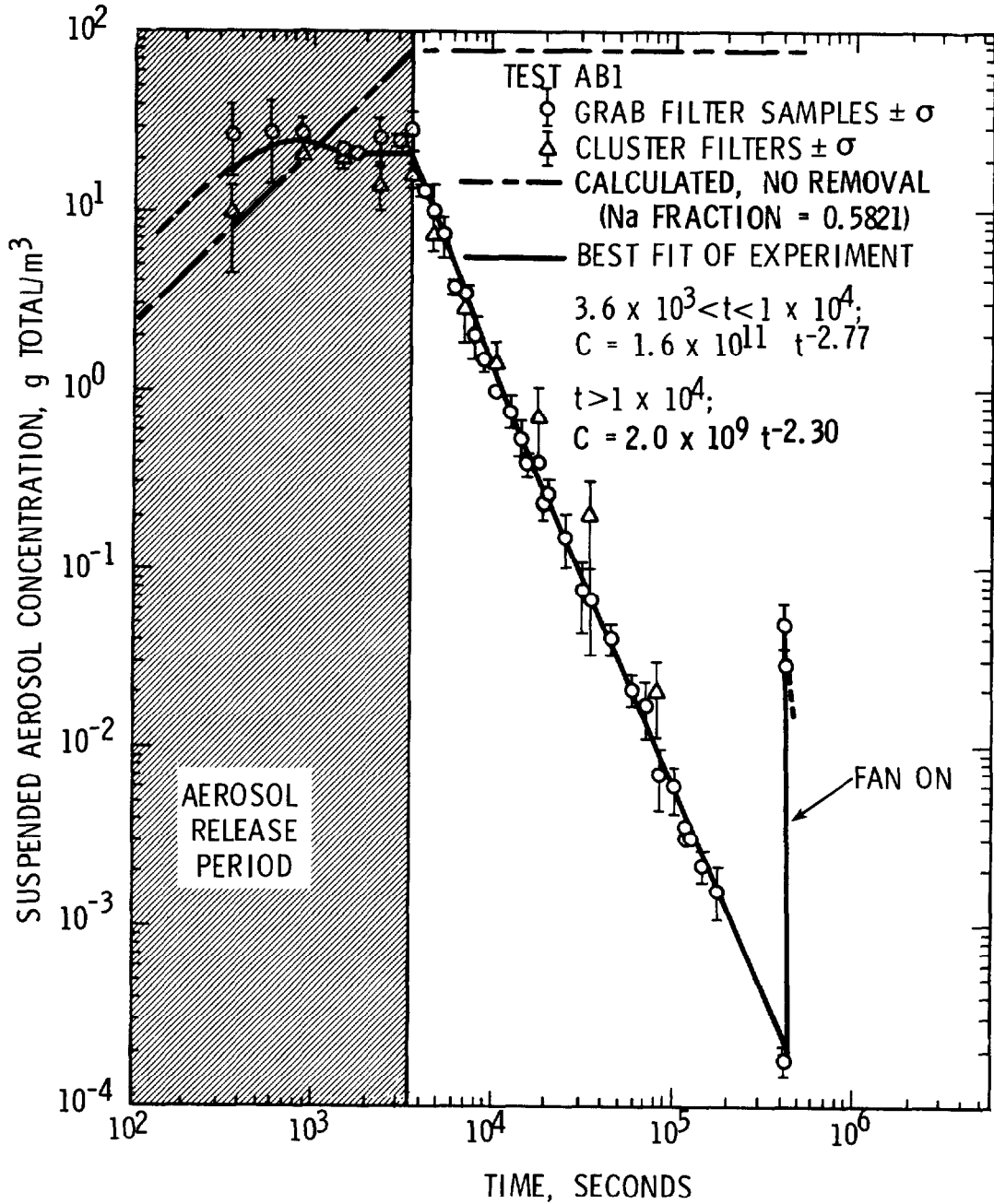
Table VI. Suspended mass concentration - test AB2.

Time ^(a) sec	Suspended mass concentration, g/m ³ ^(c)	
	Sodium	Total Mass
3.60 (2)	7.32 (0) ± 4.3 (0)	1.74 (1) ± 1.0 (1)
7.20 (2)	1.09 (1) ± 1.5 (0)	2.22 (1) ± 3.6 (0)
1.02 (3)	7.30 (0) ± 1.5 (0)	1.49 (1) ± 3.3 (0)
1.44 (3)	9.83 (0) ± 1.3 (0)	2.18 (1) ± 3.5 (0)
1.80 (3)	8.97 (0) ± 1.5 (0)	2.22 (1) ± 4.2 (0)
2.40 (3)	1.09 (1) ± 2.9 (0)	2.73 (1) ± 7.8 (0)
3.24 (3)	1.11 (1) ± 1.8 (0)	2.85 (1) ± 5.5 (0)
3.60 (3)	1.26 (1) ± 2.5 (0)	3.60 (1) ± 8.2 (0)
4.32 (3)	9.11 (0) ± 2.5 (0)	3.14 (1) ± 3.4 (0)
4.80 (3)	6.22 (0) ± 1.1 (0)	2.30 (1) ± 4.8 (0)
5.40 (3)	4.29 (0) ± 9.1 (-1)	1.59 (1) ± 3.8 (0)
6.30 (3)	3.26 (0) ± 6.1 (-1)	1.21 (1) ± 2.6 (0)
7.20 (3)	2.24 (0) ± 2.5 (-1)	8.00 (0) ± 1.4 (0)
8.20 (3)	9.92 (0) ± 5.9 (-1)	6.86 (0) ± 2.3 (0)
9.00 (3)	1.61 (0) ± 6.0 (-1)	5.75 (0) ± 2.3 (0)
1.13 (4)	6.58 (-1) ± 2.3 (-1)	2.35 (0) ± 8.9 (-1)
1.29 (4)	3.03 (-1) ± 3.0 (-2)	1.08 (0) ± 1.9 (-1)
1.47 (4)	2.86 (-1) ± 7.2 (-2)	1.02 (0) ± 3.0 (-1)
1.63 (4)	2.53 (-1) ± 9.0 (-3)	9.05 (-1) ± 1.3 (-1)
1.94 (4)	1.88 (-1) ± 2.2 (-2)	6.48 (-1) ± 1.2 (-1)
2.53 (4)	1.20 (-1) ± 1.1 (-2)	4.00 (-1) ± 6.5 (-2)
3.21 (4)	7.07 (-2) ± 2.5 (-3)	2.35 (-1) ± 3.2 (-2)
3.75 (4)	4.90 (-2) ± 5.6 (-3)	1.63 (-1) ± 2.9 (-2)
4.50 (4)	3.28 (-2) ± 3.6 (-3)	1.09 (-1) ± 1.9 (-2)
6.06 (4)	2.05 (-2) ± 2.1 (-3)	6.61 (-2) ± 1.1 (-2)
7.35 (4)	1.57 (-2) ± 1.2 (-3)	5.06 (-2) ± 9.0 (-3)
8.61 (4)	1.08 (-2) ± 9.1 (-4)	3.48 (-2) ± 6.3 (-3)
9.60 (4)	7.63 (-3) ± 2.2 (-3)	2.38 (-2) ± 7.8 (-3)
1.10 (5)	6.05 (-3) ± 5.1 (-4)	1.89 (-2) ± 3.3 (-3)
1.28 (5)	4.95 (-3) ± 1.1 (-3)	1.55 (-2) ± 4.2 (-3)
1.46 (5)	3.17 (-3) ± 2.9 (-4)	1.02 (-2) ± 1.8 (-3)
1.73 (5)	2.15 (-3) ± 3.9 (-4)	6.72 (-3) ± 1.6 (-3)
1.91 (5)	1.50 (-3) ± 1.4 (-4)	4.69 (-3) ± 8.6 (-4)
4.02 (5)	1.72 (-4) ± 1.1 (-5)	5.06 (-4) ± 8.0 (-5)
4.43 (5) ^(b)	<3.0 (-5)	<8.8 (-5)

(a) Numbers in parentheses are exponents of base 10.

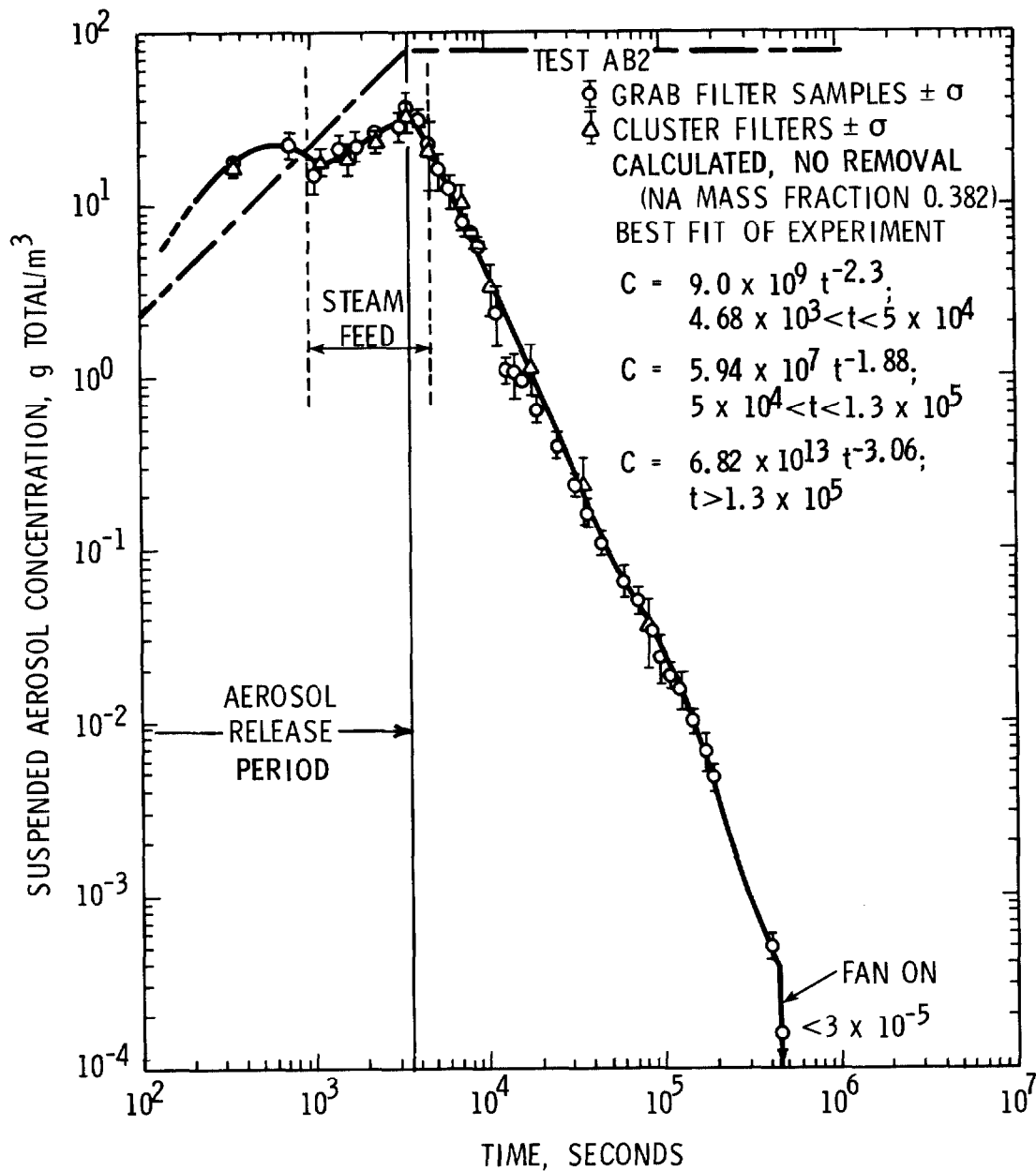
(b) Ventilation fan started at 4.42 (5) sec.

(c) Mean of four sampling locations.



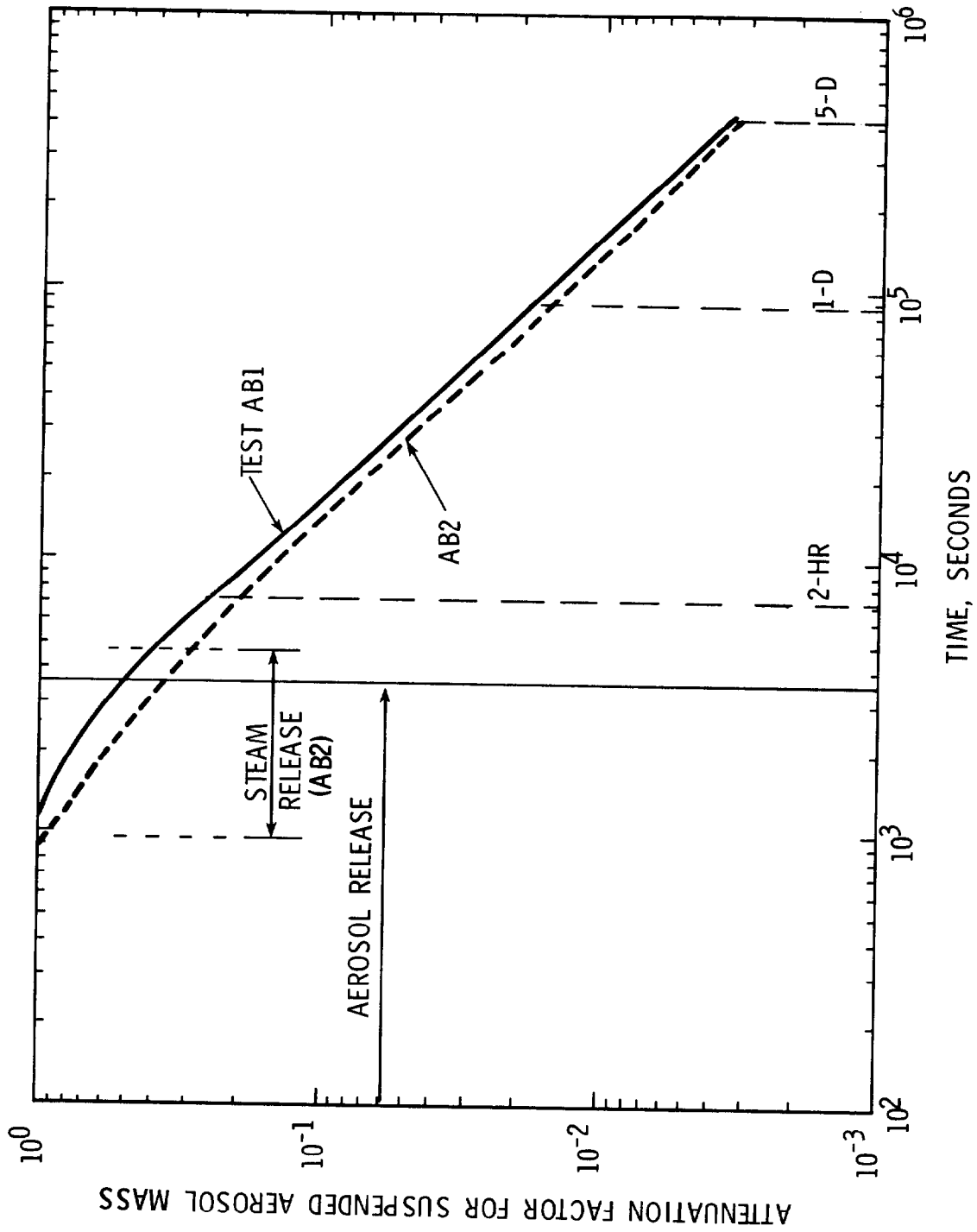
HEDL 7806-14.8

Figure 8. Suspended mass concentration—test AB1.



HEDL 7806-14.7

Figure 9. Suspended mass concentration—test AB2.



HEDL 7806-14.5

Figure 10. Attenuation factors for suspended mass concentration available for leakage.

Aerosol Physical Properties

Particle Size Distribution. The aerodynamic size distribution of the suspended aerosol mass was measured by inserting two types of cascade impactors directly into the containment atmosphere in a horizontal position. Although there was no inlet tube, some deposition did occur in the nose sections upstream of the first stages. This material was neglected in analyzing the data. The two types of cascade impactors were an eight-stage multi-circular jet type (Anderson Mark III) and a six-stage multi-rectangular jet type (Sierra Model 226). A typical example of the data plotted on log-normal paper as the stage cut-off diameter vs. the mass fraction penetrating that stage is shown in Figure 11. If the particle distribution is log-normal, a straight line should be obtained and the two major parameters of particle size distribution can be obtained: the aerodynamic mass median diameter, AMMD, and the geometric standard deviation, σ_g . Most of the 44 cascade impactor samples taken in these tests gave good approximations to a straight line on log-normal paper, though a few showed significant deviations from it.

Samples were taken simultaneously from high and low containment locations. No consistent difference was found for the two locations, which supports the conclusion made earlier that the gas space was well mixed. The results for the upper and lower samples were averaged and plotted as a function of time in Figures 12 and 13 for the AMMD and σ_g , respectively. The rectangular jet impactor gave a significantly larger median diameter than the circular jet impactor, especially at early times when the particles were larger. The reason for this discrepancy has not been resolved. Possible, as suggested by Allen and Briant⁽¹⁵⁾, this is caused by interception of very large particles of lower than average density on the first few stages, but it is not known why a rectangular geometry would accentuate this effect.

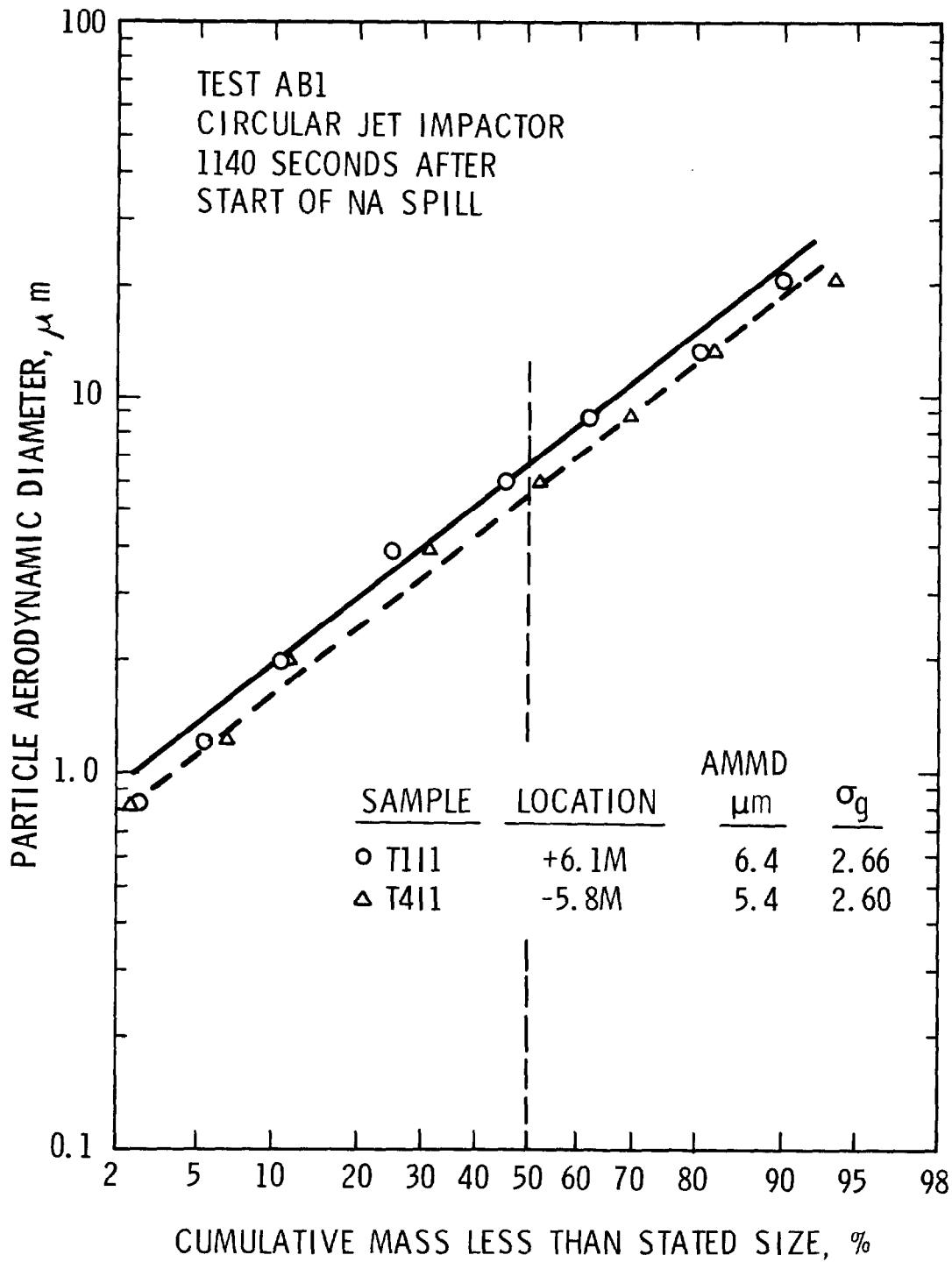
A comparison of the cascade impactor results with the settling diameter, d_s , calculated from the rate of depletion of airborne concentration is given in Figures 14 and 15. If the distribution is log-normal, the aerodynamic settling diameter can be calculated from the cascade impactor by equation (1).

$$d_s = \text{AMMD} \exp(\ln^2 \sigma_g) \quad (1)$$

The aerodynamic settling diameters were also calculated from the airborne concentration curves (Figures 8 and 9) by differentiating the curves and equating with the Stokes settling removal term. This neglects wall plateout, which is reasonable in view of the fact that 93% of the mass settled and only 7% plated. Thus,

$$\frac{dC}{dt} = - \frac{u_t A_s C}{V} \quad (2)$$

where C = time dependent suspended mass concentration
 u_t = terminal settling velocity
 A_s = horizontal surface
 V = gas volume.



HEDL 7806-14.2

Figure 11. Typical cascade impactor data plot on log-normal paper.

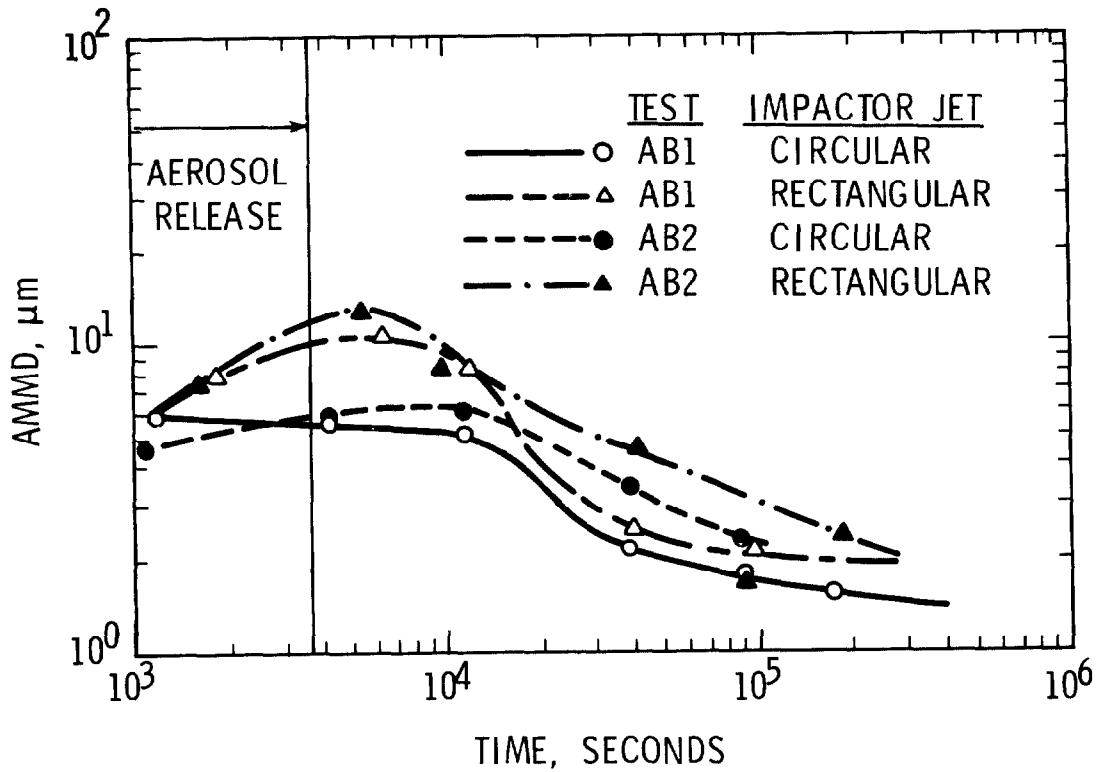


Figure 12. Aerodynamic mass median diameter of suspended particles.

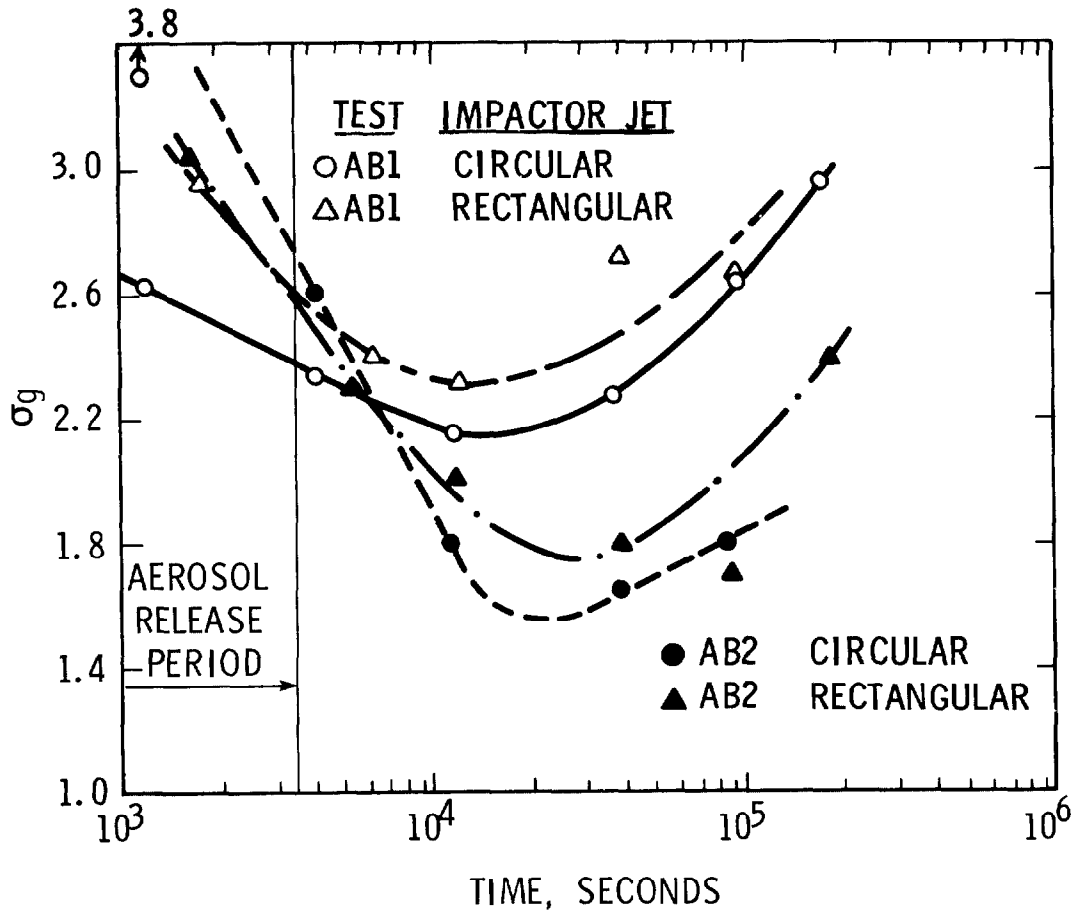


Figure 13. Standard geometric deviation of suspended particle size.

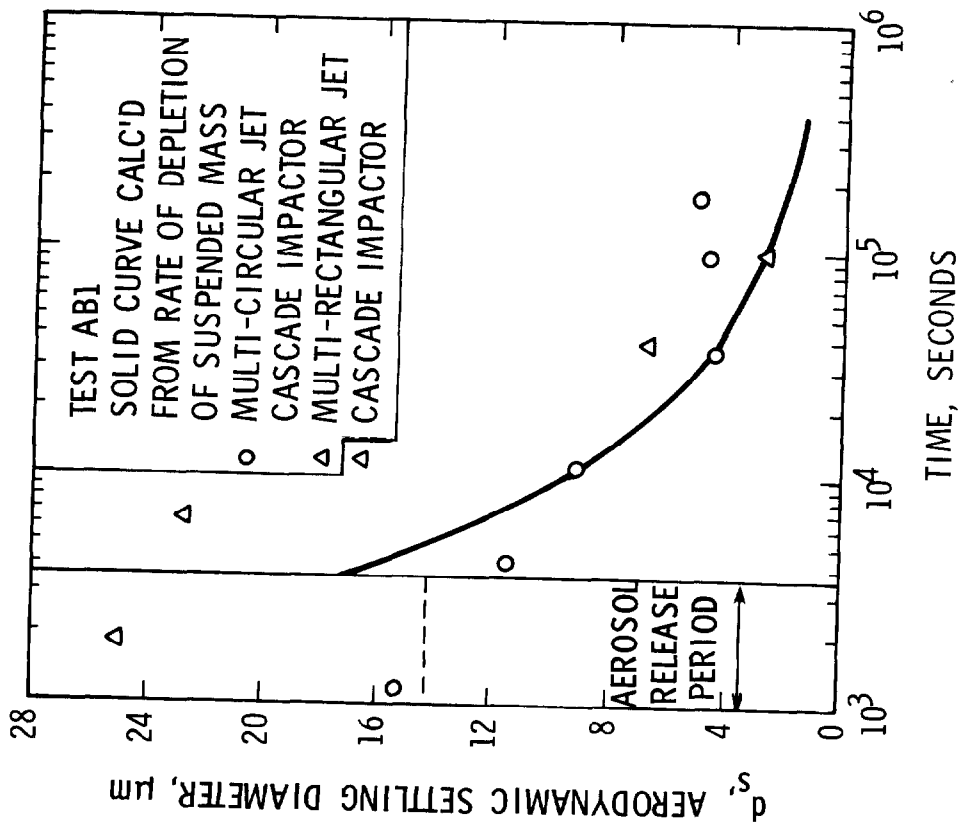


Figure 14. Comparison of aerodynamic settling diameters from cascade impactor and airborne depletion data—test AB1.

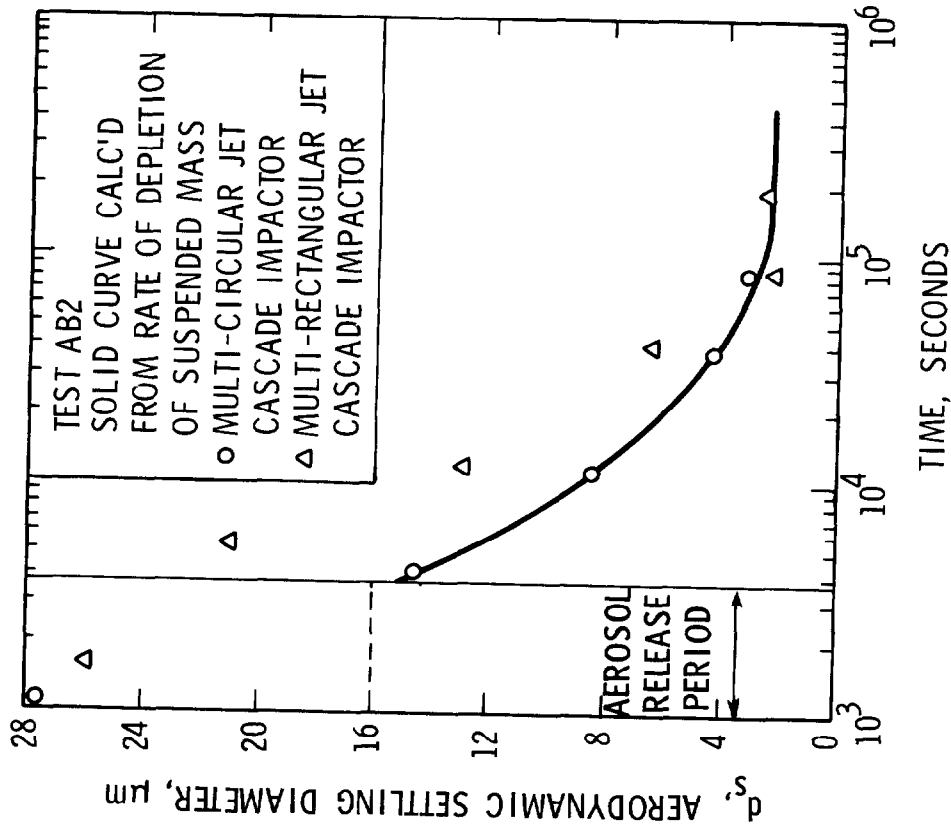


Figure 15. Comparison of aerodynamic settling diameter from cascade impactor and airborne depletion data—test AB2.

HEDL 7806-14.1

15th DOE NUCLEAR AIR CLEANING CONFERENCE

The settling velocity, u_t , was calculated by equation (2) and the settling diameter calculated from Stoke's law:

$$d_s = \left(\frac{18 \mu_f u_t}{g \rho_p} \right) \quad (3)$$

where μ_f = fluid viscosity
 g = acceleration due to gravity
 ρ_p = effective particle density.

In using equation (3), the particles were assumed to be spherical with unit density in order to compare with the similar assumption used for the cascade impactor data. Figures 14 and 15 show that fairly good agreement was obtained with the circular jet impactor.

Particle Density. The bulk density of the composite deposited aerosol materials recovered from the floor after test AB1 was determined by weight and volume measurements to be 0.33 ± 0.03 g/cm³. This agrees well with the value of 0.32 reported by First and Yusa⁽¹⁹⁾. After tapping 100 times in a graduated cylinder, the bulk density increased to 0.60 ± 0.10 g/cm³. The material density of the AB1 material was not determined, but a similar sample with the same nominal composition (test AB3) was found to have a material density of 2.3 ± 0.3 g/cm³ by immersion in acetone. The handbook value, based on the analysis of sample S5 in Table IV is 2.30 g/cm³.

No density measurements were made of the aerosol material in test AB2, but it was believed to have been liquid during most of the test. At the end of the test 13.4 liters of 65 wt% NaOH solution was drained from the vessel. However, portions of the vessel surface had a deposit of solid material. The agglomerated aerosol particles probably contained some void space due to oxygen gas emitted by the reaction of Na₂O₂ and water and to the insolubility of the small amounts of sodium carbonate which formed. No direct measurements were made of the particle density.

Electron Microscope. Electron microscope grids were exposed briefly to the containment atmosphere at various times. They were protected from exposure to ambient air by withdrawing the holder into an o-ring sealed protector before removing it from the containment vessel. Figure 16 shows some typical photo micrographs of samples taken at four times during test AB1. The indices shown in the figure are set at 10 μ m. The projected diameter of the primary particles ranged from 0.1 to 0.5 μ m. The settled agglomerates were irregular shapes of approximately 1-5 μ m diameter at 8 minutes. They had grown to 1-30 μ m diameter spheres by the end of the sodium fire. The larger particles appeared to contain voids, but this observation is suspect because the vacuum in the transmission electron microscope may have altered the geometry of the particles. Shadowing techniques were not used, but stereoscopic examination showed the particles to be approximate spheres.

AEROSOL PARTICLES AT 8 MINUTES DURING TEST ABI



Figure 16a. Time 8 min.

AEROSOL PARTICLES AT 56 MINUTES DURING TEST ABI

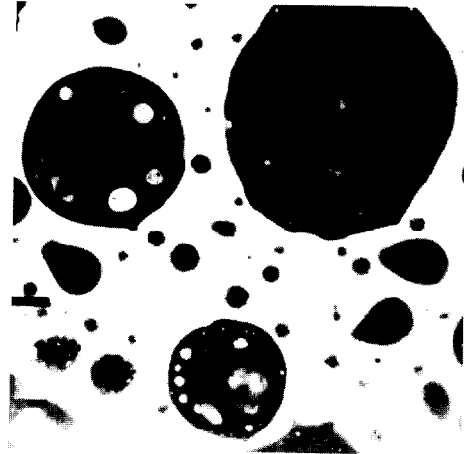


Figure 16b. Time 56 min.

AEROSOL PARTICLES AT 190 MINUTES DURING TEST ABI

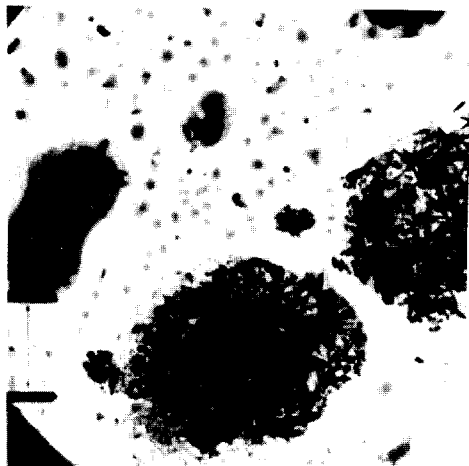


Figure 16c. Time 190 min.

AEROSOL PARTICLES AT 25 HR DURING TEST ABI



Figure 16d. Time 1500 min.

Figure 16. Electron photomicrographs of gravity settled particles at various times in test ABI.

15th DOE NUCLEAR AIR CLEANING CONFERENCE

Electric Charge

Particle charge distributions were measured by the use of a parallel plate charge analyzer of the type described by Gillespie and Langstroth⁽¹⁶⁾. For both tests the sample flow was started 30 minutes after the sodium spill and lasted for 10 minutes. Filtered sheath air flow at 11 cm³/sec was recirculated by a small diaphragm pump and a net sample flow of 2 cm³/sec was bled through the analyzer and its backup filter. The apparatus was operated at 10,000 V for AB1 and 4000 V for test AB2. Any particle with a mobility greater than 7.7×10^{-6} and 1.9×10^{-5} cm²/volt sec, respectively, would be collected on one of the plates. Table VII gives the distribution.

Table VII. Particle charge distribution.

	<u>AB1</u>	<u>AB2</u>
Mass fraction on positive plate	0.46	0.07
Mass fraction on negative plate	0.45	0.07
Mass fraction on backup filter	0.09	0.86
Limiting mobility, cm ² /v-5	7.7×10^{-6}	1.9×10^{-5}
Equivalent charge on 7- μ m dia. particle	7	18
Equivalent charge on 1- μ m dia. particle	1	3

The data of Table VII indicate that the "dry" particles in test AB1 had a higher charge than the wet aerosol, but that the net charge was close to zero in both tests.

IV. Discussion and Conclusions

The results of these tests support the following conclusions and generalized observations. The sodium burned at an average rate of 34 kg Na/hr m², releasing 8.8 kg Na/hr m² as aerosol. The presence of a steam source in the atmosphere had no significant effect on the mass release rate. The mean atmosphere temperatures increased by 64.5 and 75.5°C for the dry and wet tests, respectively. The additional heat generated in test AB2 was due to the condensation on and reaction of steam with the aerosol particles.

It is hypothesized that the aerosol particles were formed by reaction of sodium vapor with oxygen within a few centimeters of the sodium pool surface, rapid nucleation to form a high concentration of primary particles in the high temperature plume, and rapid agglomeration to form aggregate particles during the plume rise and dispersal throughout the vessel. Essentially uniform suspended mass concentration was accomplished very quickly, but the few seconds in the high concentration plume caused the particles to grow to diameter of the order of one micrometer by the time they were dispersed.

The aerosol was formed as Na₂O₂ particles in the oxygen-rich atmosphere. As these particles were dispersed throughout the vessel atmosphere, they reacted very rapidly with the water vapor present in the normal air test. Sufficient water vapor was present to convert approximately half of the total released aerosol to NaOH. Within a

15th DOE NUCLEAR AIR CLEANING CONFERENCE

few minutes the aerosol was in the form of sodium hydroxide solution particles. As more Na_2O_2 particles were generated, they agglomerated with the sodium hydroxide particles. Some of the water of dilution in the sodium hydroxide solution particles diffused to the co-agglomerate Na_2O_2 to react to NaOH and release oxygen gas. The released gas caused a volume increase, with corresponding reduction in the effective density of the particle. Some reaction with the CO_2 occurred, but the supply of CO_2 was limited. In the test where additional water vapor was added as steam, sufficient water was available to convert all the aerosol to NaOH with excess water of solution. The overall result in both tests was an aerosol that varied with time in chemical composition, density and shape.

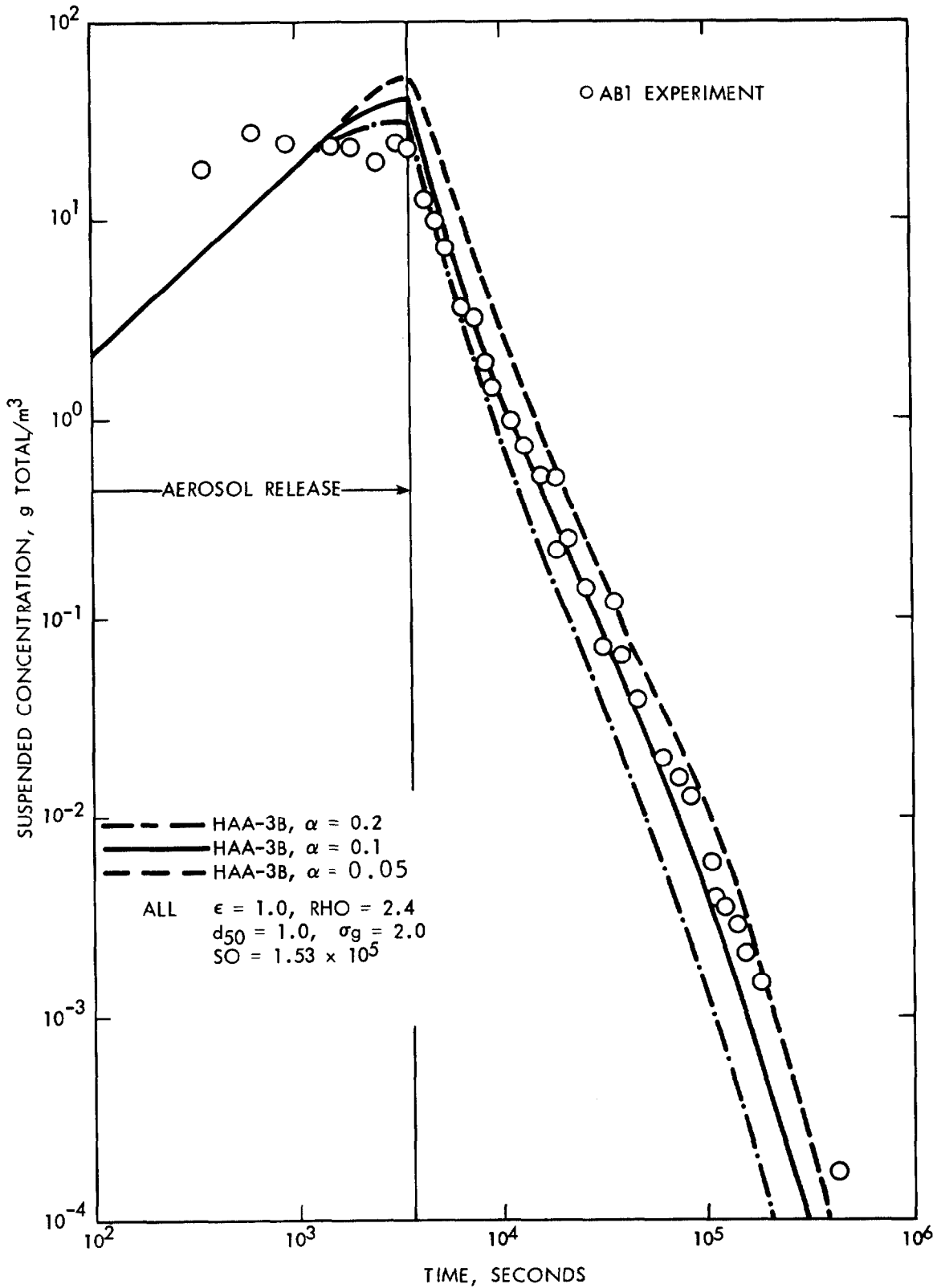
Cascade impactor samples showed that the size distribution of the suspended particles was approximately log-normal. Samples taken later than 24 hr indicated some departure from log-normal. Approximately 7.3% of the released mass was recovered from the vertical walls, while 92.7% settled on horizontal surfaces. All horizontal surfaces collected aerosol by sedimentation, although deposition trays exposed for the entire test put 0.4 m below an overhanging ledge received only ~70% as much as unshadowed trays. This shows that aerosol models should consider all horizontal surfaces, not just the vessel cross section.

No attempt was made in this paper to evaluate specific aerosol behavior models and computer codes. However, it is of interest to note that pre-test predictions of the suspended mass concentration using the HAA-3B⁽¹⁷⁾ and HAARM⁽¹⁸⁾ codes agreed reasonably well with the experiment. One problem encountered in the pre-test predictions was the need for an accurate method to forecast the aerosol mass release rate. Even when conditions are well known, as in the present tests, there was a large uncertainty in the source rate. The HAA-3B code was rerun post-test, using the average experimentally determined source rate. The HAA-3B predictions for suspended mass concentration are compared with experimental results in Figure 17. Good agreement is shown except at the very early times, where the code underpredicts because it does not account for condensation of water vapor. The HAA-3B code predicted that 6.2% of the total release would be plated on walls and 93.8% settled to horizontal surfaces. This compares well with 7.3% and 92.7%, respectively, for the experiments. A more complete evaluation of aerosol codes is underway at HEDL and elsewhere.

It is concluded that the results of these large-scale tests in the CSTF will contribute importantly to increased confidence in the ability to understand and predict nuclear aerosol behavior during accidents in sodium cooled facilities.

V. References

1. M.A. Greenfield, R.L. Koontz and D.F. Hausknecht, "Characterization of Aerosols Produced by Sodium Fires, Vol II, Comparisons of Experiments with a General Equation for the Coagulation of Heterogeneous Aerosols", AI-AEC-12878, Atomic International, October 1969.



HEDL 7806-331.1

Figure 17. Comparison of HAA-3B computer code predictions with experiment.

15th DOE NUCLEAR AIR CLEANING CONFERENCE

2. J.A. Gieseke, R.C. Behn, A.S. Chace, and L.D. Reed, "Analytic Studies of Aerosol Behavior Predictions For Fast Reactor Studies", BMI-1932, Battelle Columbus Laboratories, March 18, 1975.
3. F.L. Horn and A.W. Castleman, Jr., "PuO₂-UO₂-Na Aerosols Produced by Vaporization of Fast Reactor Core Materials", BNL-12757, Brookhaven National Laboratory, August 1968.
4. W.C. Hinds, E.F. Mallove, and M.W. First, "Evaluation of In-Vessel Emergency Air Cleaning Systems For an LMFBR", CONF-760882, p. 927, 14th ERDA Air Cleaning Conference, August 1976.
5. R.E. Adams, T.S. Kress, and L.F. Parsly, Jr., "Sodium Oxide Aerosol Study: NSPP Runs 101-105, Data Record Report", ORNL/NUREG/TM-179, Oak Ridge National Laboratory, April 1978.
6. H.J. Ettinger, W.D. Moss, and H. Busey, "Characteristics of the Aerosol Produced from Buring Sodium and Plutonium", Nuc. Sc. & Eng., 30, pp 1-13 (1967).
7. W.O. Schikarski, "The Aerosol Behavior in LMFBR Accidents: Results of TUNA Experimental Program and Comparison with PARADISEKO Code", Karlsruhe Nuclear Research Center, CONF-760882, p. 885, 14th ERDA Air Cleaning Conference, August 1976.
8. Y. Fruchard et al., "Sodium Fire Studies in France, Safety Tests and Applications on an LMFBR", CEA, Cadarache, CONF-761001, p. 1945, Proceedings of International Meeting on Fast Reactor Safety and Related Physics, October 1976.
9. S. Kitani et al., "Behavior of Sodium Oxide Aerosol in a Closed Chamber", J. Nuc. Sc. & Tech., 10, pp 566-573 (September 1973)
10. J.F. van de Vate et al., "Deposition of Aerosols Formed by HCDA Due to Decay Heat Transport in LMFBR Inner Containment Atmospheres", Netherlands Energy Research Foundation, CONF-761001, p. 1915, Proceedings of International Meeting on Fast Reactor Safety and Related Physics, October 1976.
11. R.K. Hilliard, J.D. McCormack and A.K. Postma, "Evaluation of Air Cleaning System Concepts for Emergency Use in LMFBR Plants", HEDL-TME 76-41, Hanford Engineering Development Laboratory, December 1976.
12. J.D. McCormack and R.K. Hilliard, "Large Scale Air Cleaning Tests in the Containment Systems Experiment", CONF-700816, p. 102, Proceedings of the Eleventh AEC Air Cleaning Conference, August 1970.
13. J.M. Atwood, "Sodium Engineering and Technology Technical Progress Report, July, August, September, 1977", HEDL-TME 77-38, p. 79, December 1977.
14. P.C. Reist and W.C. Hinds, "Optical Properties of Sodium Aerosols", CONF-700816, p. 425, Proceedings of the Eleventh AEC Air Cleaning Conference, August 1970.

15th DOE NUCLEAR AIR CLEANING CONFERENCE

15. M.D. Allen and J.K. Briant, "Characterization of LMFBR Fuel-Sodium Aerosols", BNWL-SA-6481, Battelle Northwest Laboratories, undated.
16. T. Gillespie and G.O. Langstroth, Can. J. Chem, 30, 1056, (1952).
17. R.S. Hubner et al., "HAA-3 User Report", AI-AEC-13088, Atomic International, March 30, 1973.
18. L.D. Reed and J.A. Gieseke, "HAARM-2 Users Manual", BMI-X-665, Battelle Columbus Laboratories, October 31, 1975.
19. M.W. First and H. Yusa, "Heat Transfer of Sodium Compounds Deposited on Surfaces from Aerosols", CONF-700816, p. 423, Proceedings of the Eleventh AEC Air Cleaning Conference, August 1970.

DISCUSSION

SCHIKARSKI: I congratulate you on your fine experiments. I want to make two remarks. In the presence of enough moisture and CO₂ in the air, the reaction to sodium carbonates is fast. This, I guess, agrees with your findings. It is a favourable effect because Na₂CO₃ is not a chemically aggressive material. The change of composition of particles in the vessel affects many parameters assumed to be constant in the codes (HAARM-2, PARADISEKO IIIb, etc.). I think these codes should be improved in that respect.

HILLIARD: Thank you, Dr. Schikarski. I agree that the conversion to carbonate is very rapid when you have water vapor present. I think Jerry McCormack is going to speak on Thursday about some filter loading tests in which we injected carbon dioxide and steam and found it produced sodium carbonate very quickly, just a few minutes. But, in a sealed containment vessel that has a limited supply of carbon dioxide, i.e., no added carbon dioxide, we found an excess of sodium hydroxide. All the carbon dioxide was used up and there was no more available. Therefore, the chemical composition depends on the size of the sodium hydroxide release relative to the vessel size. Your point regarding new input to the codes is certainly relevant. I think that the density and shape of the particles is important. These will be different for dry carbonate compared to moist sodium hydroxide.

15th DOE NUCLEAR AIR CLEANING CONFERENCE

ATTENUATION OF PARTICLES THROUGH LEAK PATHS

by

C. Nelson

R. Johnson

Atomics International Division
Rockwell International
8900 De Soto Avenue
Canoga Park, California 91304

Abstract

Particulates of sodium oxide were passed through narrow leak passages. The particulates impacted on the walls and built up plugs which eventually stopped the flow. Conditions under which plugging occurs were determined. Material which did pass through the leaks was increased in size because of agglomeration on the wall followed by detachment. The data shows that radioactive particulates escaping through leaks following a hypothetical FBR accident will tend to plug the leaks in both the reactor vessel and the containment building. Also, the particulates will generally increase in size so as to be nonrespirable.

I. INTRODUCTION

Gas borne particulates both tend to plug small passages in leak paths and also increase in size following impaction and subsequent detachment from leak-path walls. This behavior mitigates the consequences of hypothetical LMFBR Core Disassembly Accidents (CDA) by reducing the leakage both through reactor head seals and through containment building walls.

A series of tests has been made to assess the proportion of CDA particles in the cover gas escaping through assumed displaced head seals and to assess the quantity and size of the particles which could escape into the containment building.

In a second series of tests, gas containing sodium combustion product aerosols was allowed to leak through capillary-type leak paths to determine the fraction of respirable size particulates which were transmitted. With current building leak rate measurement technology, the limit of leak detection sensitivity is usually assumed to be approximately 0.1 vol % leakage per day at a pressure differential of 0.68 atmosphere for a steel reactor containment building. Assuming the total containment leak is accommodated by a single hole, the size of the leak can be represented by a hole 1 to 2 mm in diameter.

15th DOE NUCLEAR AIR CLEANING CONFERENCE

II. PLUGGING OF HEAD SEAL LEAKAGE PATHS (TEST SERIES 1)

Following a CDA in a LMFBR, the accompanying sodium slug motion would stretch the head tiedown bolts and part of the aerosol mixture* in the cover gas could escape into the reactor containment building through broken seals. Generally, these seals would consist of a sodium filled seal, followed by a series of inflatable elastomer seals. To simulate these seals on a small scale, a multiple bend leak path was constructed, see Figure 1. This leak consisted of a series of small brass chambers having the approximate configuration of the passages in the head seal. Small diameter pipe connected the chambers together.

An airborne sodium oxide concentration of 200 to 700 g/m³ was produced in the high-temperature concentration aerosol (HTCA) Test Apparatus to characterize the plugging of a head seal leak. A schematic of the apparatus is shown in Figure 2. The apparatus consisted of a 427 liter vessel, two reservoirs (one for 530°C sodium - one for atomizing gas), sodium spray nozzles, and oxygen flooding nozzles. All the sodium was expelled in a few seconds and subsequently produced a very concentrated, high-temperature aerosol of sodium oxide carried by a mixture of nitrogen and oxygen. This aerosol was used to simulate the material presumed to escape from the reactor cover gas following a CDA - a mixture of core debris, sodium droplets, and gases.

In Test 1a, preliminary data on leak plugging in the head seal leak path was obtained by connecting the multiple bend leak path directly to the HTCA vessel. A spray of 100 g of 5 μm drops of sodium was injected into the HTCA vessel in approximately 4 seconds producing an aerosol concentration of approximately 234 g/m³. The HTCA gas and airborne particles were allowed to vent directly through the multiple bend leak path to the outside atmosphere.

The maximum gas flow rate in the leak path was 8.5 l/sec. This occurred at approximately 1.5 seconds.

*The aerosol concentration in the cover gas following a CDA has been estimated to be ~4000 g/m³.

15th DOE NUCLEAR AIR CLEANING CONFERENCE

The leak path plugged in 6 seconds. Post-test analysis of the data indicated that the plug could withstand 2.8 atmosphere differential pressure and that approximately 7 g of sodium, in the form of sodium oxide, was trapped in the leak path assembly. The mass of sodium found in each section of the assembly is shown in Table 1.

TABLE 1

Sodium Oxide Aerosol Collected in Multiple Bend Leak Path
(Test 1a)

Leak Path Section	Type of Leak Path	Mass of Sodium in Leak Path (g)	Percentage of Mass
S-1 (LPa)	Na Seal	6.37	91.15
S-2 (LPb)	Margin Seal No. 1	0.57	8.16
S-3 (LPc)	Dynamic Seal	0.027	0.39
S-4 (LPd)	Margin Seal No. 2	0.018	0.26
Exit	--	~ 0.003	~ 0.04

The size of the 0.04% of the sodium oxide particles which exited the leak path assembly was measured by an eight-stage Anderson impactor. Approximately 95% of the mass collected in the impactor was $> 6.8 \mu\text{m}$. The median size of the particles before passing into the leak path was $2.5 \mu\text{m}$ (AED 50).

In another test, 1b, the leak path was exposed to a particle concentration of 30 g/m^3 at a pressure differential of 0.068 atmosphere. The plugging time for this set of conditions was less than 30 seconds.

15th DOE NUCLEAR AIR CLEANING CONFERENCE

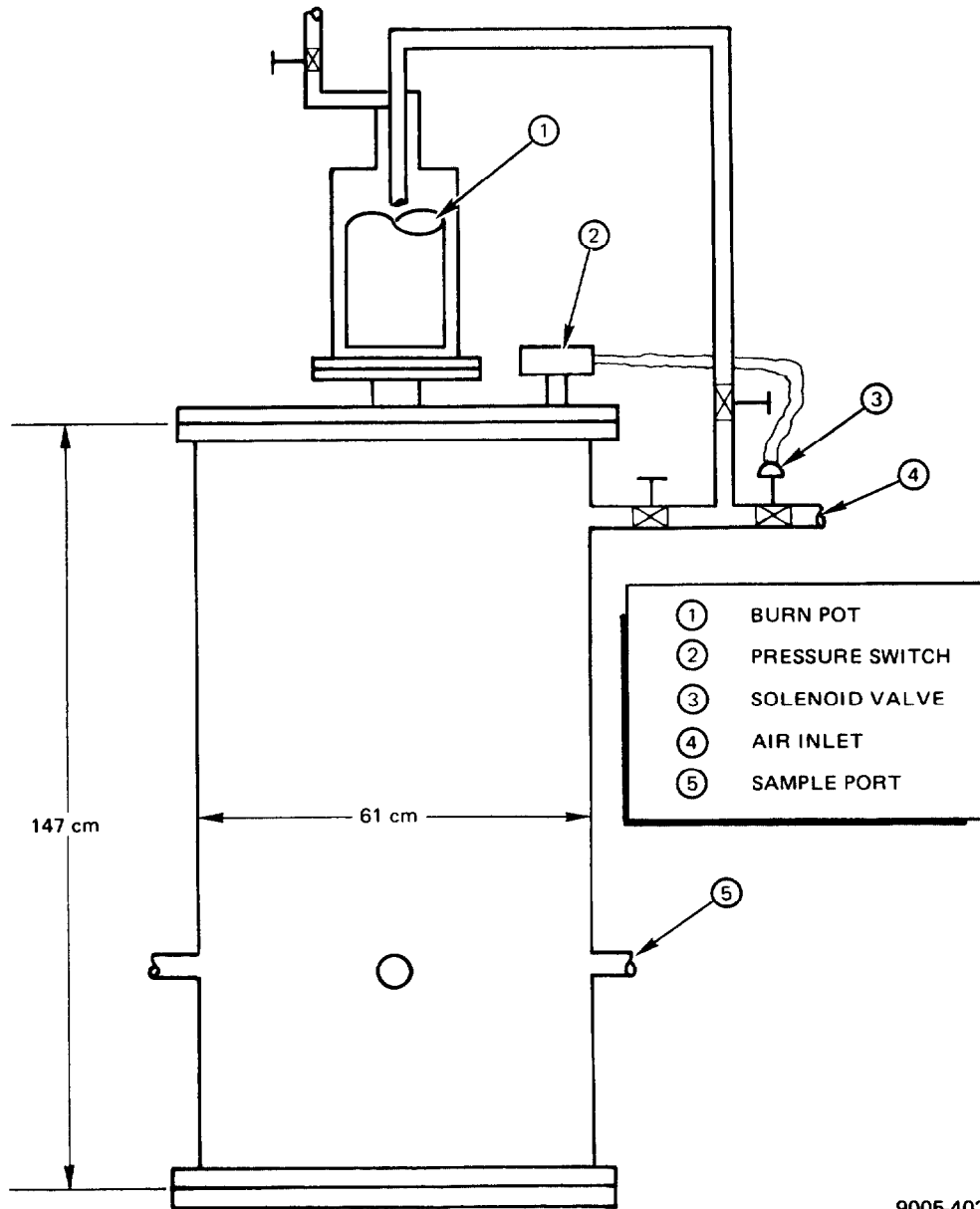
III. PLUGGING OF CONTAINMENT SHELL LEAKS (TEST SERIES 2)

In Test Series 2, sodium combustion product aerosols were allowed to pass through capillary leak paths representing flaws in a steel containment vessel to determine the attenuation of the respirable size aerosols.

These aerosol leak tests were conducted in a 427 liter vessel with flat plates on each end of the cylindrical vessel. The test vessel and simplified schematic of the injection system are shown in Figure 3. The injection system consisted of a heated pot containing sodium, an air inlet line, solenoid valve, and a pressure switch. The concentration in the vessel was regulated by a manual valve located between the solenoid valve and burn pot. A pressure switch sensed the vessel pressure and operated a solenoid valve to maintain a constant pressure in the vessel. During each test run, both total volume of gas which passed through the leak path and gas flow rate were recorded.

For the majority of the tests, the aerosol was allowed to leak through smooth capillaries 1 to 2 mm diameter by 4 cm in length. An example of the sampling methods are shown in Figures 4a and 4b. The wet test meter was modified to measure the gas flow rate as well as accumulated flow. The dry air manifold was used to determine the plug strength at the end of the test. In some tests, the air manifold was not used and the capillary entrance was mounted flush with the inner surface of the vessel wall.

Typical results for a given set of conditions in which plugging occurs is presented in Figure 5. For this series of tests, the aerosol concentration and humidity were maintained constant. The data indicates a direct relationship between pressure applied across the capillary and the mass required to plug it. In addition, measurements of the plug mass and the mass escaping have shown that the major fraction of the entering aerosol mass is the plug mass. Further tests have shown that a higher initial pressure applied across the capillary before plugging usually requires a greater pressure to unplug.



9005-40285

Figure 3. Test vessel.

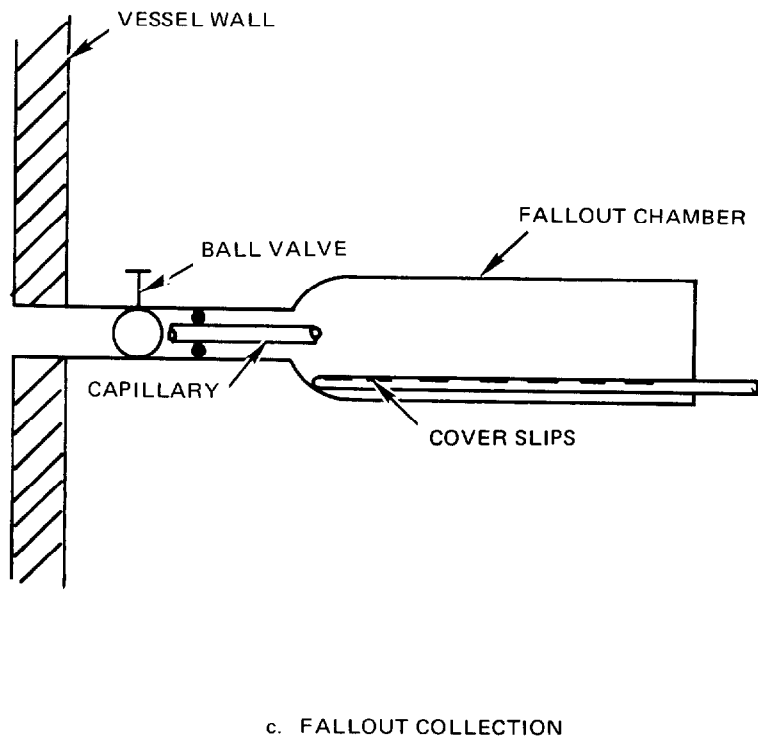
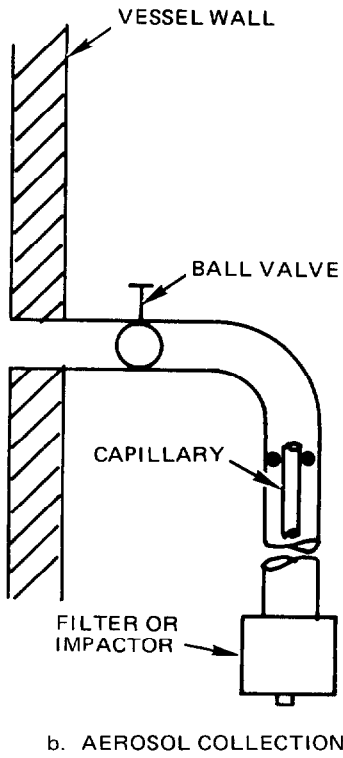
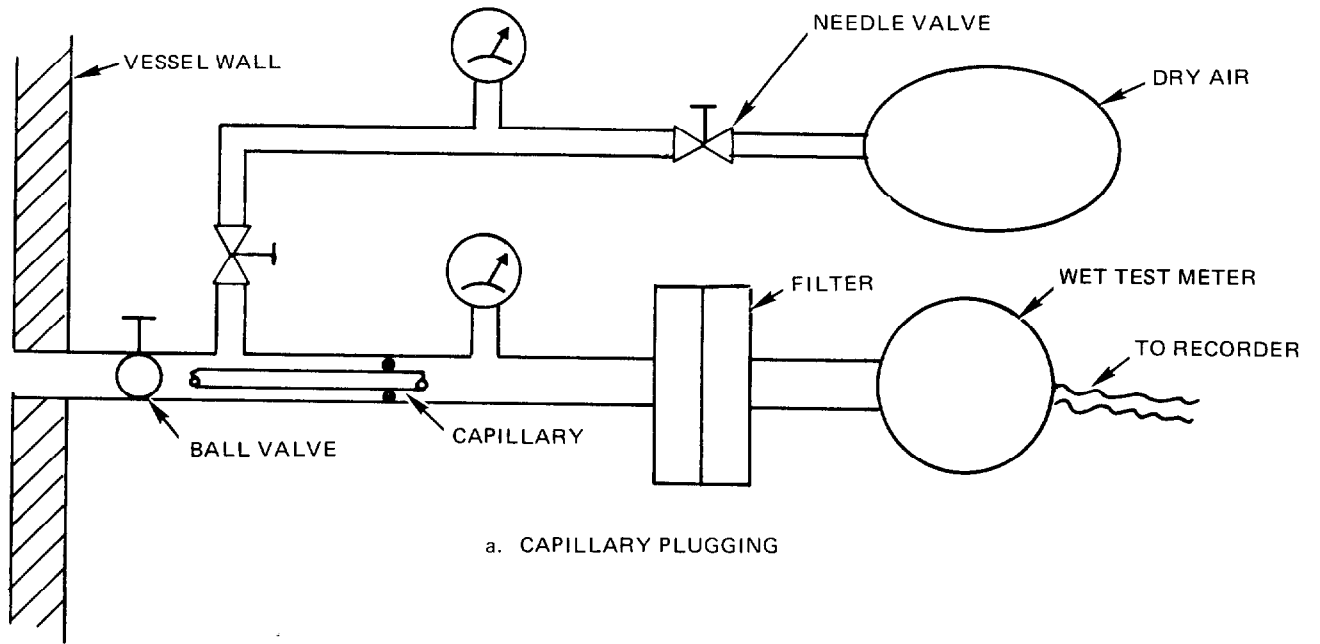


Figure 4. Sampling methods.

9005-40193

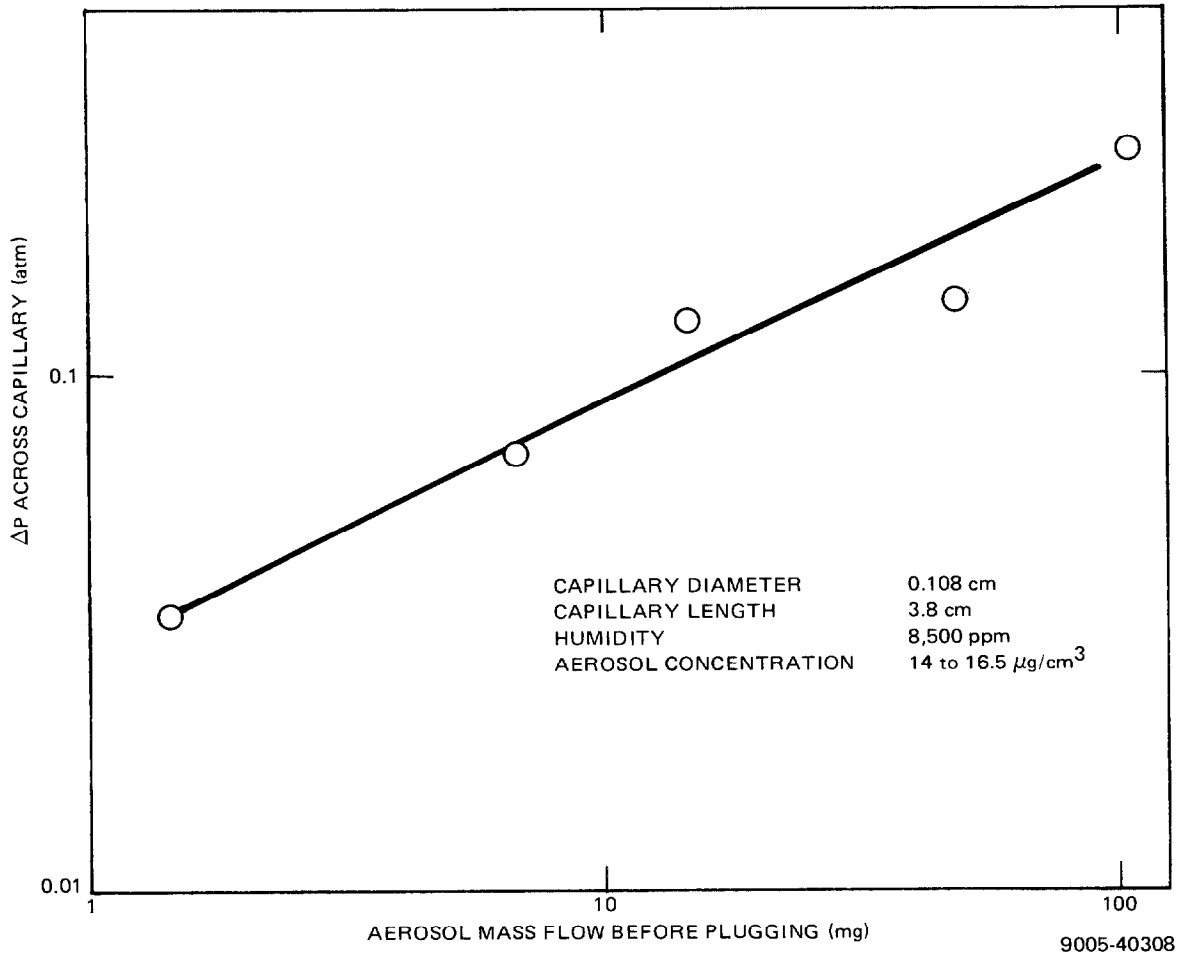


Figure 5. Pressure across capillary vs plugging mass.

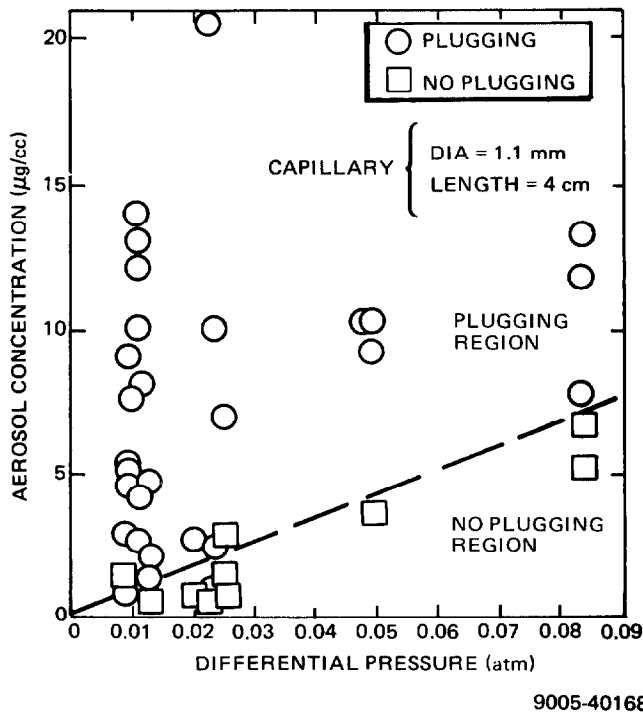


Figure 6. Conditions for Plugging.

15th DOE NUCLEAR AIR CLEANING CONFERENCE

After grouping several tests together as in Figure 6, the data indicates that given a certain pressure differential, there is an aerosol concentration above which plugging occurs and below which no plugging occurs. The line of separation depends primarily on the diameter of the leak path although humidity also plays an important part.

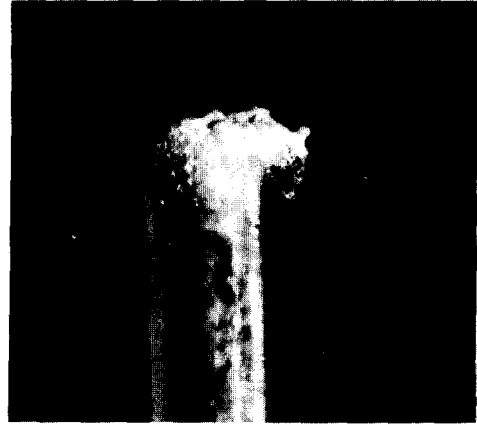
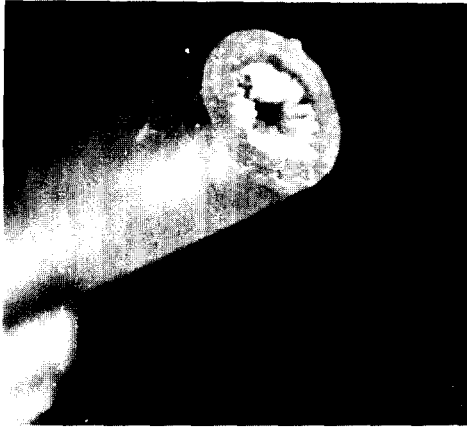
In one set of experiments, tests were performed to document by photography the particulate buildup or deposition during the plugging sequence of capillaries. These tests were performed in a sodium oxide aerosol environment which varied from 0.5 to 3.5 g/m³ in concentration and approximately 1.8 to 2.5 μ m in size (AED 50). The pressure in the vessel was maintained at 0.068 atmosphere with the dew point ranging from -10⁰C to 5⁰C (~3500 ppm).

Figure 7 shows a photograph of entrance plugging where the particulates do not follow the air stream and impact at the entrance. When such a buildup of oxide occurs the plug acts as a filter even though some gas leakage through the capillary still exists.

A plug formed inside the capillary is shown in Figure 8. For this type of leakage, deposition occurs directly on the walls of the capillary.

Figure 9 is a photograph of a capillary exit in which plug creep occurred. As can be seen, a considerable mass of oxide may accumulate before plugging terminates the gas flow.

To illustrate the events that take place when a plug does not form, a strike plate was placed approximately 10 cm from the capillary exit. The results as shown in Figure 10, indicate that large agglomerated particulates were formed in the capillary and then expelled. These particulates are shown to be considerably larger than respirable particulates (i.e., >> μ m). Before passing through the median size was about 2.8 μ m (AED).



← 5 mm →

Figure 7. Entrance plugging.

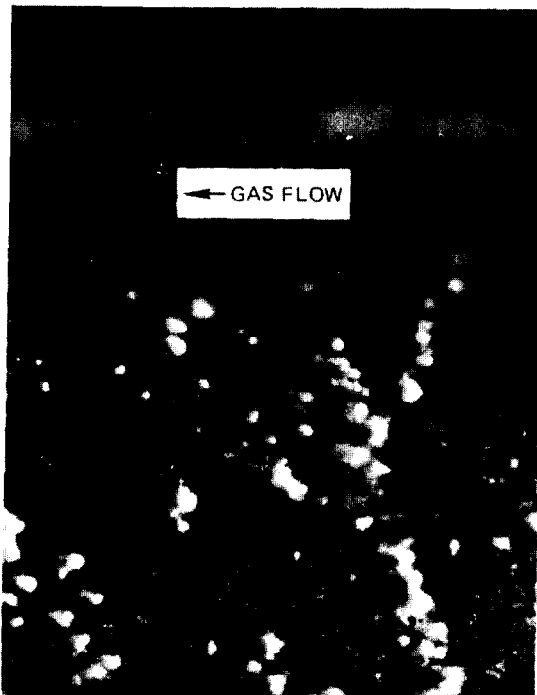


Figure 8. Inside wall of longitudinal section of capillary following plugging.

→ 2 mm ←

9005-40270

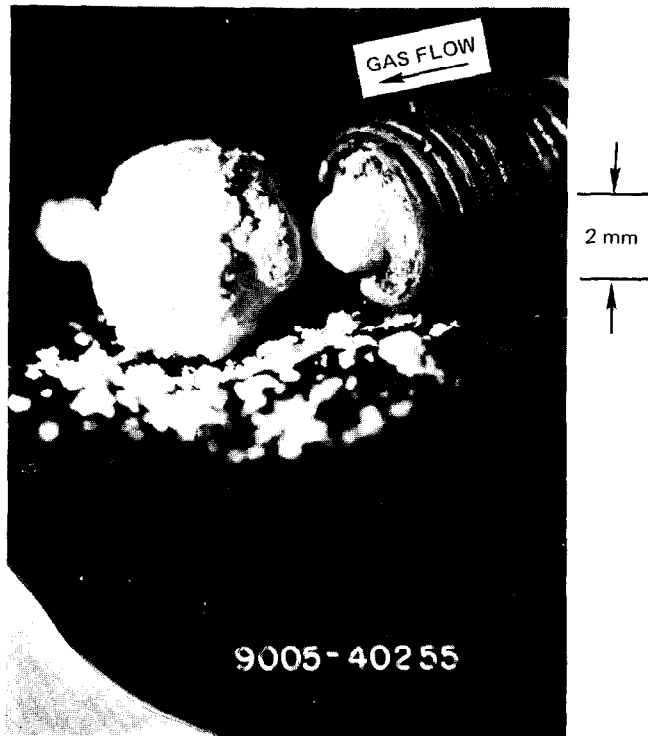


Figure 9. Capillary exit showing plug creep.

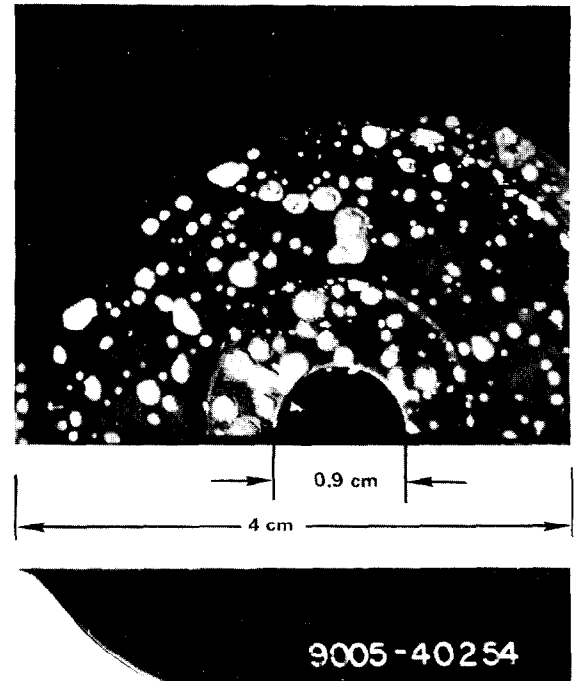


Figure 10. Expelled particulates.



Figure 11. Dendritic column of sodium oxide formed on impact plate.

15th DOE NUCLEAR AIR CLEANING CONFERENCE

In one experiment, all particulates greater than $0.95 \mu\text{m}$ were removed and the remaining particulates allowed to leak through a capillary (.03 mm diam x 1.1 mm) and strike a plate 1.7 mm from the capillary exit. The flow thru the capillary was maintained at 100 cc/min. The results are shown in Figure 11. At the impact region, a dendritic column of sodium oxide (approximately 0.06 mm diam x 1.3 mm) was produced. This column would eventually have reached the capillary and produced a plug if the flow had been continued.

IV. CONCLUSIONS

As a gas stream containing particulates passes through narrow, tortuous passages, the particulates will impinge on the walls, particularly at turns, to form deposits which tend to plug the passages. Also such particulates which are resuspended from the walls will have agglomerated to form much larger (not respirable) particulates.

The present results support the concept that particulates resulting from a hypothetical reactor accident will not flow through leak paths in the same manner as gas, but that leak paths will plug, and that the residual mass which is expelled will be larger than respirable size. An important attenuation mechanism for aerosols has been established, but further work is needed to quantify the attenuation under a wider variety of conditions. It appears that less than 0.5% of the entering aerosol mass may escape through a plugged capillary leak path as compared with the equivalent gas flow model. Of this 0.5%, only 5% will be in the respirable size range. The overall attenuation is tentatively 3×10^{-4} .

15th DOE NUCLEAR AIR CLEANING CONFERENCE

DISCUSSION

SCHIKARSKI: Have you found any dependence of particle composition on the penetration or plugging behavior?

NELSON: There's a lot of dependence on the composition as well as moisture. If you have a lot of moisture in the reactor vessel you have very wet sodium hydroxide and essentially, you have a liquid going through the capillary rather than a dry aerosol. If you have a smooth capillary such as the ones we used, it's difficult to plug them with liquid, because it just keeps on going through. However, if you have a smooth capillary and an aerosol which is extremely dry, why you have a material which does not readily plug within the capillary but forms fluffy deposits on the side. It cannot stick to the side and keeps popping out. Composition does make a lot of difference.

JORDAN: Do you measure temperature distribution in the test capillary? Do you measure particle size entering and leaving the capillary?

NELSON: We assume the leak path is in the outer containment and for this location, temperature will not be much of a problem. Normally, we measure particle size entering and leaving the capillary.

JORDAN: Do you attempt to identify this behavior with filtration theory?

NELSON: Normally, the particle size that we are working with when we expose the capillaries is somewhere between 1 and 4.5 micrometers. We have used extremely low concentrations so that the size would not increase by agglomeration. We seldom get sizes less than one micrometer.